Flows in the radiative zones of rotating stars

Abstract

Keywords: Rotating spherical shells, Anelastic approximation, Stelar radiative zones

Contents

1. Introduction

Some relevant references to start from [1, 2] and for a general overview [6, 5].

2. Mathematical model and numerical method

2.1. Anelastic equations - convective instability

We consider an electrically conducting, self-gravitating, perfect gas confined to a spherical shell. The shell rotates with a fixed angular velocity $\Omega\hat{\boldsymbol{k}}$ about the vertical axis and an entropy contrast ΔS is imposed between its inner and outer surfaces.

Assuming a gravity field proportional to $1/r^2$, a hydrostatic polytropic reference state exists of the form

$$\bar{\rho} = \rho_c \zeta^n, \quad \bar{T} = T_c \zeta, \quad \bar{P} = P_c \zeta^{n+1}, \quad \zeta = c_0 + c_1 d/r, \tag{1}$$

with parameters $c_0 = (2\zeta_o - \eta - 1)/(1-\eta)$, $c_1 = (1+\eta)(1-\zeta_o)/(1-\eta)^2$, $\zeta_o = (\eta+1)/(\eta \exp(N_\rho/n)+1)$. The parameters ρ_c, P_c and T_c are reference values of density, pressure and temperature at the middle of the shell, and the gas polytropic index n, the density scale height N_ρ and the shell thickness ratio η are defined further below. Convection and magnetic field generation set in for sufficiently large values of the entropy contrast, ΔS, and can be described by the equations of continuity, momentum, energy and magnetic flux. In the anelastic approximation [3, 4] these equations take the form

$$\nabla \cdot \bar{\rho}\boldsymbol{u} = 0, \tag{2a}$$

$$\partial_t \boldsymbol{u} + (\nabla \times \boldsymbol{u}) \times \boldsymbol{u} = -\nabla \Pi - \tau(\hat{\boldsymbol{k}} \times \boldsymbol{u}) + \frac{\mathrm{R}}{\mathrm{Pr}} \frac{S}{r^2} \hat{\boldsymbol{r}} + \boldsymbol{F}_\nu \tag{2b}$$

$$\partial_t S + \boldsymbol{u} \cdot \nabla S = \frac{1}{\mathrm{Pr} \bar{\rho} \bar{T}} \nabla \cdot \bar{\kappa} \bar{\rho} \bar{T} \nabla S + \frac{c_1 \mathrm{Pr}}{\mathrm{R} \bar{T}} Q_\nu, \tag{2c}$$

where $\boldsymbol{u}$ is the velocity, $\boldsymbol{B}$ is the magnetic flux density, S is the entropy and $\nabla \Pi$ includes all terms that can be written as gradients. The viscous force and the viscous heating,

$$\boldsymbol{F}_\nu = \frac{\rho_c}{\bar{\rho}} \nabla \cdot \hat{\boldsymbol{S}}, \quad Q_\nu = \hat{\boldsymbol{S}} : \boldsymbol{e}, \tag{3}$$

are defined in terms of the deviatoric stress tensor

$$\hat{S}_{ij} = 2 \bar{\nu} \bar{\rho} (e_{ij} - e_{kk} \delta_{ij}/3), \quad e_{ij} = (\partial_i u_j + \partial_j u_i)/2,$$

where double-dots (**:**) denotes the Frobenius inner product. We assume that the viscosity and the entropy diffusivity vary in radius as $\bar{\nu}(r) = \nu_c \bar{\rho}^k$ and $\bar{\kappa}(r) = \kappa_c \bar{\rho}^k$ with some negative power $k \leq 0$, where ν_c and κ_c are their reference values at midshell. The governing equations have been nondimensionalised using the thickness of the shell $d = r_o - r_i$ as a unit of length, d^2/ν_c as a unit of time, ΔS as a unit of entropy, $\nu_c \sqrt{\mu_0 \rho_c}/d$ as a unit of magnetic induction, ρ_c as a unit of density and T_c as a unit of temperature. Here, r_i and r_o are the inner and the outer radius, λ and μ_0 are the magnetic diffusivity and permeability, respectively. The system is then characterized by eight dimensionless parameters: the radius ratio, the polytropic index of the gas, the density scale number, the radial dependence power, the Rayleigh number, the ordinary and the magnetic Prandtl numbers and the Coriolis number, defined as

$$\eta = r_i/r_o, \quad n, \quad N_\rho = \ln\Big(\bar{\rho}(r_i)/\bar{\rho}(r_o)\Big), \quad k,$$
$$\mathrm{R} = \frac{c_1 T_c d^2 \Delta S}{\nu_c \kappa_c}, \quad \mathrm{Pr} = \frac{\nu_c}{\kappa_c}, \quad \mathrm{Pm} = \frac{\nu_c}{\lambda}, \quad \tau = \frac{2\Omega d^2}{\nu_c}, \tag{4}$$

respectively.

Since the mass flux $\bar{\rho}\boldsymbol{u}$, and the magnetic flux density $\boldsymbol{B}$ are solenoidal vector fields, it is advantageous to employ a decomposition in poloidal and toroidal components,

$$\bar{\rho} \boldsymbol{u} = \nabla \times (\nabla \times \hat{\boldsymbol{r}} r v) + \nabla \times \hat{\boldsymbol{r}} r^2 w, \tag{5}$$

where $\hat{\boldsymbol{r}}$ is the radial unit vector, r is its length, v, w, h and g are the poloidal and toroidal scalars of the momentum and magnetic field, respectively. Equations (2a) are then satisfied by construction. Scalar equations for v and w are obtained, and effective pressure gradients are eliminated by taking $\hat{\boldsymbol{r}} \cdot \nabla \times \nabla \times$ and $\hat{\boldsymbol{r}} \cdot \nabla \times$ of equation (2b). Similarly, equations for h and g are obtained by taking $\hat{\boldsymbol{r}} \cdot \nabla \times$ and $\hat{\boldsymbol{r}} \cdot$ of equation (**??**). The resulting poloidal-toroidal equations are somewhat lengthy and will not be listed here (or may be listed in an appendix). A minor disadvantage of this representation is that a fourth-order poloidal equation is obtained.

2.2. Boundary conditions

We explore various assumptions for the boundary conditions imposed on velocity, entropy and magnetic flux at the surface of the shell. The alternatives are listed below and the particular choice will be specified in each individual case. At a no-slip, impenetrable boundary we impose

$$v = 0, \quad \partial_r v = 0, \quad w = 0. \tag{6}$$

At a stress-free, impenetrable boundary we require

$$v = 0, \quad \partial_r^2 v - \frac{\bar{\rho}'}{\bar{\rho} r} \partial_r (r v) = 0, \quad \partial_r w - \frac{\bar{\rho}'}{\bar{\rho}} w = 0. \tag{7}$$

Values of the entropy may be fixed at the boundaries, then

$$S = 1 \text{ at } r = r_i, \qquad S = 0 \text{ at } r = r_o. \tag{8}$$

Alternatively, the entropy flux may be specified at the top,

$$\partial_r S = 0 \text{ at } r = r_o. \tag{9}$$

Boundary conditions for the magnetic field may be derived from the assumption of an electrically insulating external region. The poloidal function h is then matched to a function $h^{(e)}$, which describes an external potential field,

$$g = 0, \quad h - h^{(e)} = 0, \quad \partial_r(h - h^{(e)}) = 0. \tag{10}$$

Alternatively, a perfectly conducting external region may be assumed, requiring

$$\partial_r g = 0, \quad h = 0. \tag{11}$$

Finally, the, so-called, "pseudo-vacuum" condition offers another choice,

$$g = 0, \quad \partial_r h = 0. \tag{12}$$

2.3. Numerical method

For the numerical solution of the problem we have adapted the pseudo-spectral method described by [7]. The scalar unknowns v, w, h, g and S, are expanded in Chebychev polynomials T_p in the radial direction r, and in spherical harmonics in the angular directions (θ, φ) e.g.,

$$v = \sum_{l=1}^{N_l} \sum_{m=-l}^{l} \sum_{p=0}^{N_r} V_{lp}^m(t)\, T_p\Big(x(r)\Big)\, P_l^m(\cos\theta)\, \exp(im\varphi), \tag{13}$$

where P_l^m denotes the associated Legendre functions, $x(r) = 2(r - r_i) - 1$, and N_l and N_r are truncation parameters. A system of equations for the coefficients in these expansions is obtained by a combination of a Galerkin spectral projection of the governing equations in the angular directions and a collocation constraint in radius. Computation of nonlinear terms in spectral space is expensive, so nonlinear products and the Coriolis term are computed in physical space and then projected to spectral space at every time step. A standard 3/2-dealiasing in θ and φ is used at this stage. A hybrid of a Crank-Nicolson scheme for the diffusion terms and a second order Adams-Bashforth scheme for the nonlinear terms is used for integration in time.

A range of numerical resolutions has been used in this study varying from ($N_r = 61$, $N_l = 96$) in less demanding cases to ($N_r = 121$, $N_l = 144$) in more strongly stratified or turbulent runs. Correspondingly, the physical gridpoints on which non-linear terms are evaluated have been varied up to $N_r = 121$, $N_\theta = 216$, $N_\varphi = 437$.

2.4. Model of a baroclinic star

The equations are modified to

$$\nabla \cdot \bar{\rho}\boldsymbol{u} = 0, \tag{14a}$$

$$\partial_t \boldsymbol{u} + (\nabla \times \boldsymbol{u}) \times \boldsymbol{u} = -\nabla\Pi - \tau(\hat{\boldsymbol{k}} \times \boldsymbol{u}) + \frac{\mathrm{R}}{\mathrm{Pr}}\frac{S}{r^2}\hat{\boldsymbol{r}} + \boldsymbol{F}_\nu + Zr\frac{\zeta_o^n - \zeta(r)^n}{\zeta_o^n - \zeta_i^n}\cos(\theta)\hat{\boldsymbol{k}} \tag{14b}$$

$$\partial_t S + \boldsymbol{u} \cdot \nabla S = \frac{1}{\mathrm{Pr}\bar{\rho}\bar{T}}\nabla \cdot \bar{\kappa}\bar{\rho}\bar{T}\nabla S + \frac{c_1\mathrm{Pr}}{\mathrm{R}\bar{T}}Q_\nu, \tag{14c}$$

At $Z = 0$ the usual anelastic equations (2) are obtained.

We set $\mathrm{R} < 0$ to model a convectively stable situation and increase Z from zero until a visible effect is obtained.

The term red is obtained in a way similar to [5]?

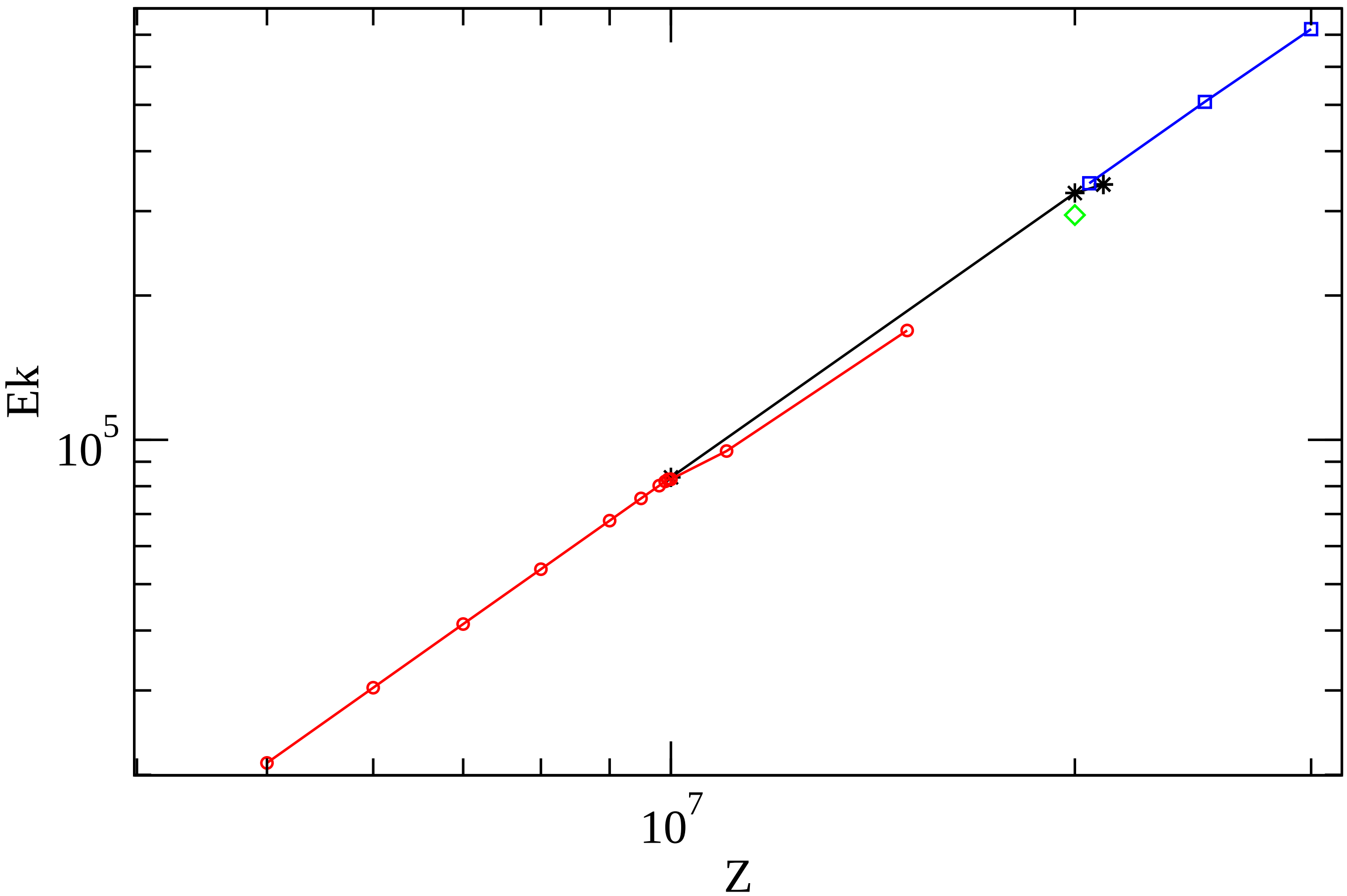

Figure 1: Kinetic energy in a sequence of cases with increasing parameter Z as indicated in the plot. The other parameters are $\eta = 0.3$, $P = 1$, $\tau = 10^4$, $R = -10$, polytropic index $n = 2$, density scale hight $N_\rho = 3$. Results are somewhat resolution dependent and the symbols represent numerical resolution as follows. Black stars – 16-fold azimuthal symmetry is imposed which forces the simulations to be essentially axisymmetric. Red circles – r=31, l=64, m=129. Green diamond – r=41, l=96, m=193. Blue squares — r=61, $\theta = 144$, $\phi = 289$; n=61, l=96, m=193

3. Numerical results

Please, see plots at the end of the draft. - There are two sets of plots. In the first set u_r is plotted at the spherical surface $r = r_i + 0.7$. In the second set u_r is plotted at the spherical surface $r = r_i + 0.5$.

We set $\mathrm{R} < 0$ to model a convectively stable situation.

We increase Z from zero. Initially a stationary axisymmetric solutions are found. Above certain value of Z, see below, instabilities develop. However, it is not clear whether the instabilities are physical states or numerical artefacts. The reason why I suspect numerical artefacts are that (a) instabilities have a rather unusual spatial structure, (b) there is some periodic time dependence that shows an extremely high frequency. (c) the instabilities shift to higher values of Z when numerical resolution is increases or when a smaller time-step is used. At the highest resolution attempted (n=61, l=96, m=193) instabilities have not yet developed.

The following plots at the end of the draft illustrate these remarks further.

An overview of the cases computed so far is given in Figure 1.

3.1. Axisymmetric solutions

One of the sequences of cases shown in Figure 1 was started from zero initial conditions (prepared with "remesh"). Since the equations include a forcing term, flows develop from zero initial conditions for any non zero value of Z.

The cases in this sequence have imposed axial symmetry. This is achieved by forcing a 16-fold azimuthal symmetry. The axial symmetry is imposed in order to obtain purely axisymmetric solutions and study their instabilities to non-axisymmetric perturbations.

Three cases are computed – shown in black stars in Figure 1.

case	z value	comments
a.e03p1t10r-10m16n2N3z1e7sgn	1e7	steady
a.e03p1t10r-10m16n2N3z2e7sgn	2e7	steady
a.e03p1t10r-10m16n2N3z2.1e7sgn.a	2.1e7	oscillations

3.2. No imposed axisymmetry

Obviously, some sort of instability (or artefact) occurs in the last case of the previous section (a.e03p1t10r-10m16n2N3z2.1e7sgn.a, Figs **??** and **??**). Because of the imposed axisymmetry this cannot properly develop. For this reason, I remove the axisymmetry assumption and use full-resolution.

3.2.1. Sequence at r=31, l=64, m=129

case	z value	comments
a.e03p1t10r-10m1n2N3z1e6	1e6	steady
a.e03p1t10r-10m1n2N3z05e7	0.5e7	steady
a.e03p1t10r-10m1n2N3z06e7	0.6e7	steady
a.e03p1t10r-10m1n2N3z07e7	0.7e7	steady
a.e03p1t10r-10m1n2N3z08e7	0.8e7	steady
a.e03p1t10r-10m1n2N3z09e7	0.9e7	steady
a.e03p1t10r-10m1n2N3z095e7	0.95e7	steady
a.e03p1t10r-10m1n2N3z098e7	0.98e7	steady
a.e03p1t10r-10m1n2N3z099e7	0.99e7	steady
a.e03p1t10r-10m1n2N3z0995e7	0.9995e7	instability, time-step=0.200D-05
a.e03p1t10r-10m1n2N3z1e7	1e7	no instability, time-step=0.100D-05
a.e03p1t10r-10m1n2N3z1e7a	1e7	
a.e03p1t10r-10m1n2N3z1.1e7	1.1e7	
a.e03p1t10r-10m1n2N3z1.5e7	1.5e7	instability,time-step=0.100D-05
a.e03p1t10r-10m1n2N3z1.6e7	1.6e7	instability,time-step=0.100D-05
a.e03p1t10r-10m1n2N3z1.7e7	1.7e7	instability,time-step=0.100D-05
a.e03p1t10r-10m1n2N3z1.8e7	1.8e7	instability,time-step=0.100D-05
a.e03p1t10r-10m1n2N2z1.8e7 1.8e7		
a.e03p1t10r-10m1n2N2z2e7 2e7		

Sequence at r=61, l=96, m=129. When resolution is increased and time step is decreased instabilities decay.

case	z value	comments
a.e03p1t10r-10m1n2N3z2.05e7	2.05e6	steady so far
a.e03p1t10r-10m1n2N3z3e7	3e7	steady so far

4. Instabilities of the axisymmetric solution

The experiments in this section were carried out with an earlier version of the code that contained a wrong sign.

We now perturb the axisymmetric solutions described in the previous section 3.1 by introducing a perturbation of the type

$$\overset{\text{pert}}{V_l^m}(r,t=0) = \overset{\text{axisymm}}{V_l^m}(r) + A\sin\big(\pi(r-r_i)\big),$$

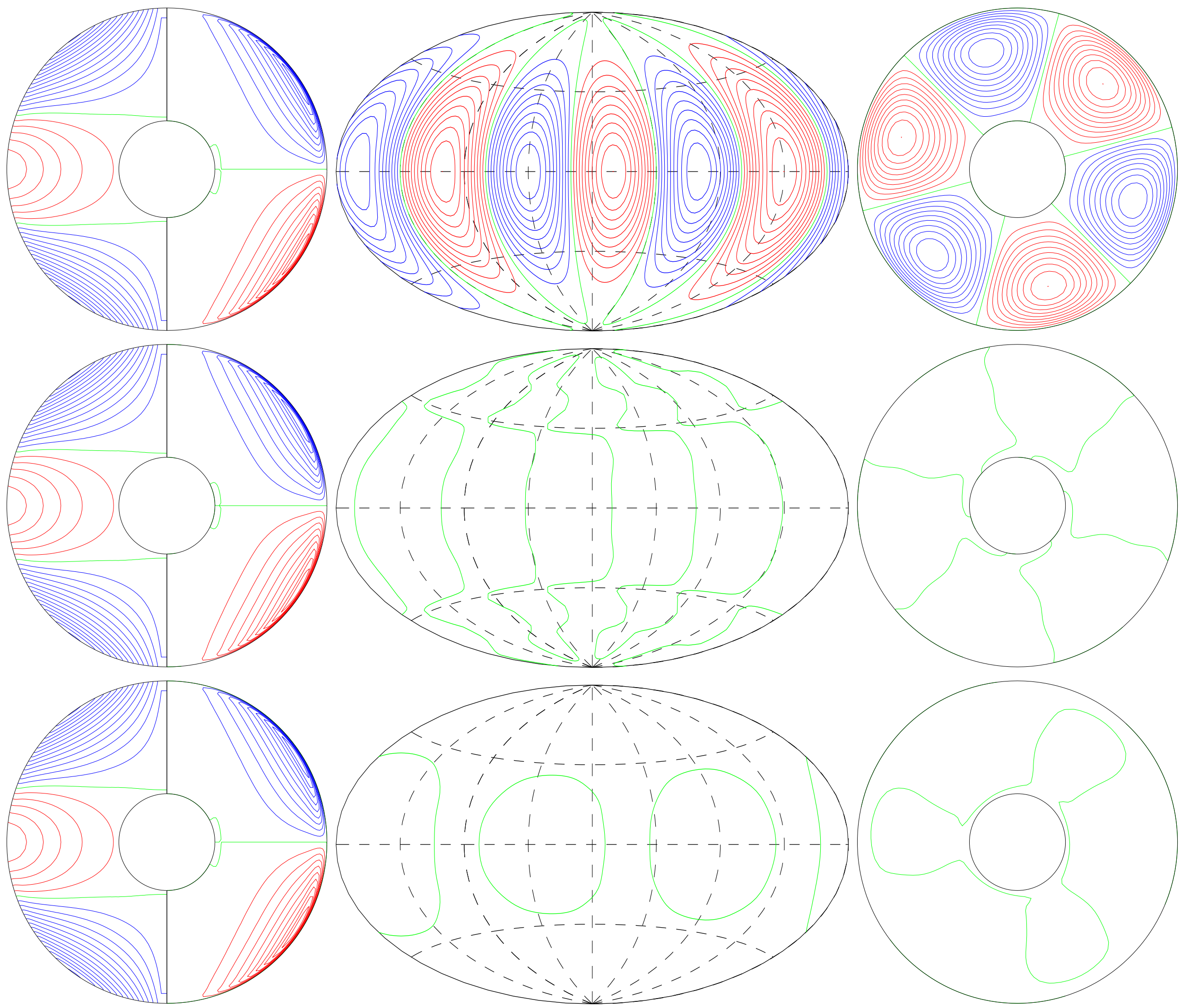

Figure 2: Left plot: Differential rotation and meridional circulation; Central plot u_r on a spherical surface; Right plot u_r in the equatorial plane. Snapshots are taken at the initial moment, at the middle and at the end of the simulation. Same case as in figure **??**.

where $V_l^m(r)$ is particular poloidal coefficient in the expansion (13), and A is the amplitude of the perturbation.

Figures **??** and **??** show results of perturbing the case $Z = 1e5$. The perturbation is quite significant in amplitude but decays and the axisymmetric solution is stable.

The parameter Z varies from 10^7 to $2 \cdot 10^7$ as indicated in figure 1 and for values of Z somewhat larger that $2 \cdot 10^7$ the numerical solution diverges. This indicates that a forcing of $Z = 10^7$ should be sufficiently strong to support instabilities of the axisymmetric solution. For this reason we, impose perturbations onto $Z = 10^7$. The results are shown in figure **??**. The axisymmetric solution appears stable again.

4.1. Conclusion

We tried imposing perturbations in a rather strongly driven case $Z = 1e7$ yet it appears stable to the perturbations. On the other hand, increasing Z further say to $Z = 2e7$ produces numerical divergence without any initial perturbations. Of course, it may be possible to offset the numerical divergence somewhat by increasing the resolution. But the resolution would become larger than typical and this is supposed to be a rather laminar problem, so maybe we should consider other options first.

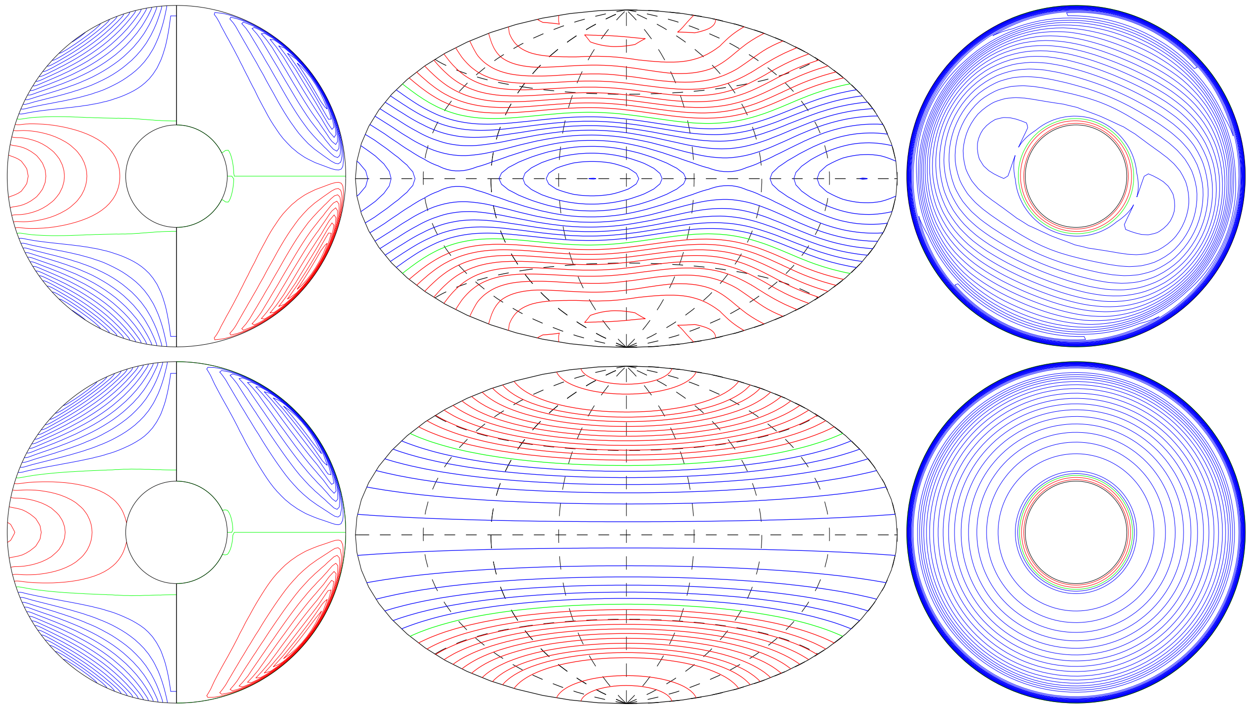

Figure 3: Left plot: Differential rotation and meridional circulation; Central plot u_r on a spherical surface; Right plot u_r in the equatorial plane. Snapshots are taken at the initial moment and at the end of the simulation. Amplitude of plots are NOT scaled wrt each other. The parameter values are $\eta = 0.3$, $P = 1$, $\tau = 10^4$, $R = -500000$, polytropic index $n = 2$, density scale hight $N_\rho = 3$, $Z = 1e7$. No azimuthal symmetry is imposed. The perturbation is of the form $V_2^2(r, t = 0) \sim \sin\left(\pi(r - r_i)\right)$.

References

[1] F. H. Busse. Do Eddington-Sweet circulations exist? Geophysical & Astrophysical Fluid Dynamics, 17(1):215–235, 1981.

[2] F. H. Busse. On the problem of stellar rotation. Astrophys. J., 259:759–766, 1982.

[3] D. O. Gough. The anelastic approximation for thermal convection. J. Atmos. Sci., 26:448, 1969.

[4] C. A. Jones, P. Boronski, A. S. Brun, G. A. Glatzmaier, T. Gastine, M. S. Miesch, and J. Wicht. Anelastic convection-driven dynamo benchmarks. Icarus, 216(1):120–135, 2011.

[5] M. Rieutord. The dynamics of the radiative envelope of rapidly rotating stars. Astronomy and Astrophysics, 451(3):1025–1036, 2006.

[6] M. Rieutord. On the dynamics of radiative zones in rotating stars. EAS Publications Series, 21:275–295, 2006.

[7] A. Tilgner. Spectral methods for the simulation of incompressible flows in spherical shells. Int. J. Numer. Meth. Fluids, 30(6):713–724, 1999.

a.e03p1t10r-10m1n2N3z1e6
times: 2.80028 2.90029 3.0003 3.10031 3.20032 3.30033

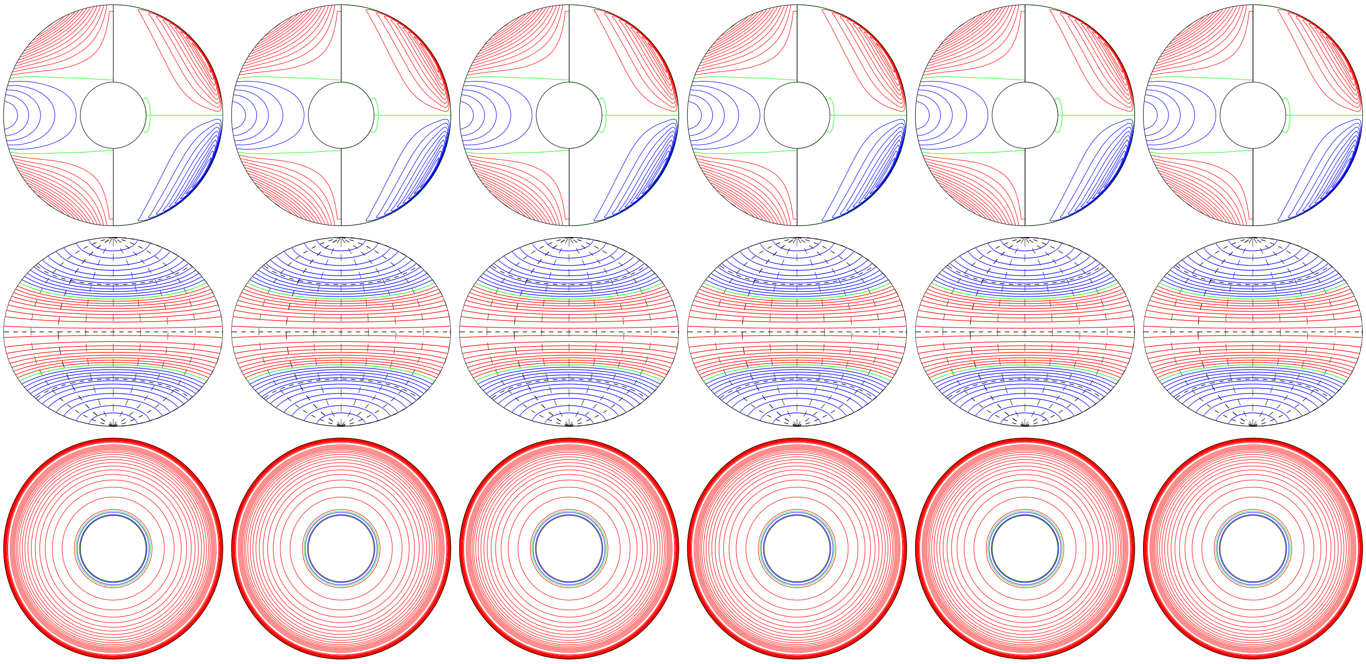

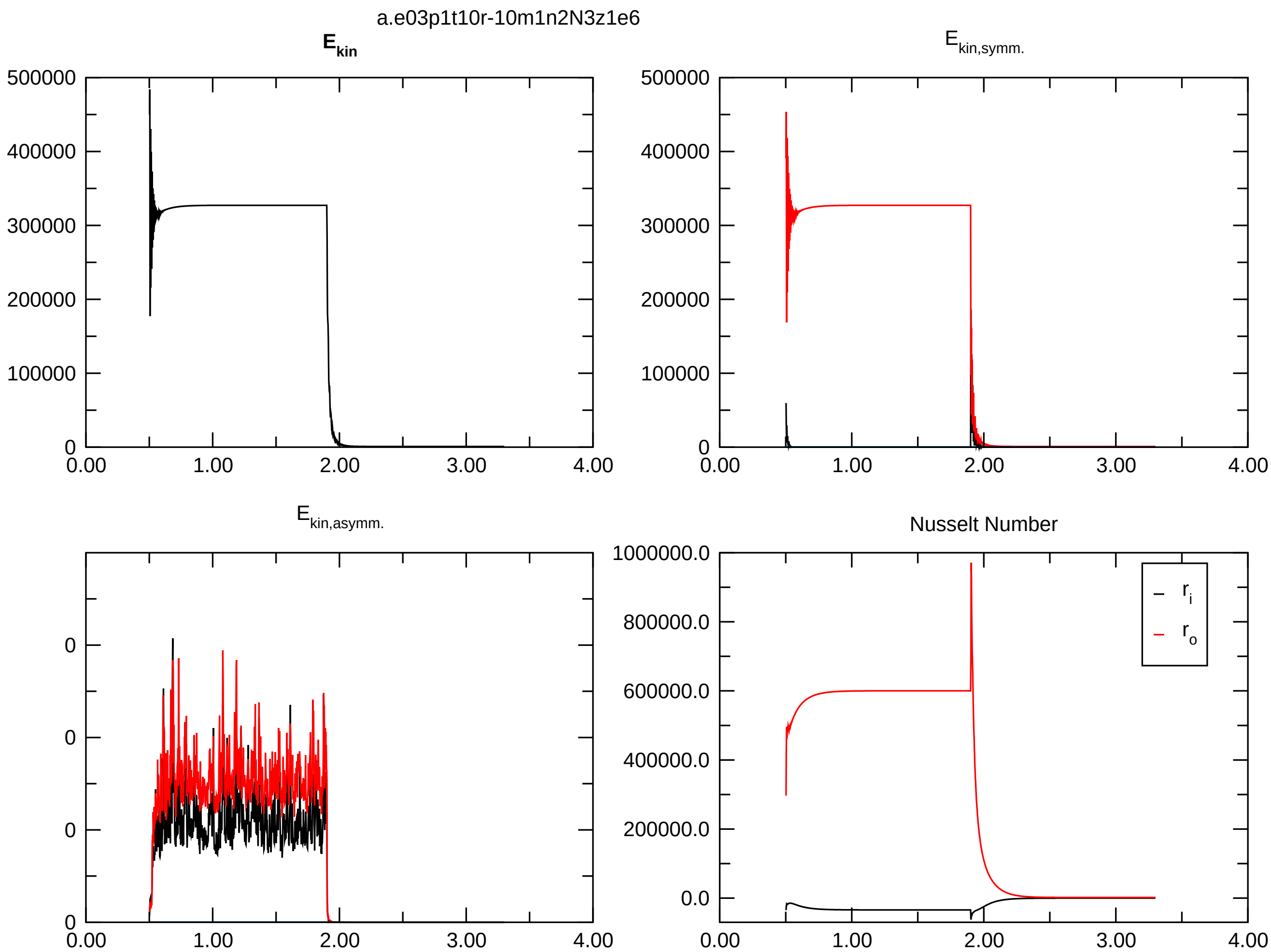

a.e03p1t10r-10m1n2N3z05e7
times: 2.80028 2.90029 3.0003 3.10031 3.20032 3.30033

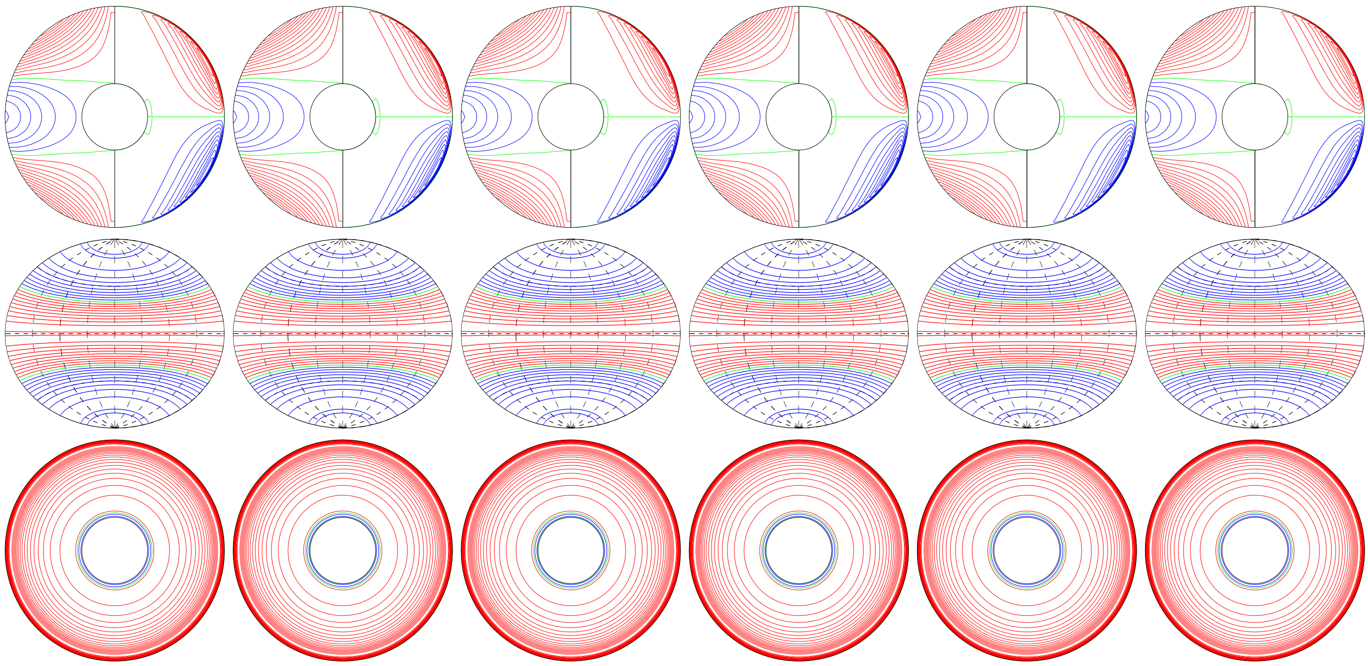

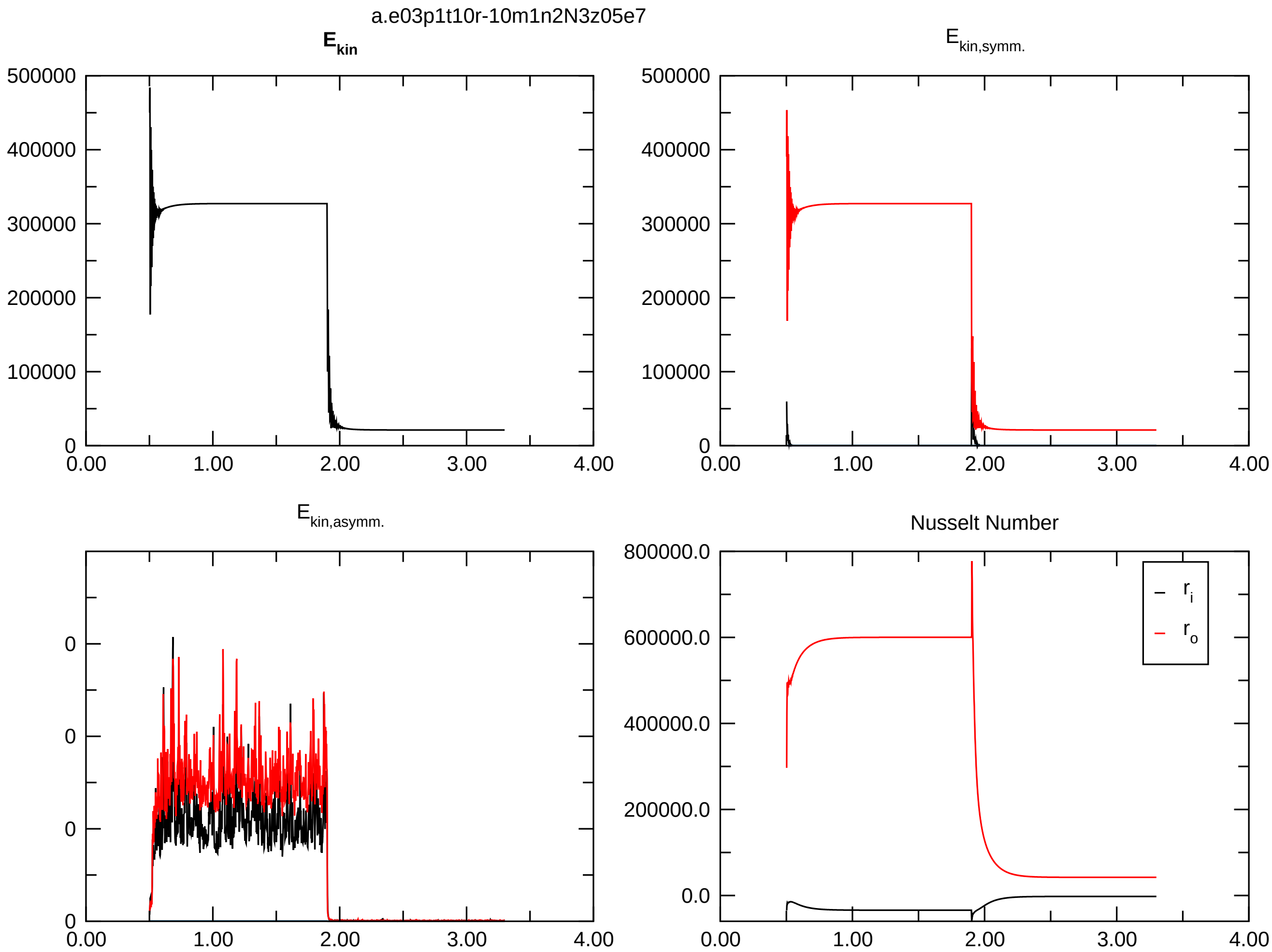

a.e03p1t10r-10m1n2N3z06e7
times: 2.80028 2.90029 3.0003 3.10031 3.20032 3.30033

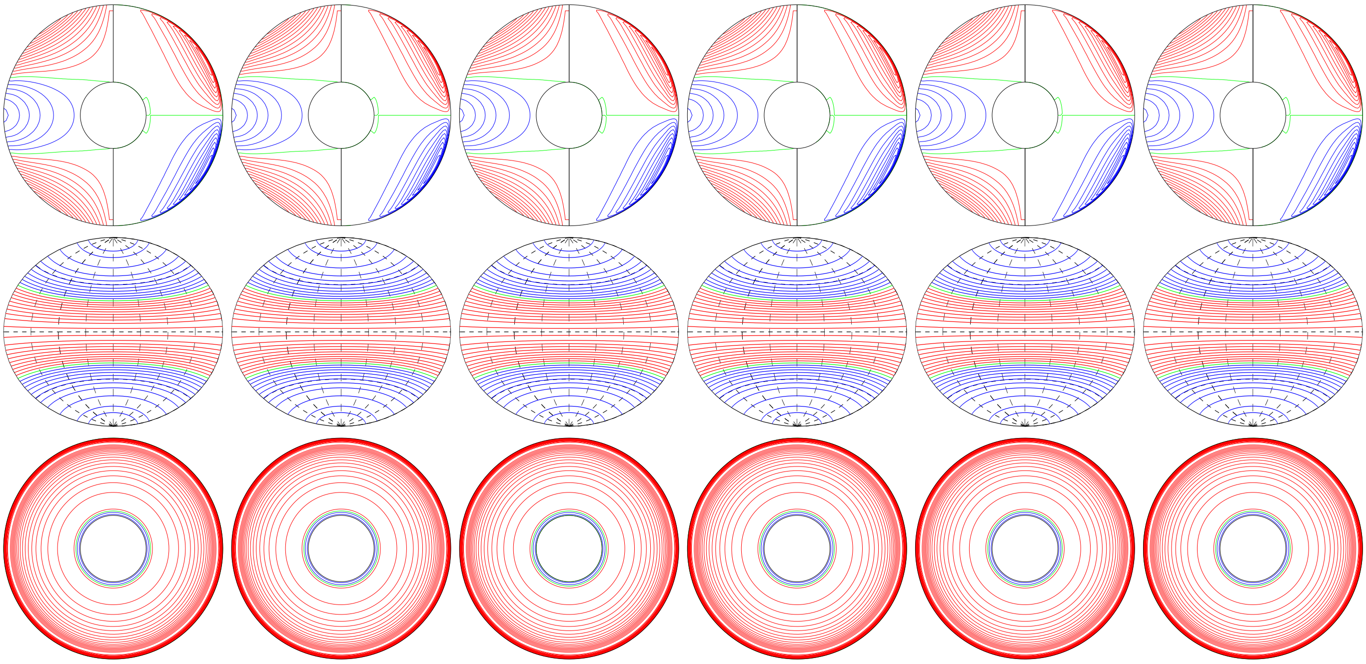

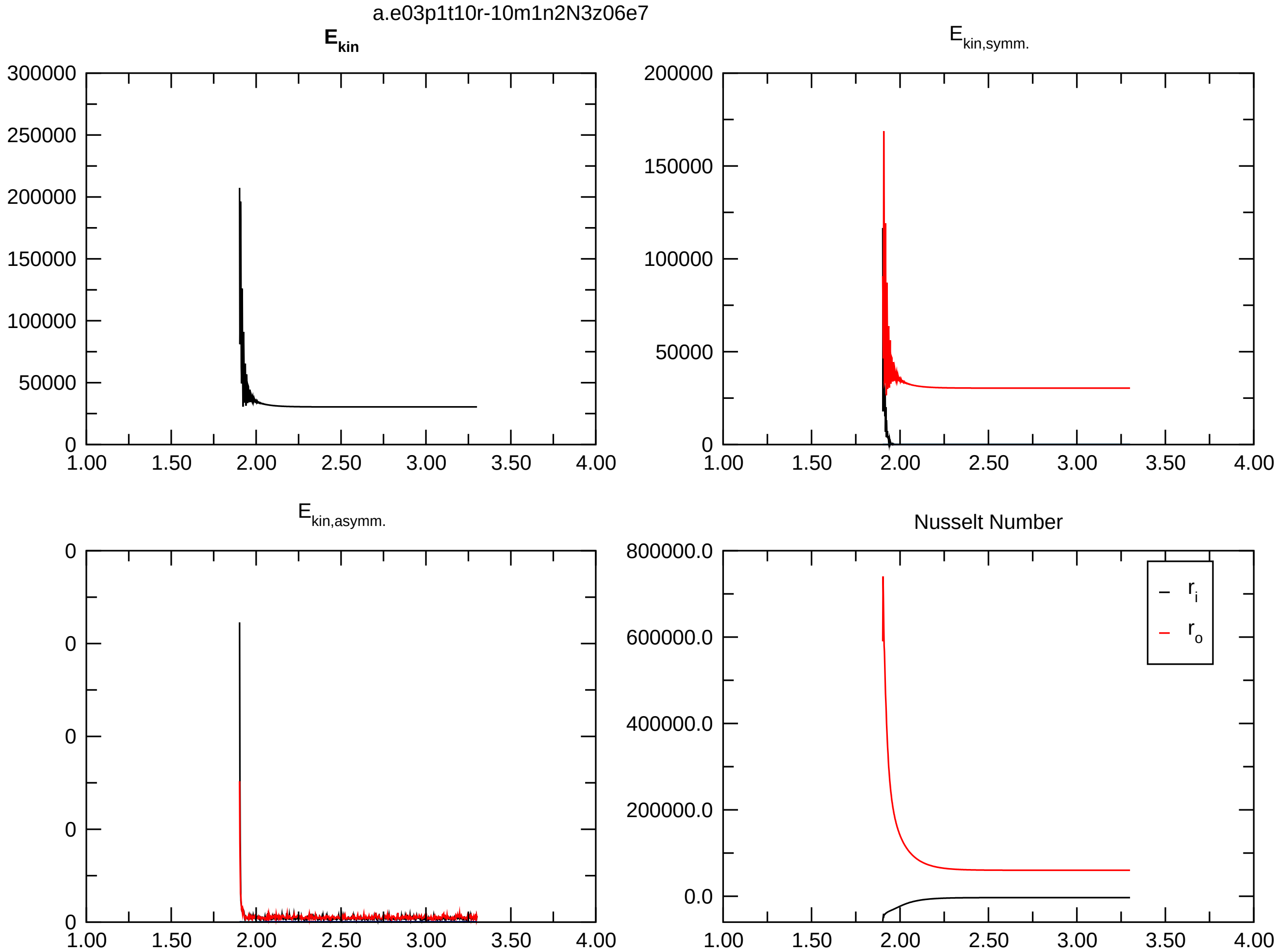

a.e03p1t10r-10m1n2N3z07e7
times: 2.80028 2.90029 3.0003 3.10031 3.20032 3.30033

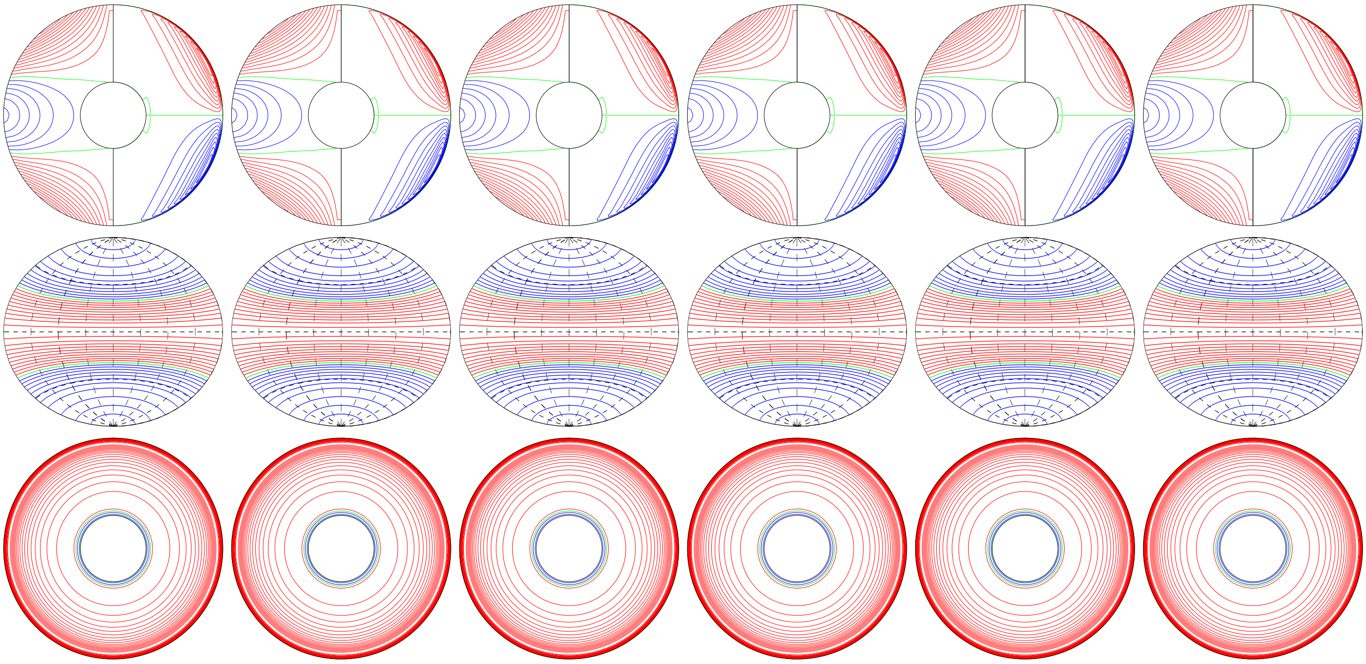

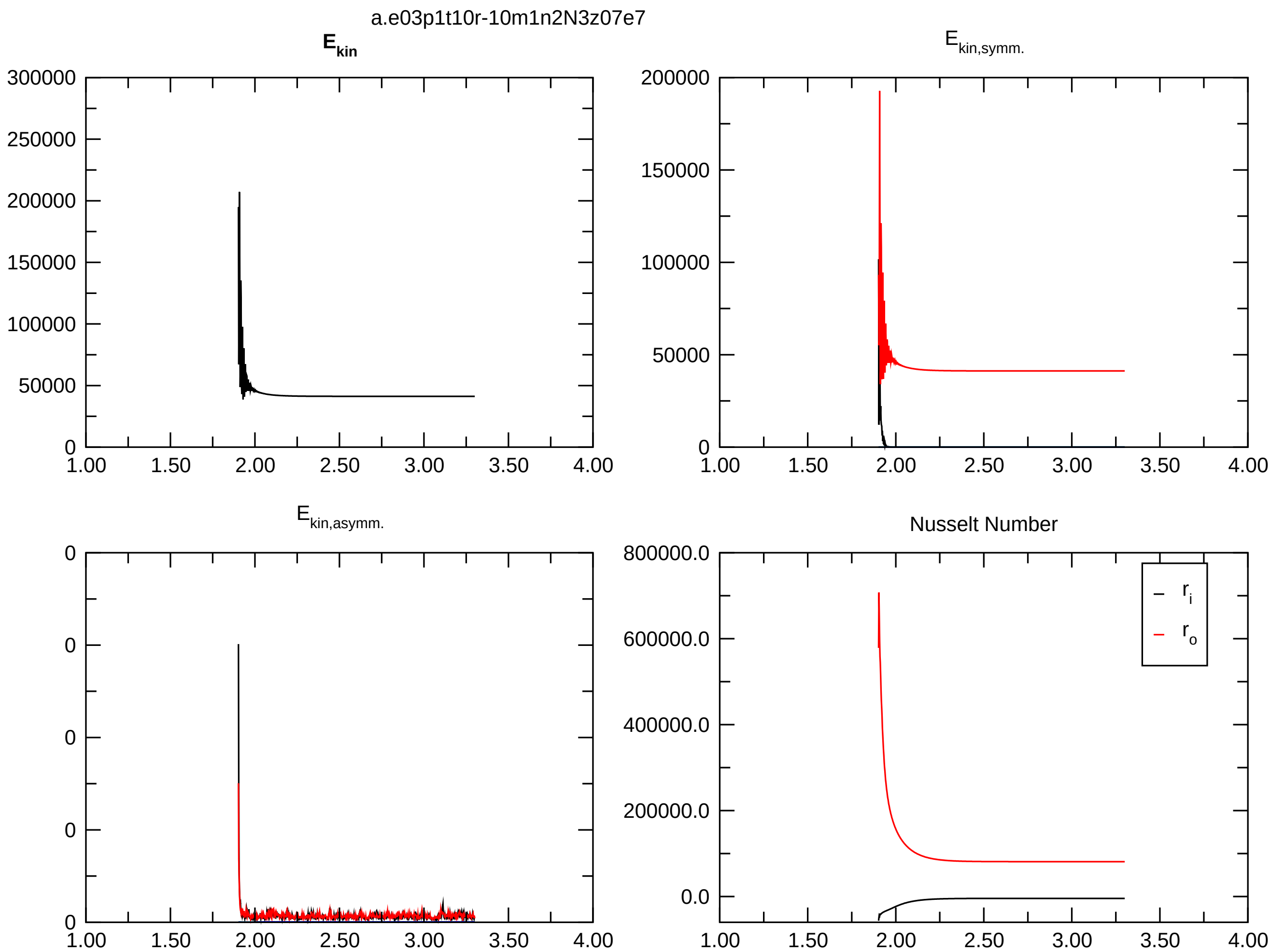

a.e03p1t10r-10m1n2N3z08e7
times: 2.80028 2.90029 3.0003 3.10031 3.20032 3.30033

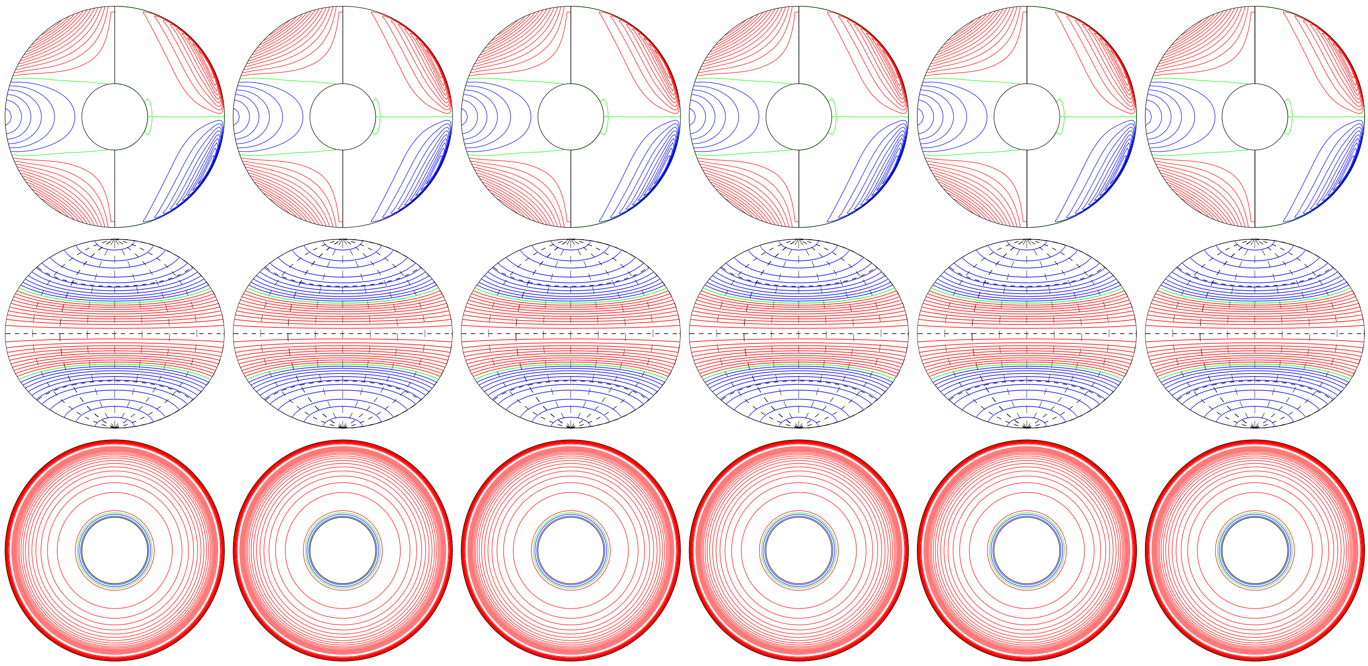

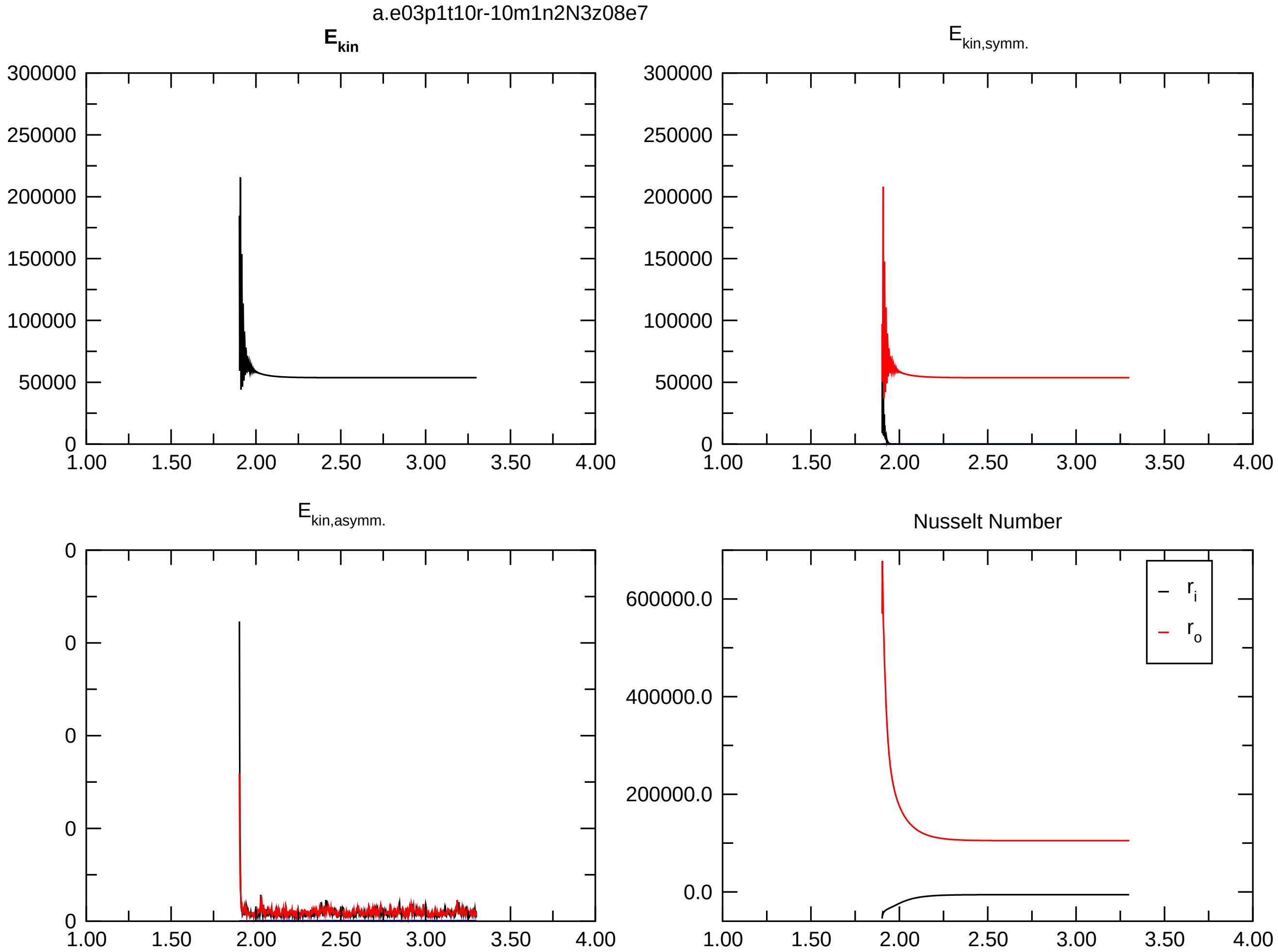

a.e03p1t10r-10m1n2N3z09e7
times: 2.80028 2.90029 3.0003 3.10031 3.20032 3.30033

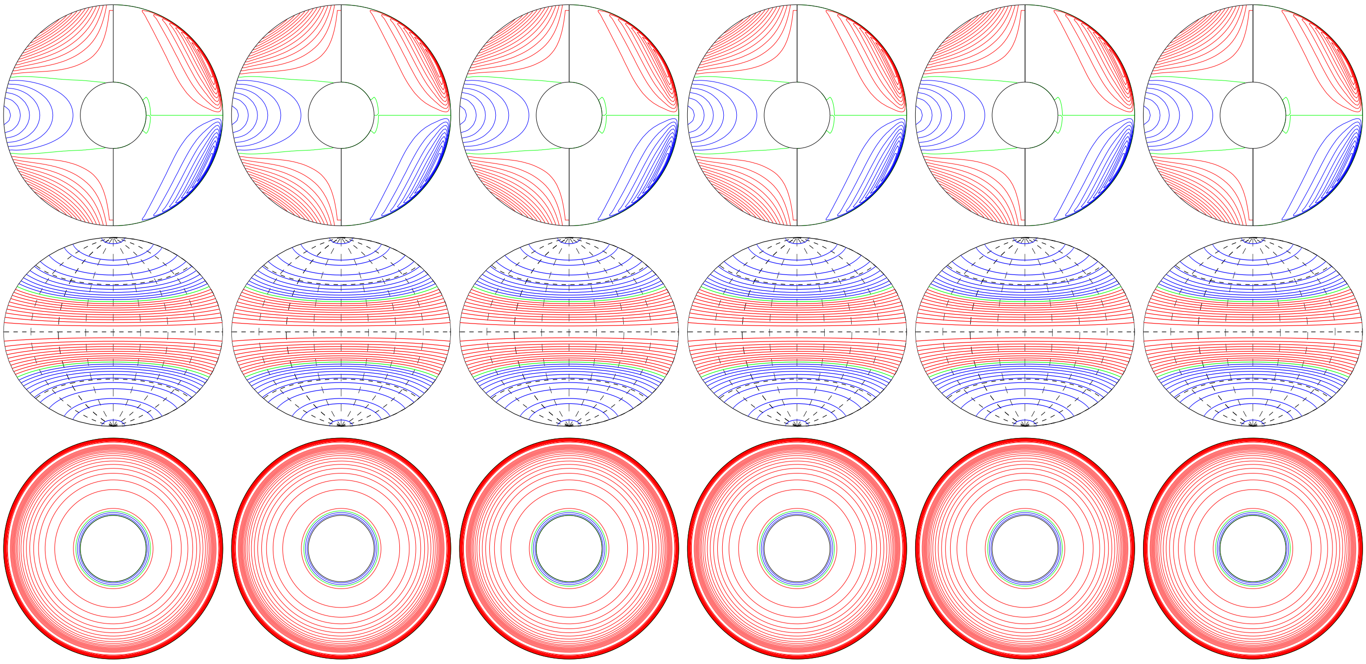

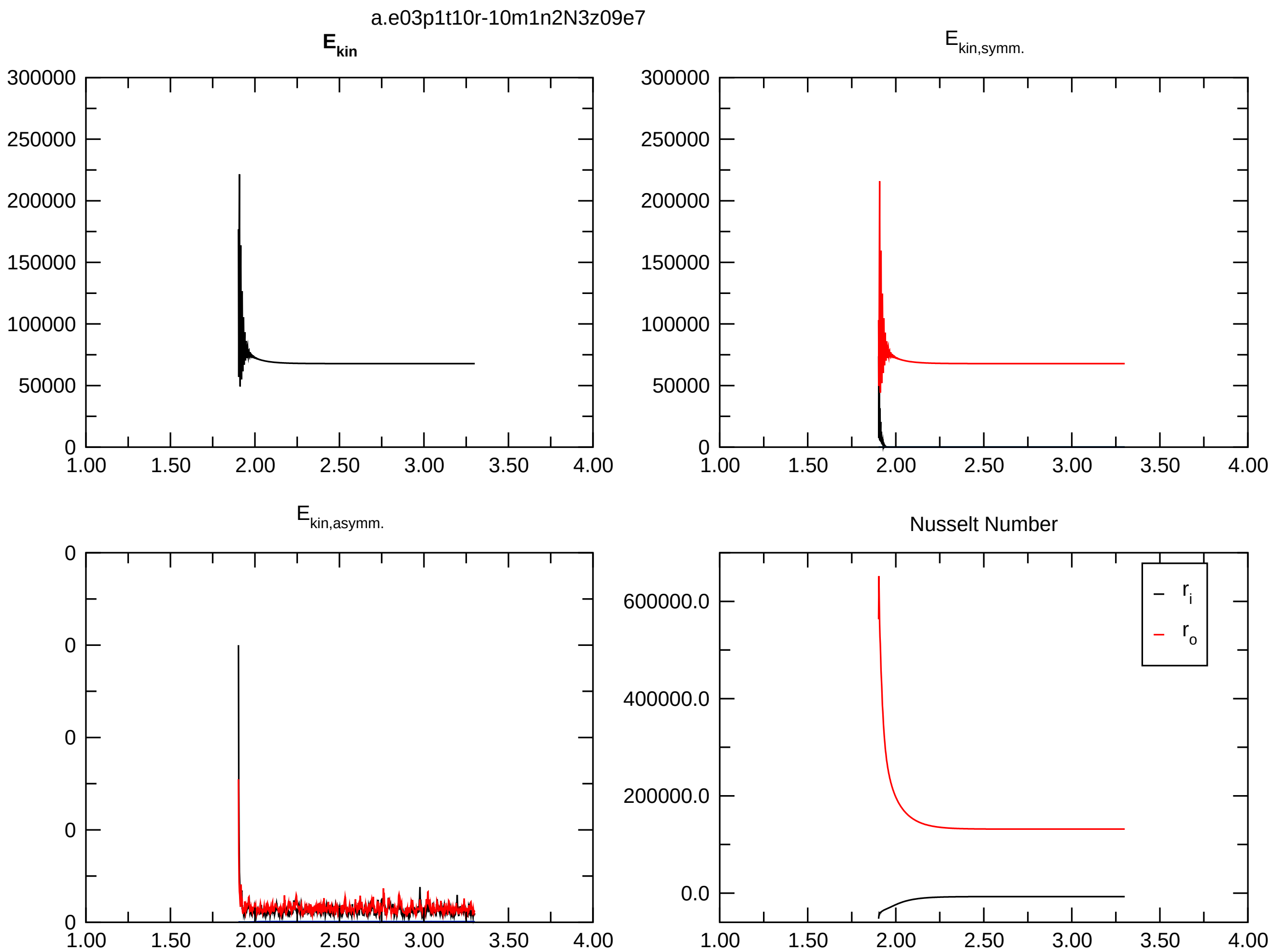

a.e03p1t10r-10m1n2N3z095e7
times: 3.650365 3.70037 3.750375 3.80038 3.850385 3.90039

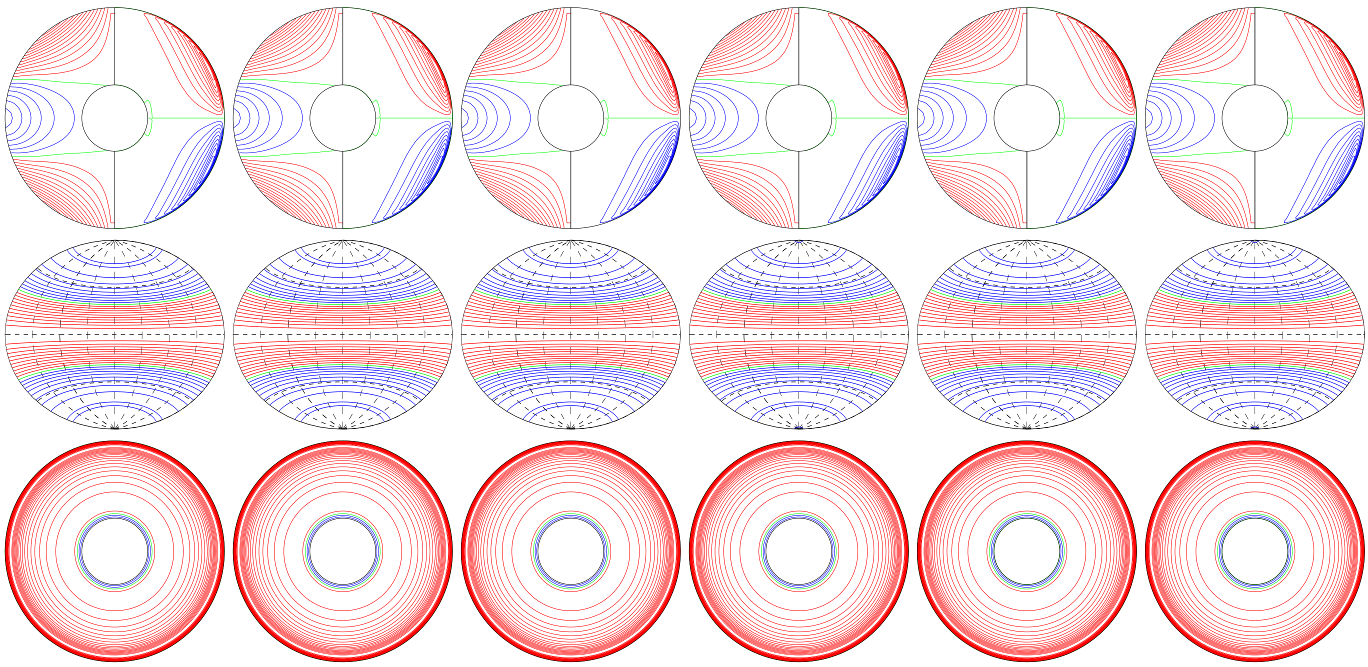

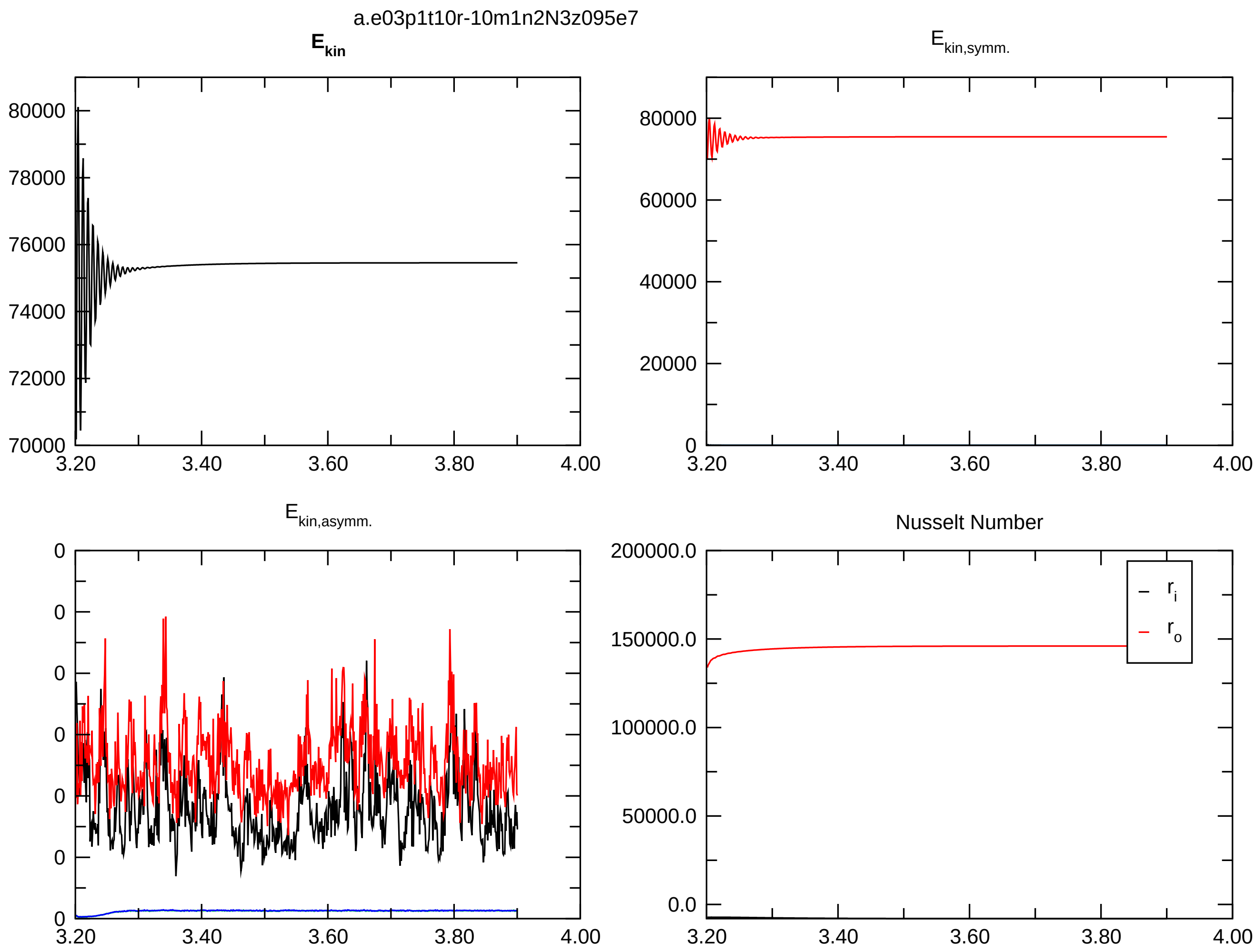

a.e03p1t10r-10m1n2N3z098e7
times: 3.560356 3.60036 3.640364 3.680368 3.720372 3.760376

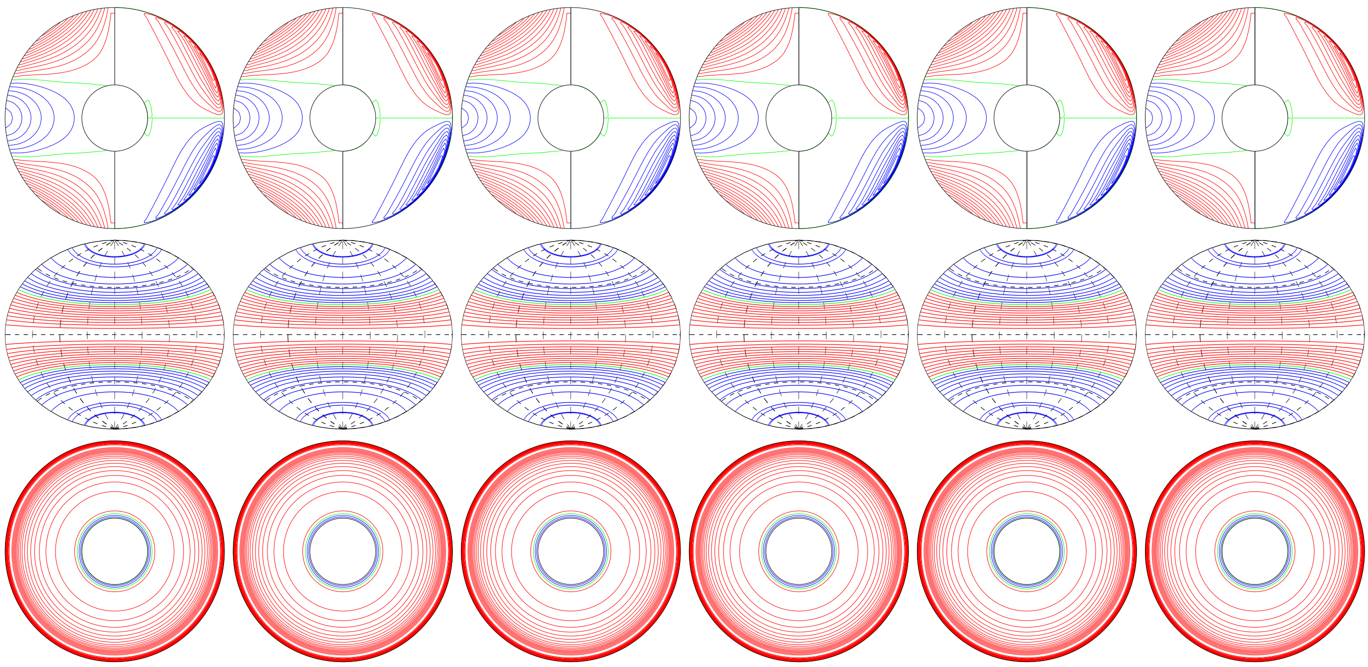

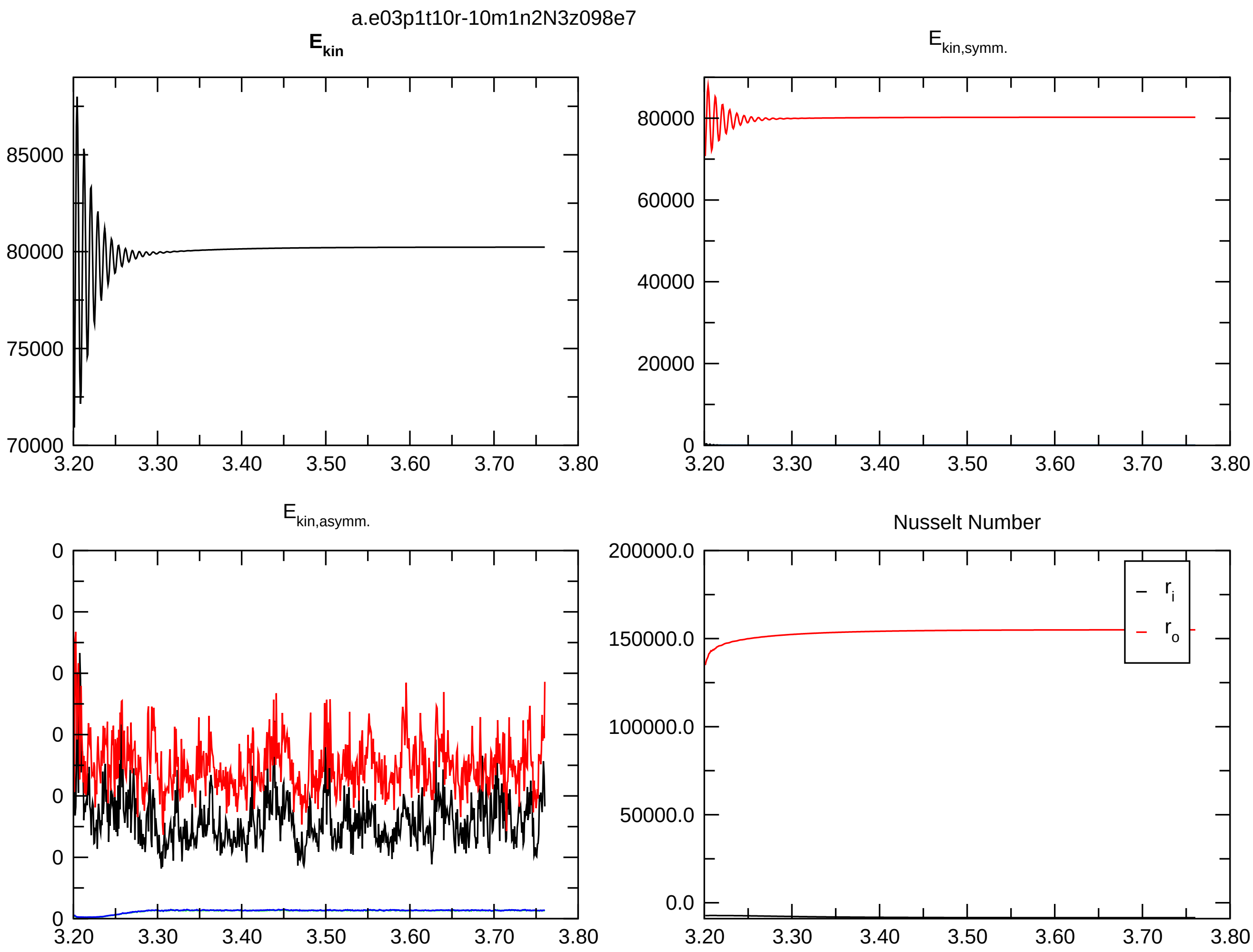

a.e03p1t10r-10m1n2N3z099e7
times: 3.940394 3.960396 3.980398 4.0004 4.020402 4.040404

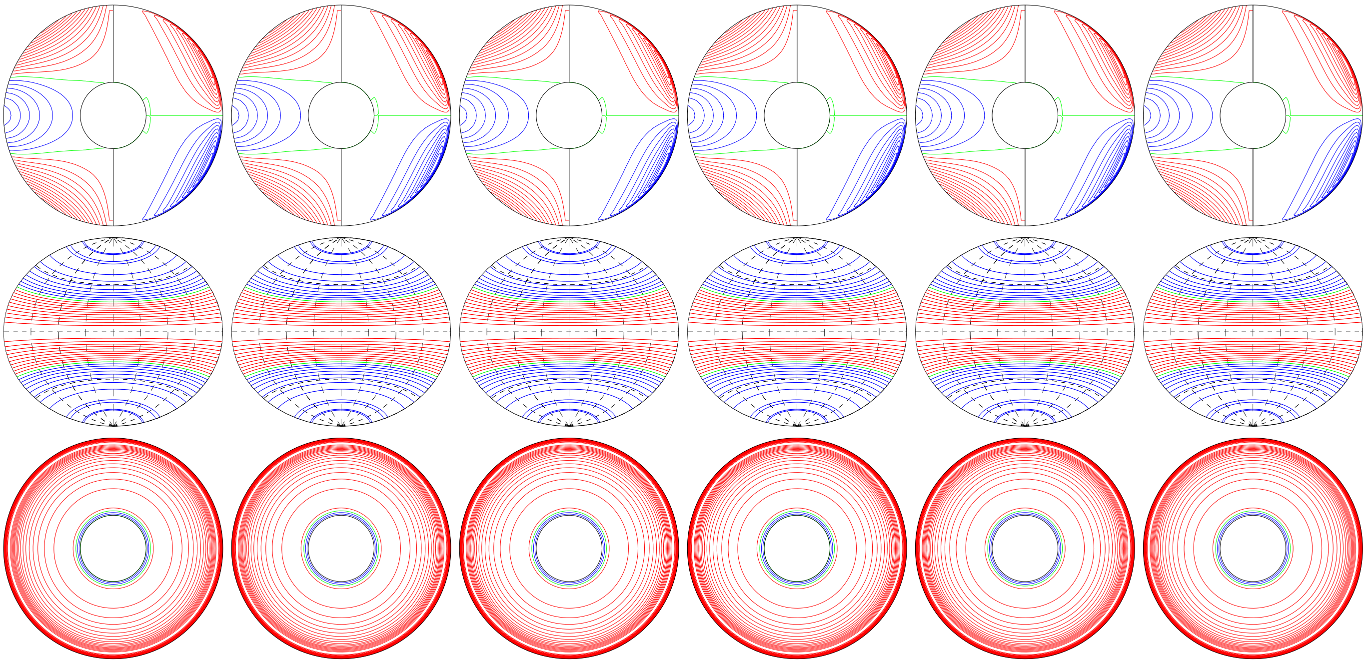

a.e03p1t10r-10m1n2N3z099e7

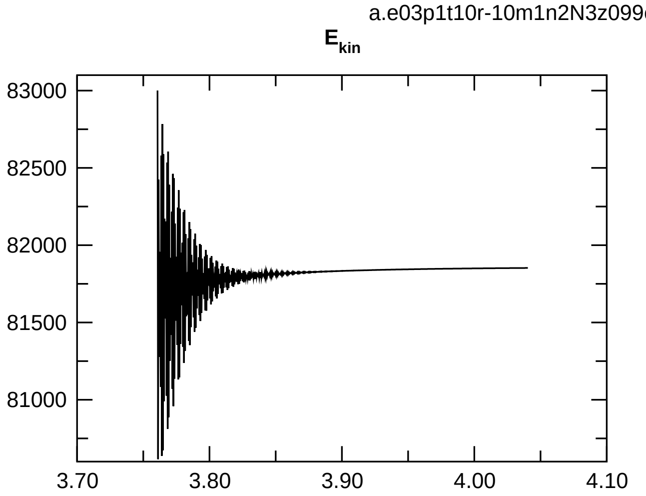

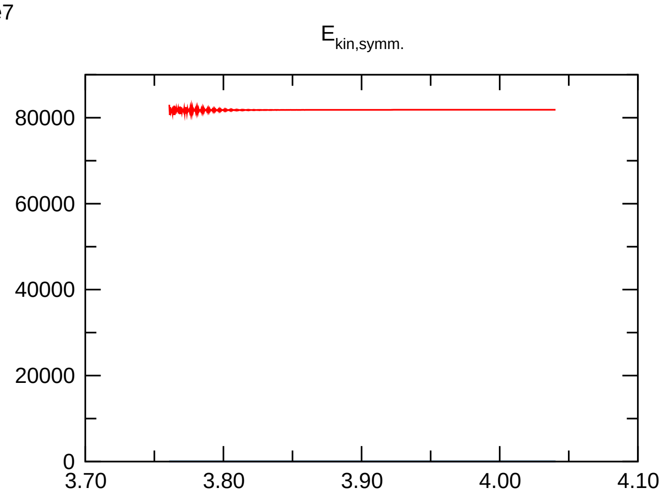

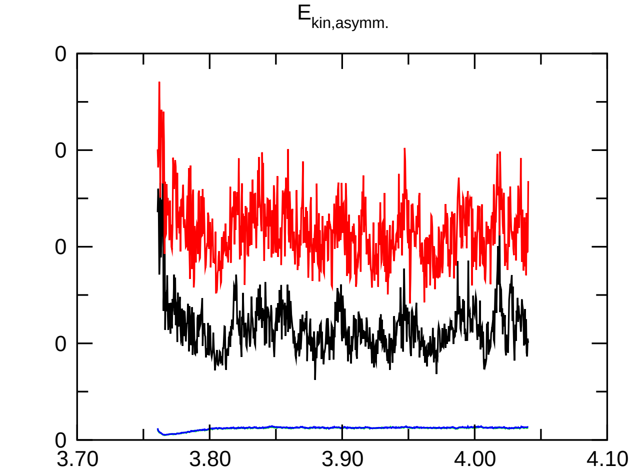

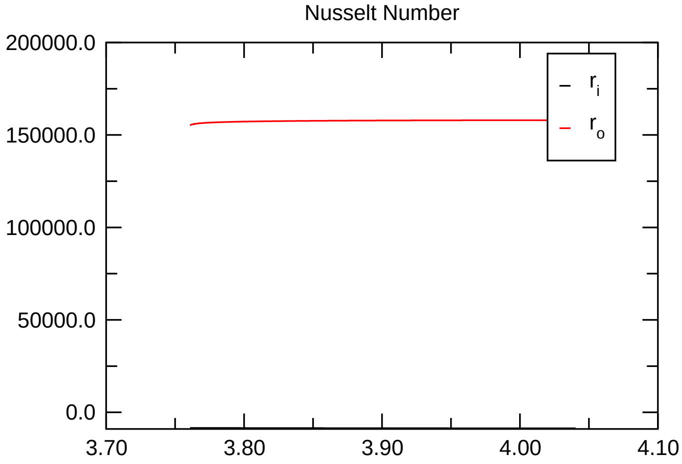

a.e03p1t10r-10m1n2N3z0995e7

times: 5.840464 5.900466 5.960468 6.02047 6.080472 6.140474

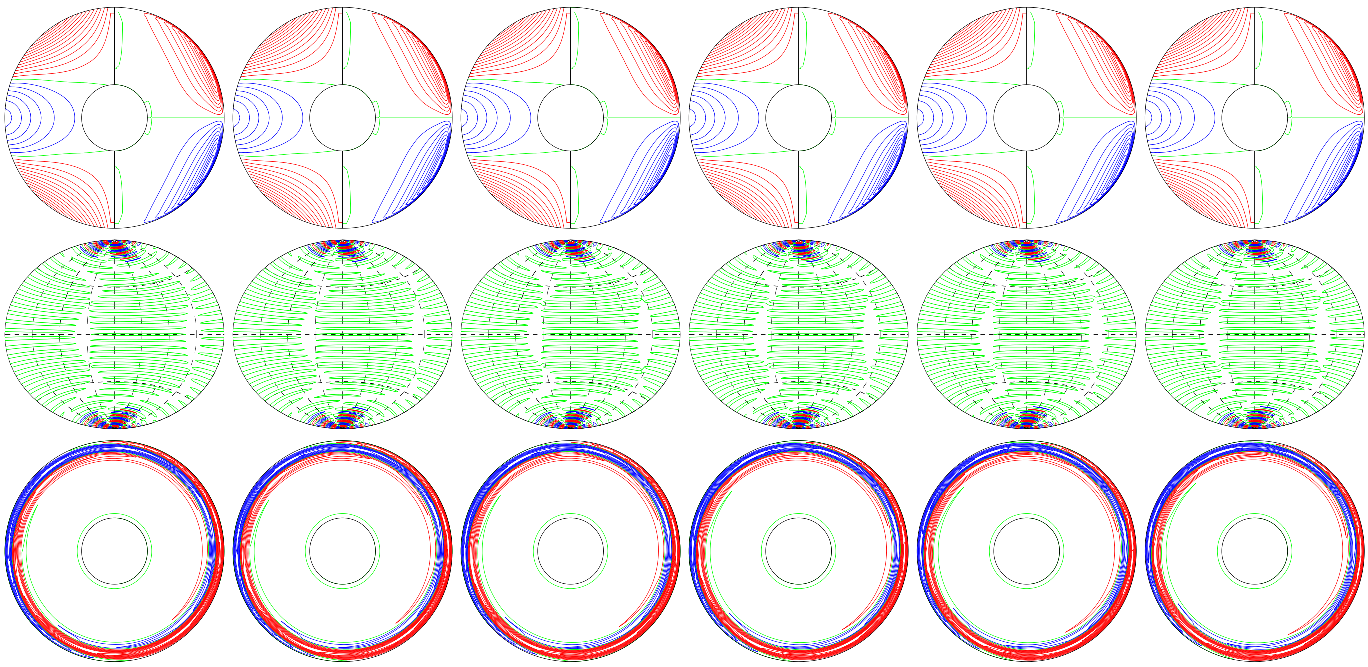

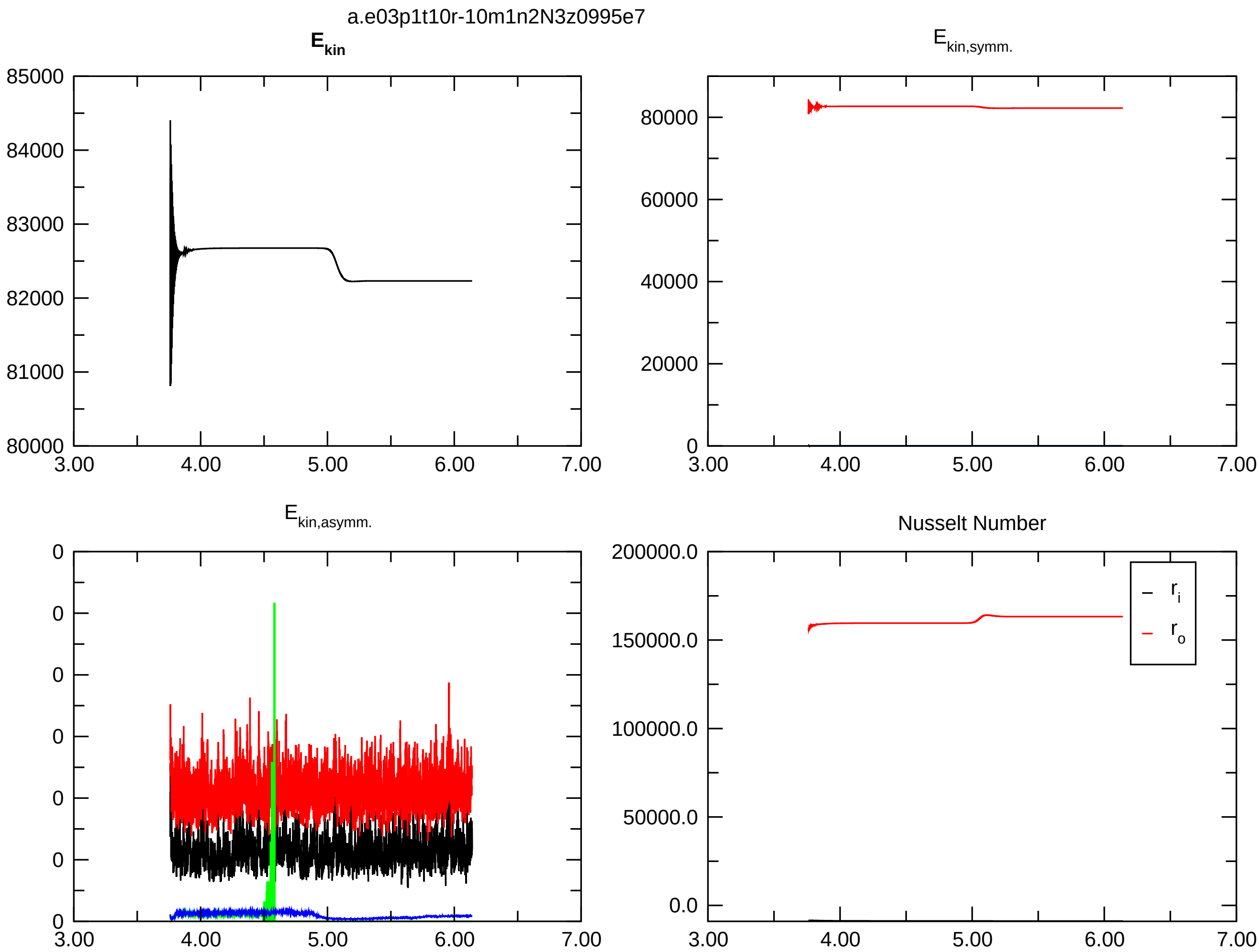

a.e03p1t10r-10m1n2N3z1e7
times: 2.910281 2.940282 2.970283 3.000284 3.030285 3.060286

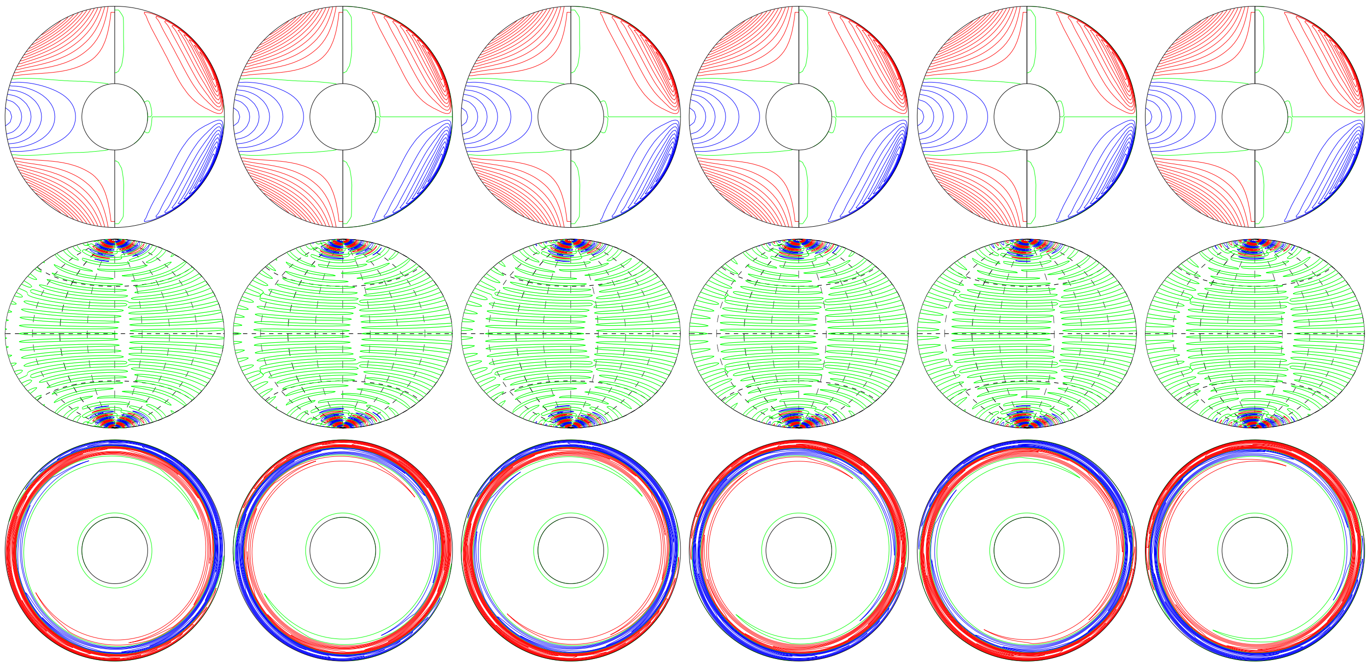

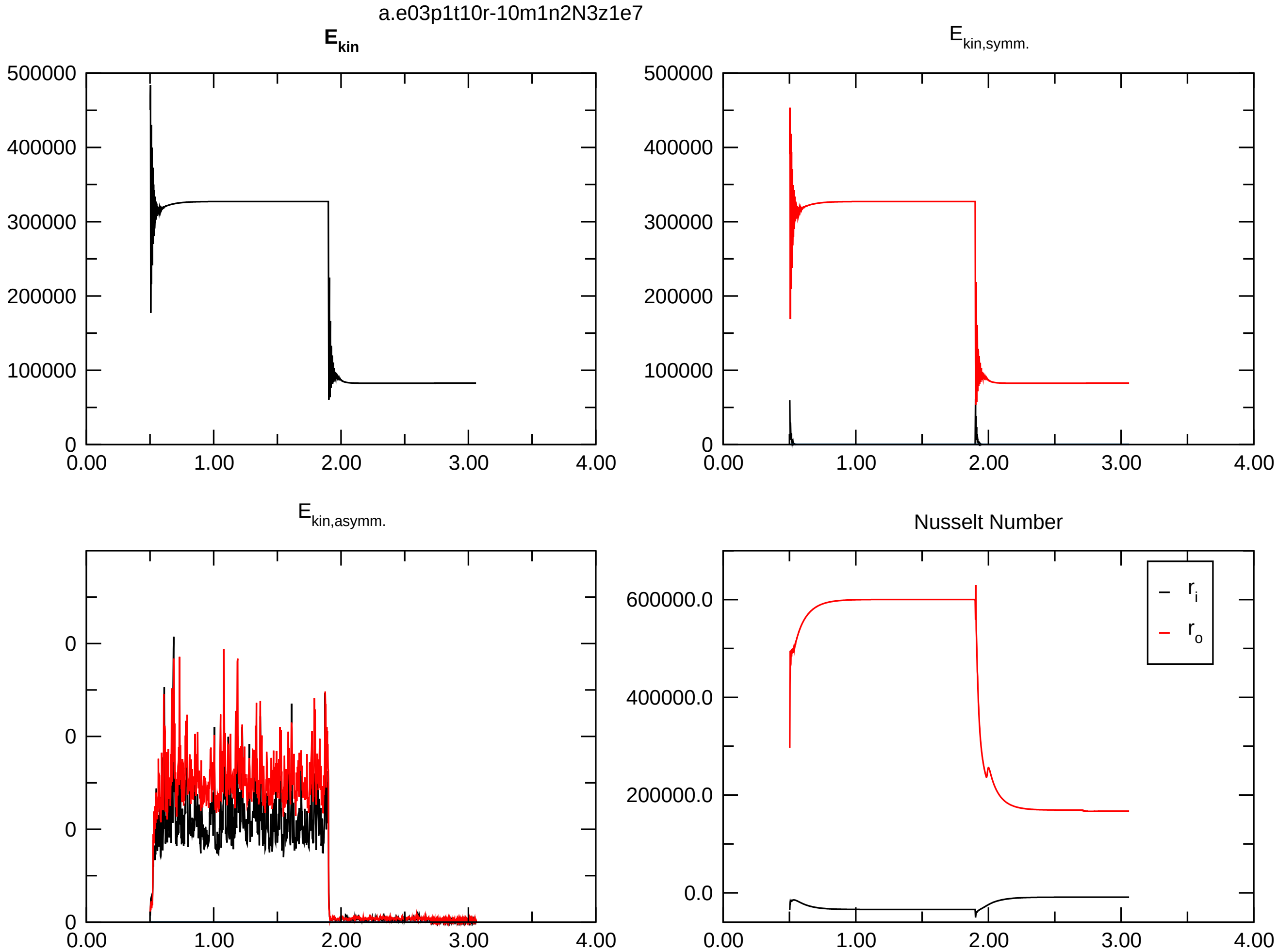

a.e03p1t10r-10m1n2N3z1e7a
times: 5.180488 5.22049 5.260492 5.300494 5.340496 5.380498

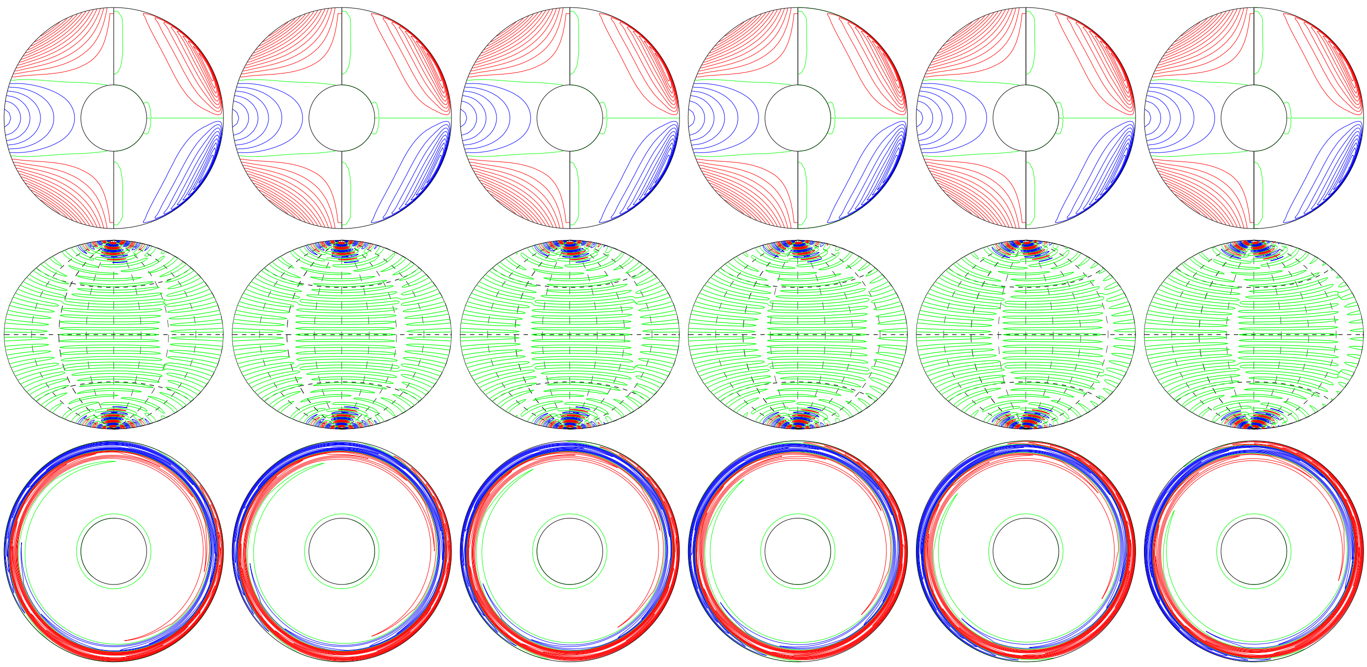

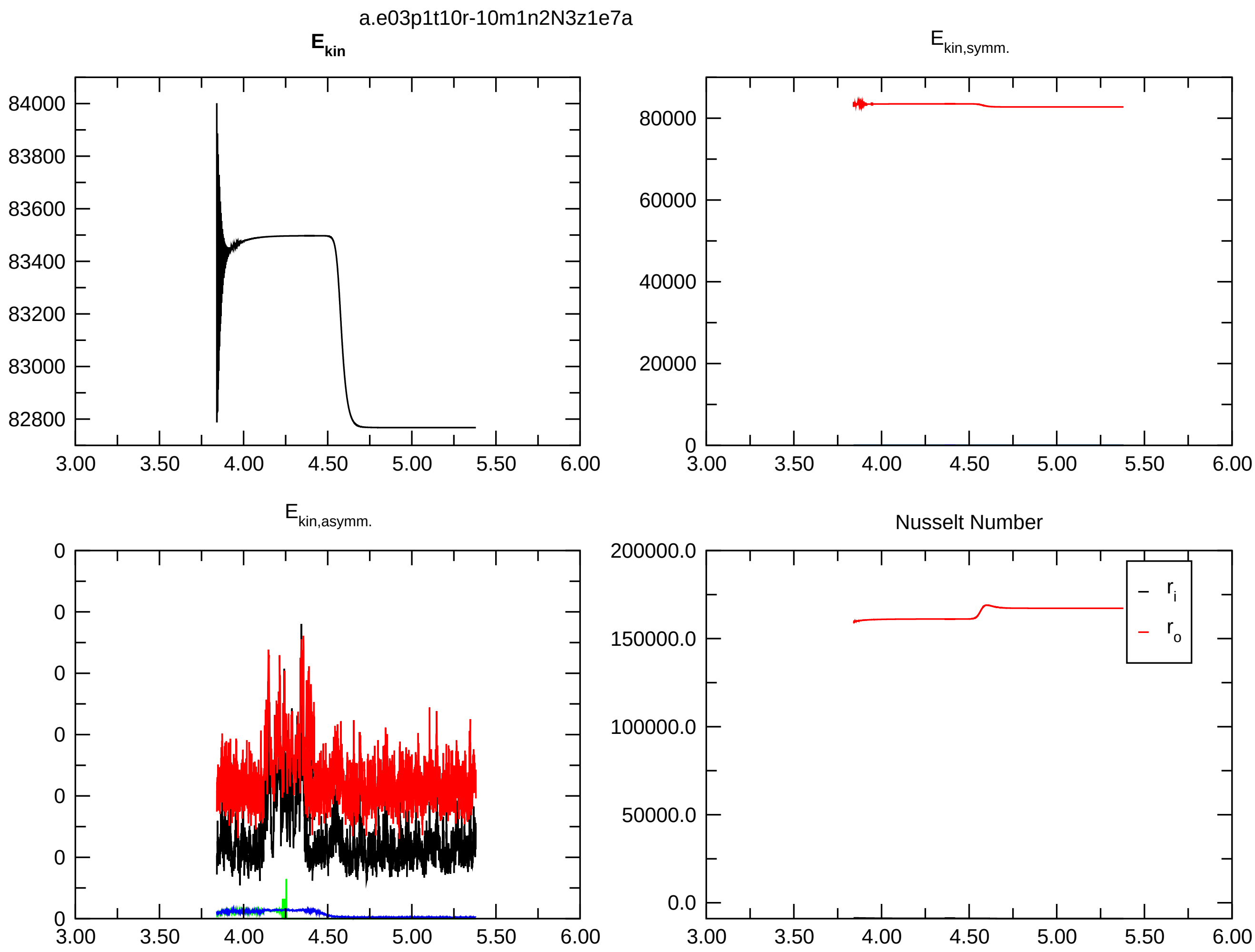

a.e03p1t10r-10m1n2N3z1.1e7

times: 5.820564 5.840566 5.860568 5.88057 5.900572 5.920574

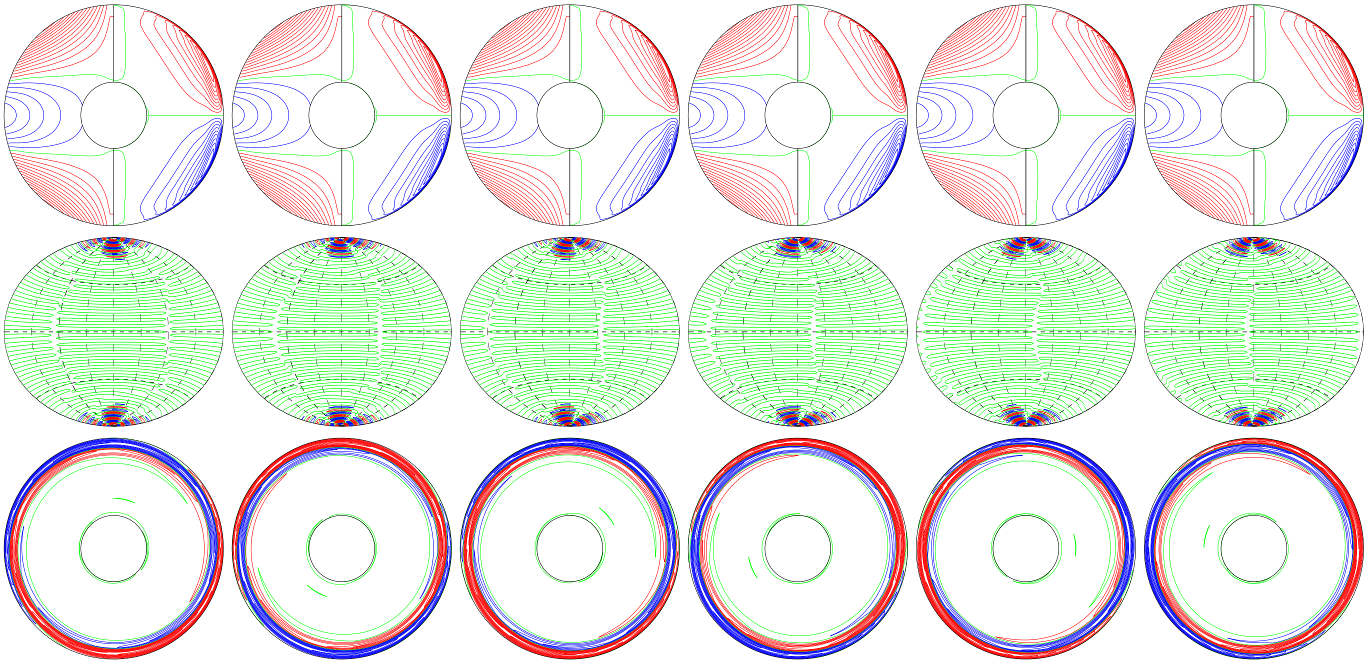

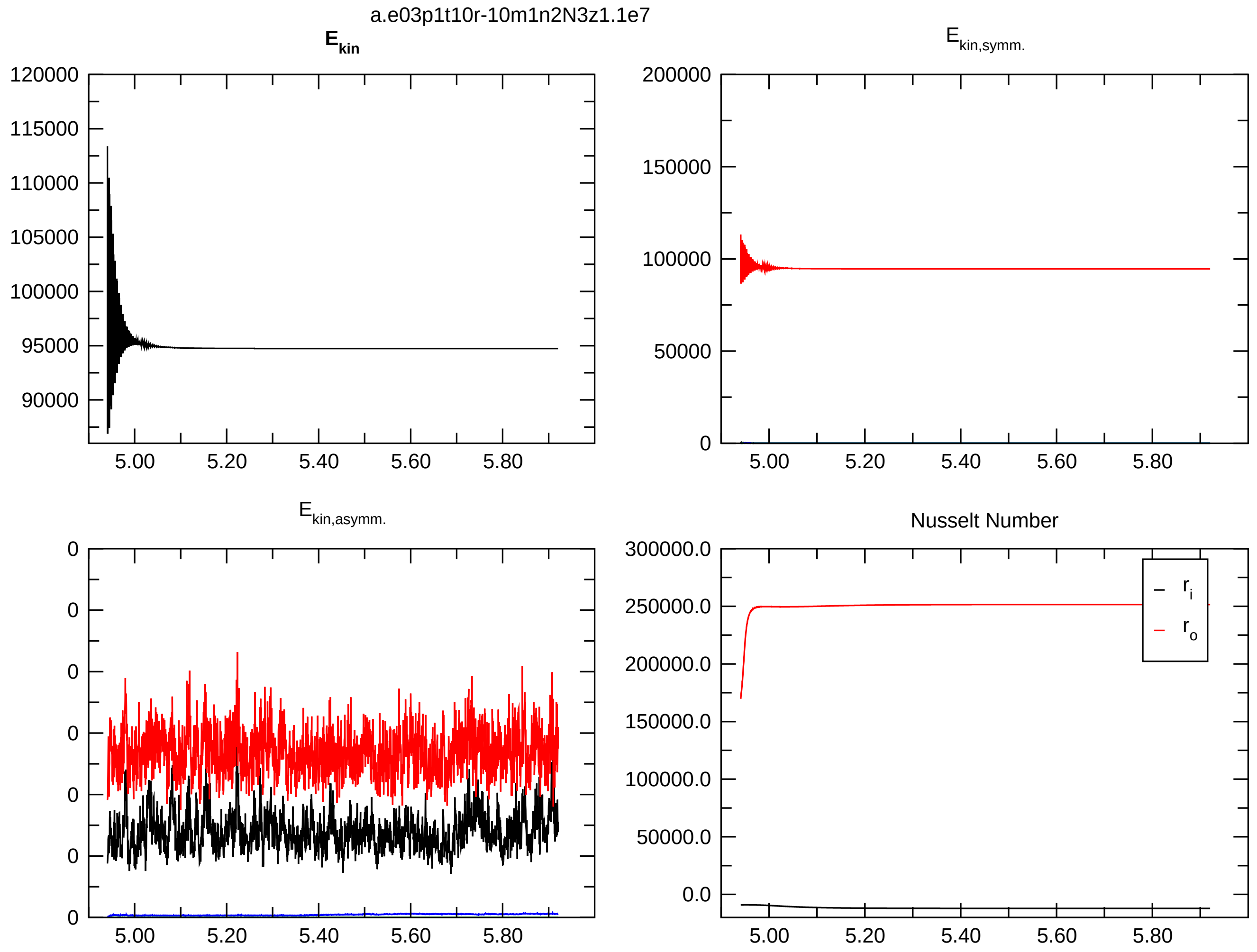

a.e03p1t10r-10m1n2N3z1.5e7
times: 7.67056 7.710561 7.750562 7.790563 7.830564 7.870565

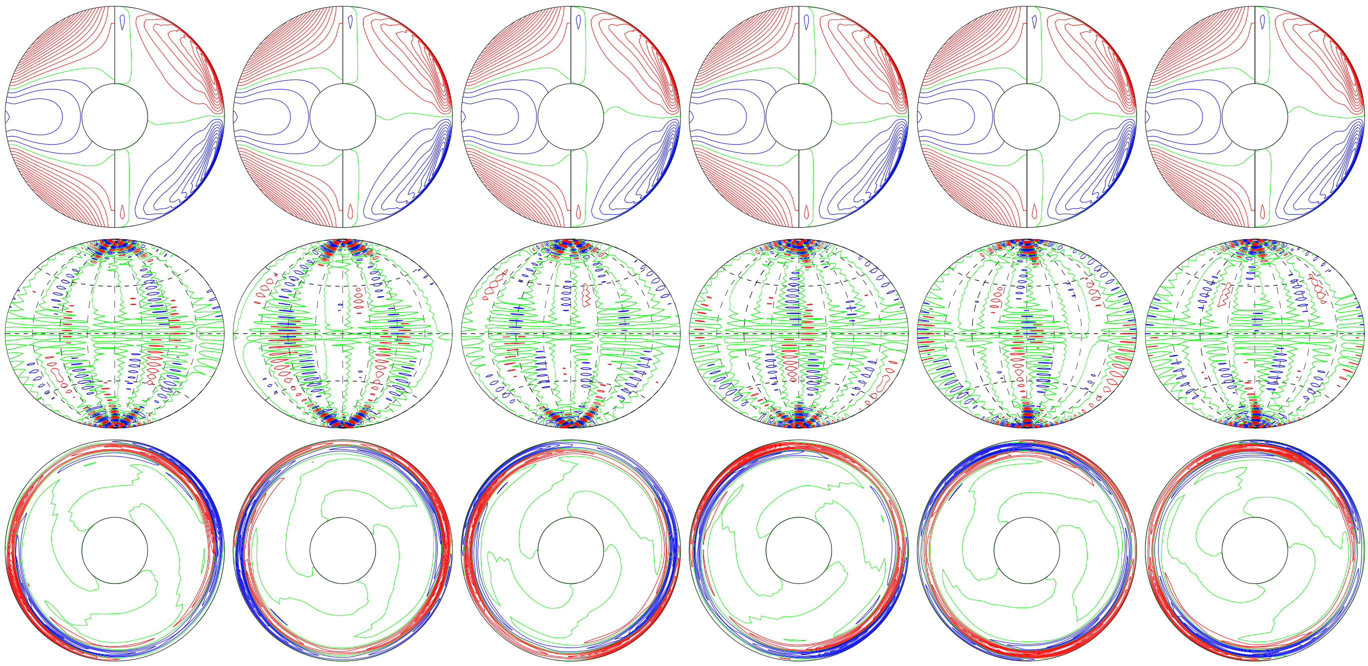

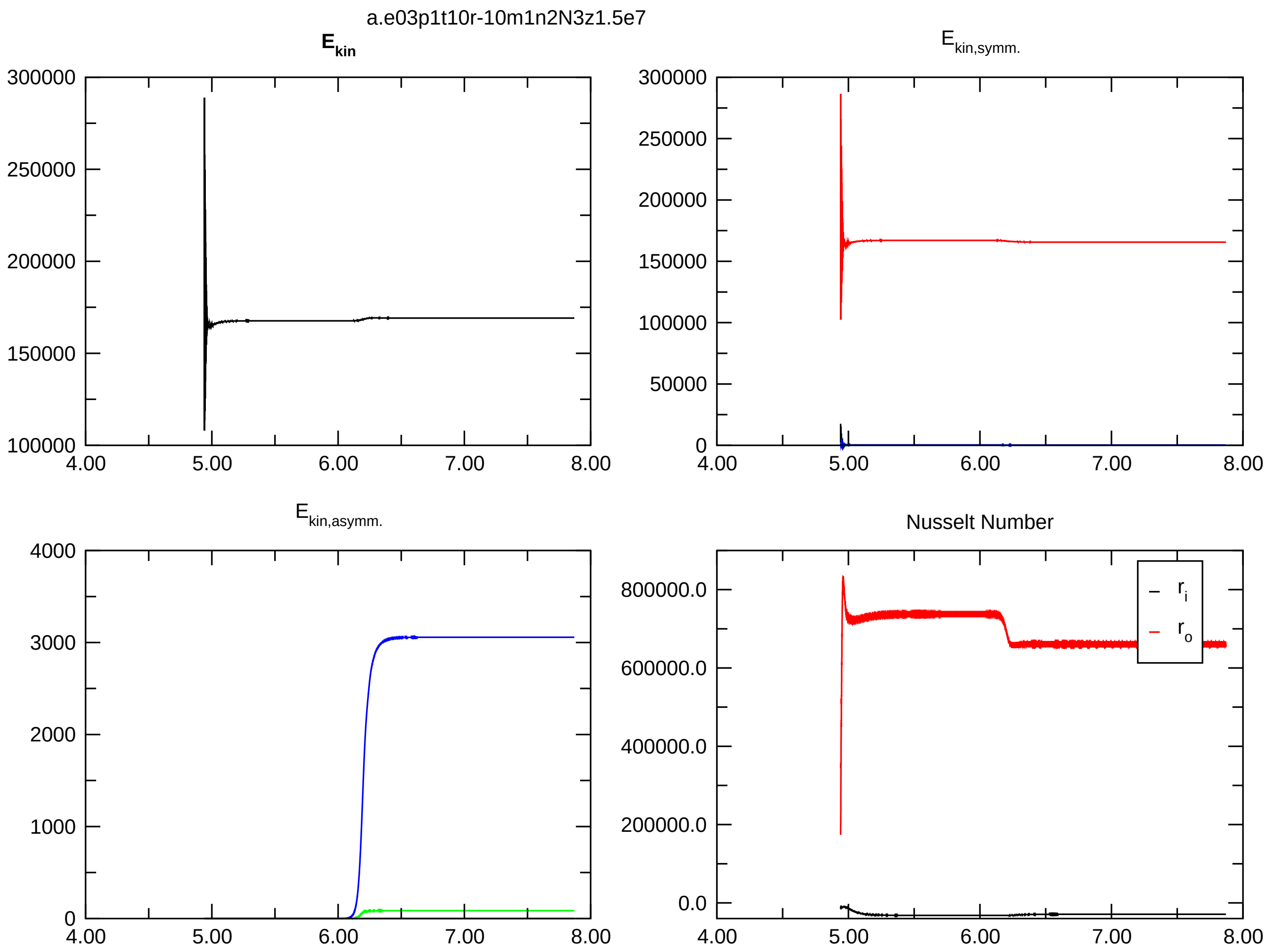

a.e03p1t10r-10m1n2N3z1.6e7
times: 8.030568 8.040569 8.05057 8.060571 8.070572 8.080573

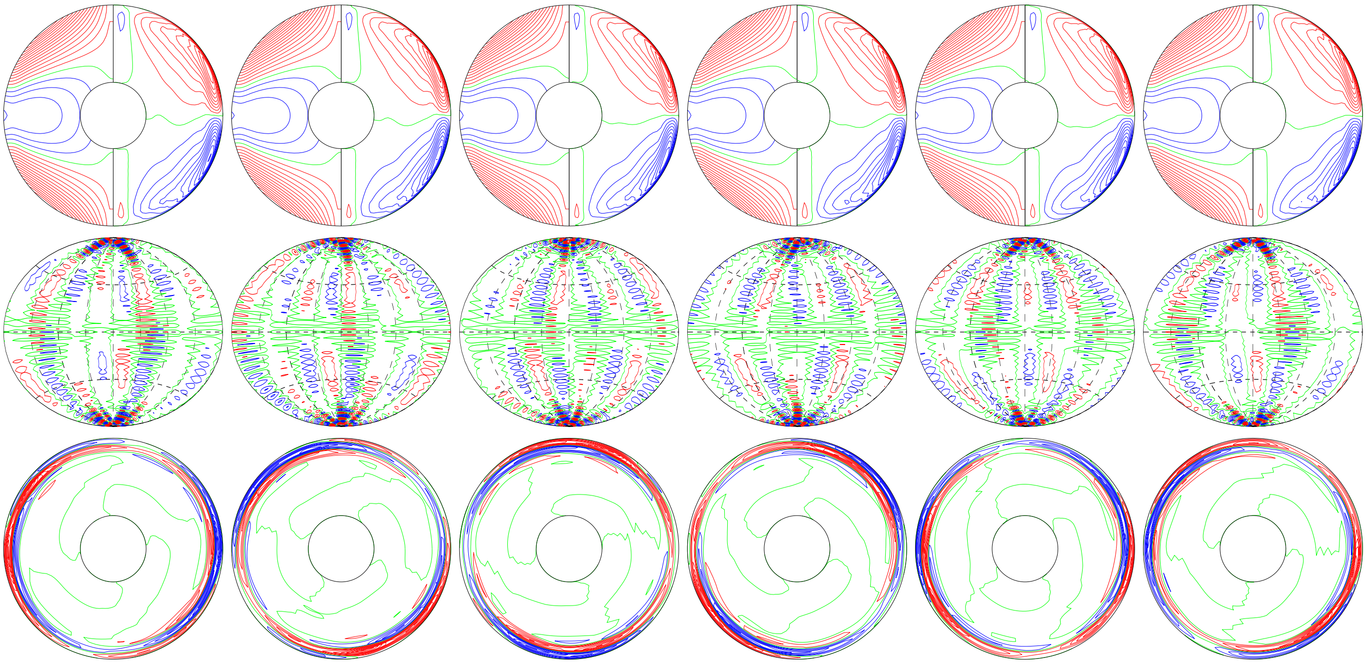

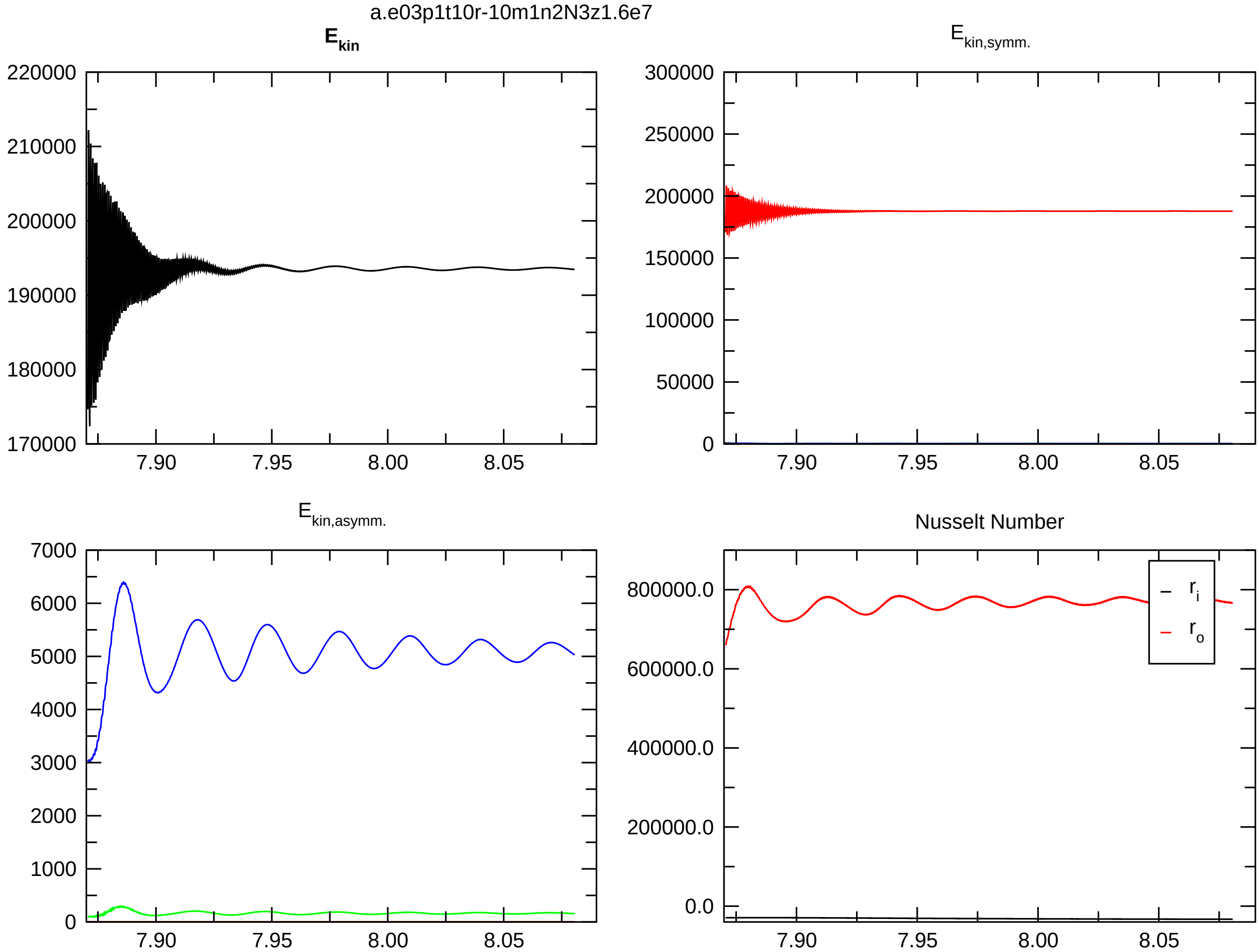

a.e03p1t10r-10m1n2N3z1.7e7
times: 8.030568 8.040569 8.05057 8.060571 8.070572 8.080573

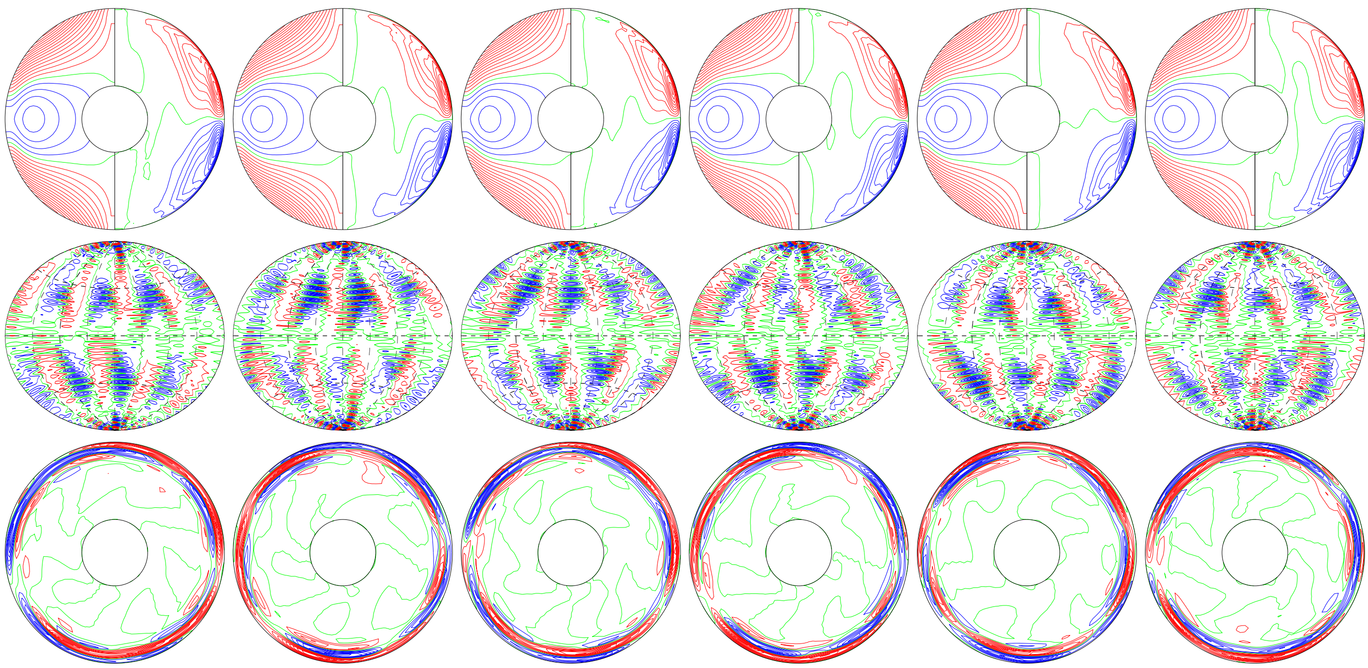

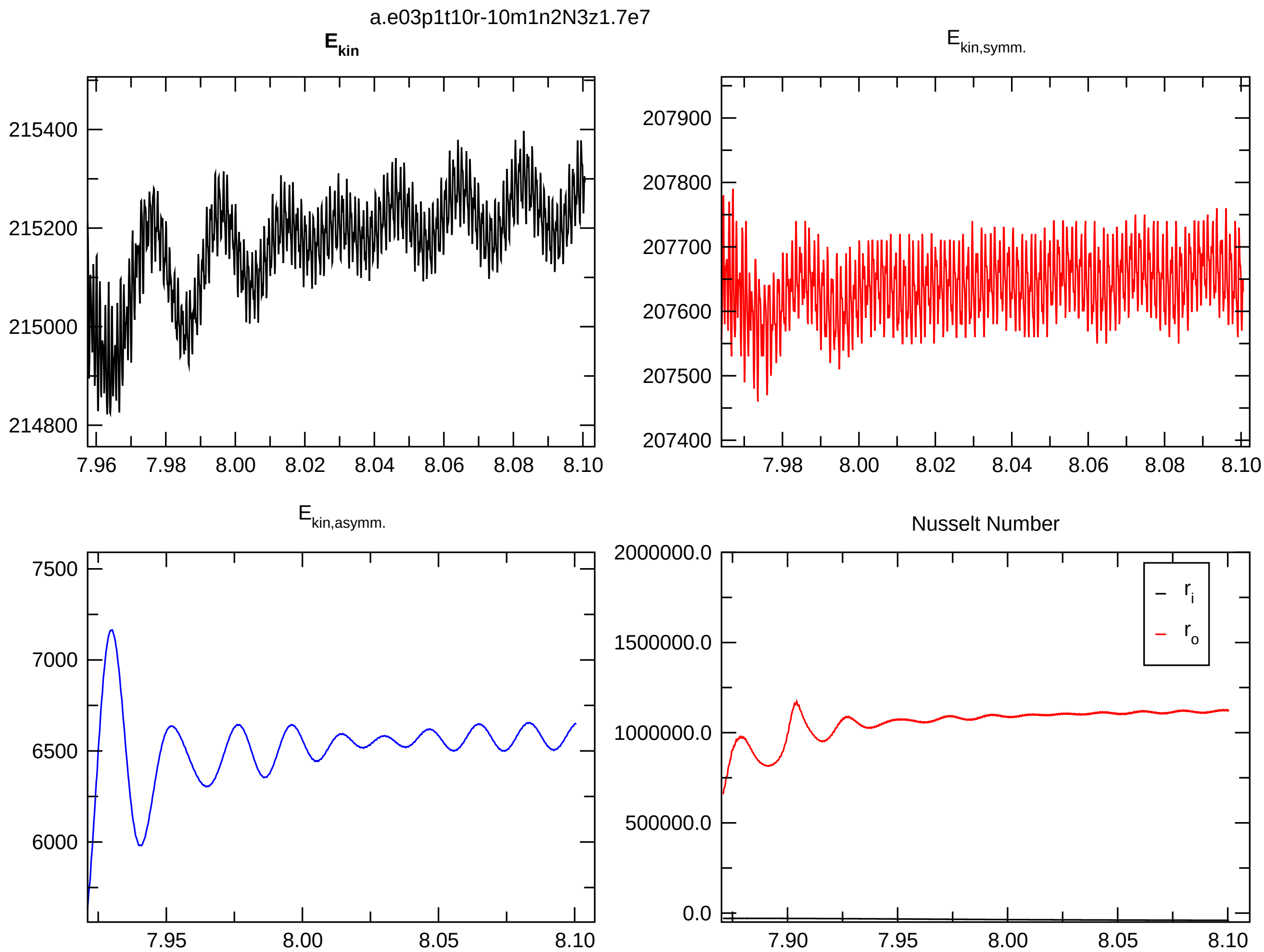

a.e03p1t10r-10m1n2N3z1.8e7

times: 7.998565 8.004565 8.010565 8.016565 8.022565 8.028565

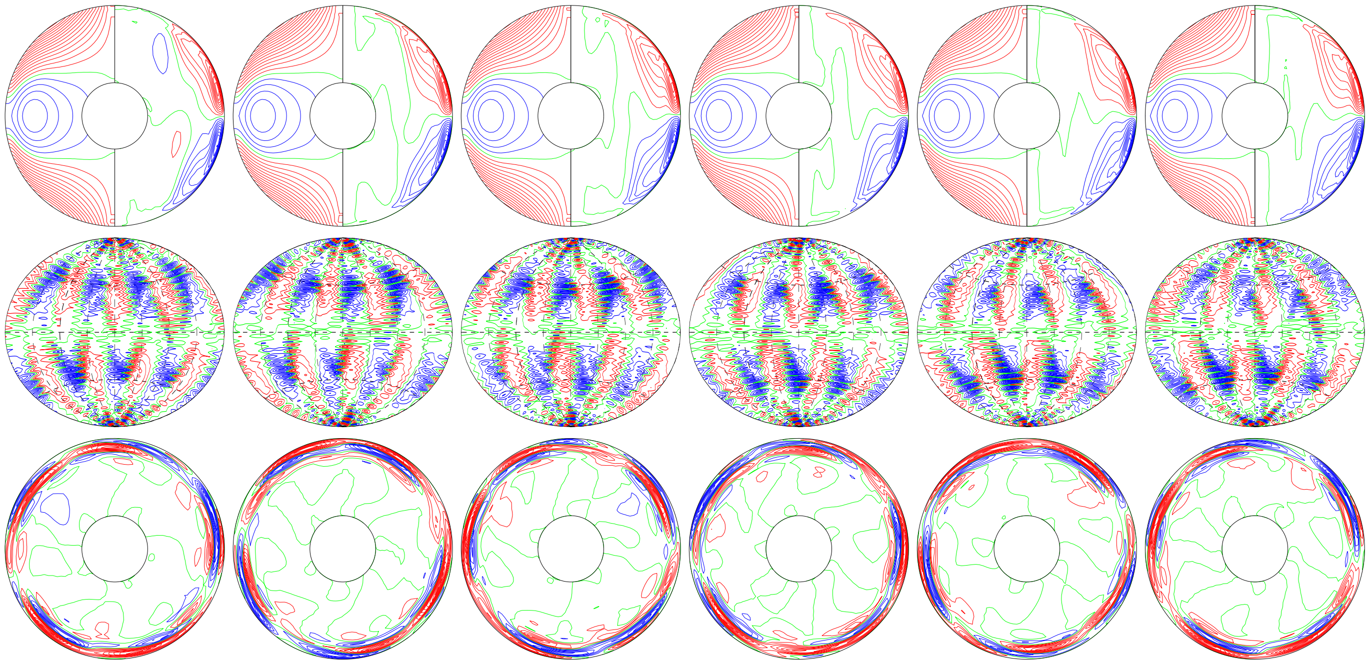

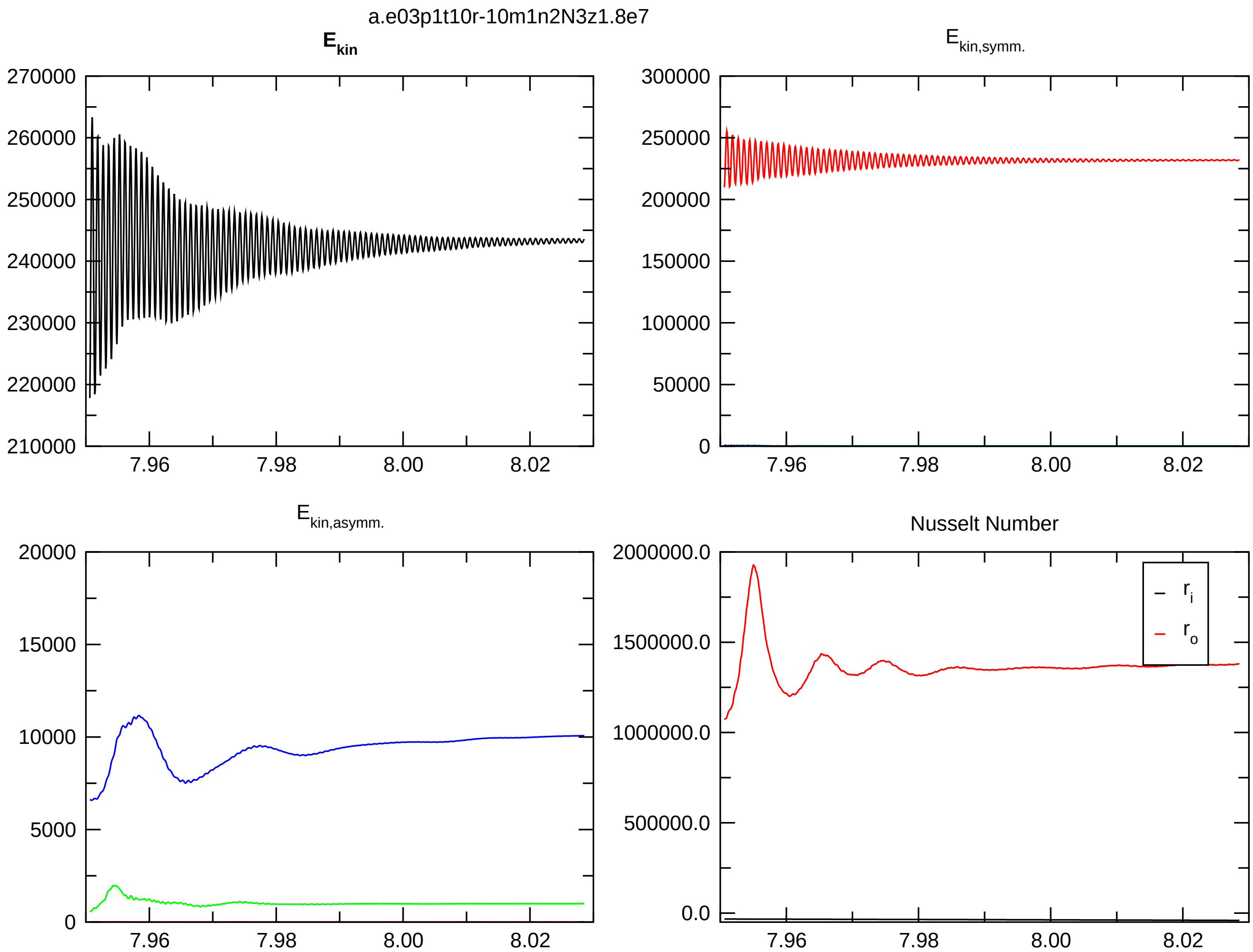

a.e03p1t10r-10m1n2N3z2e7
times: 4.330217 4.430218 4.530219 4.63022 4.730221 4.830222

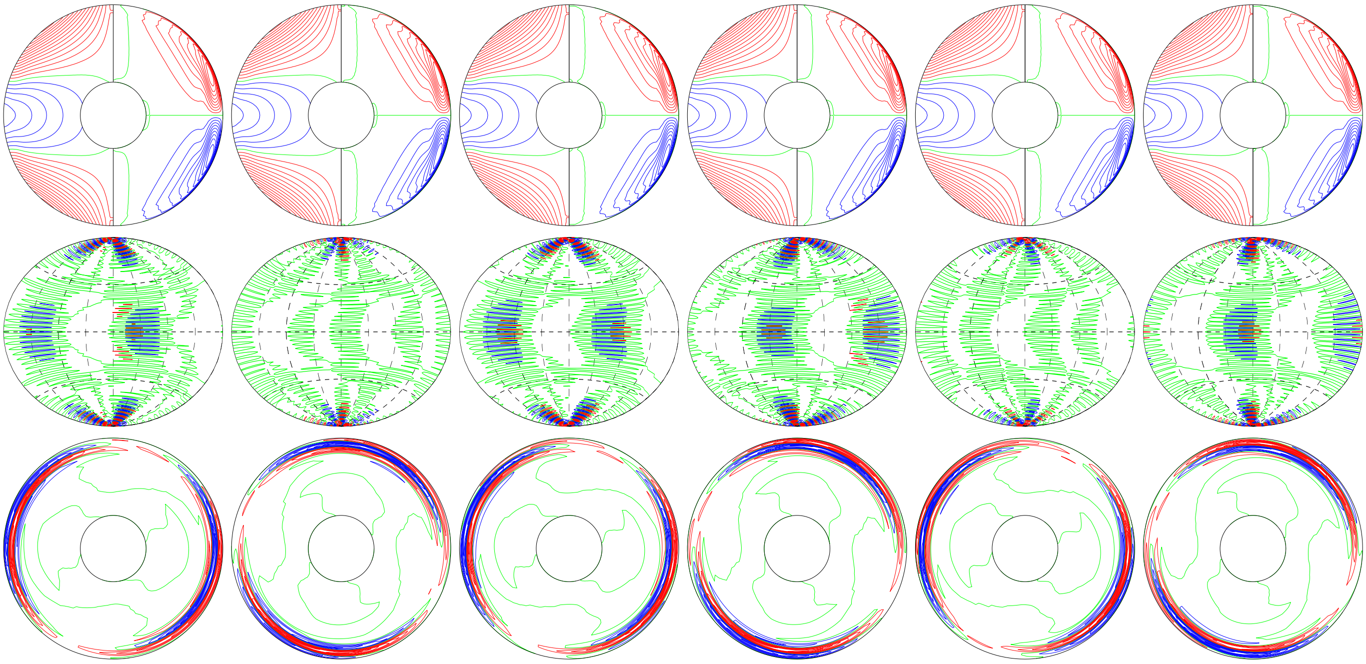

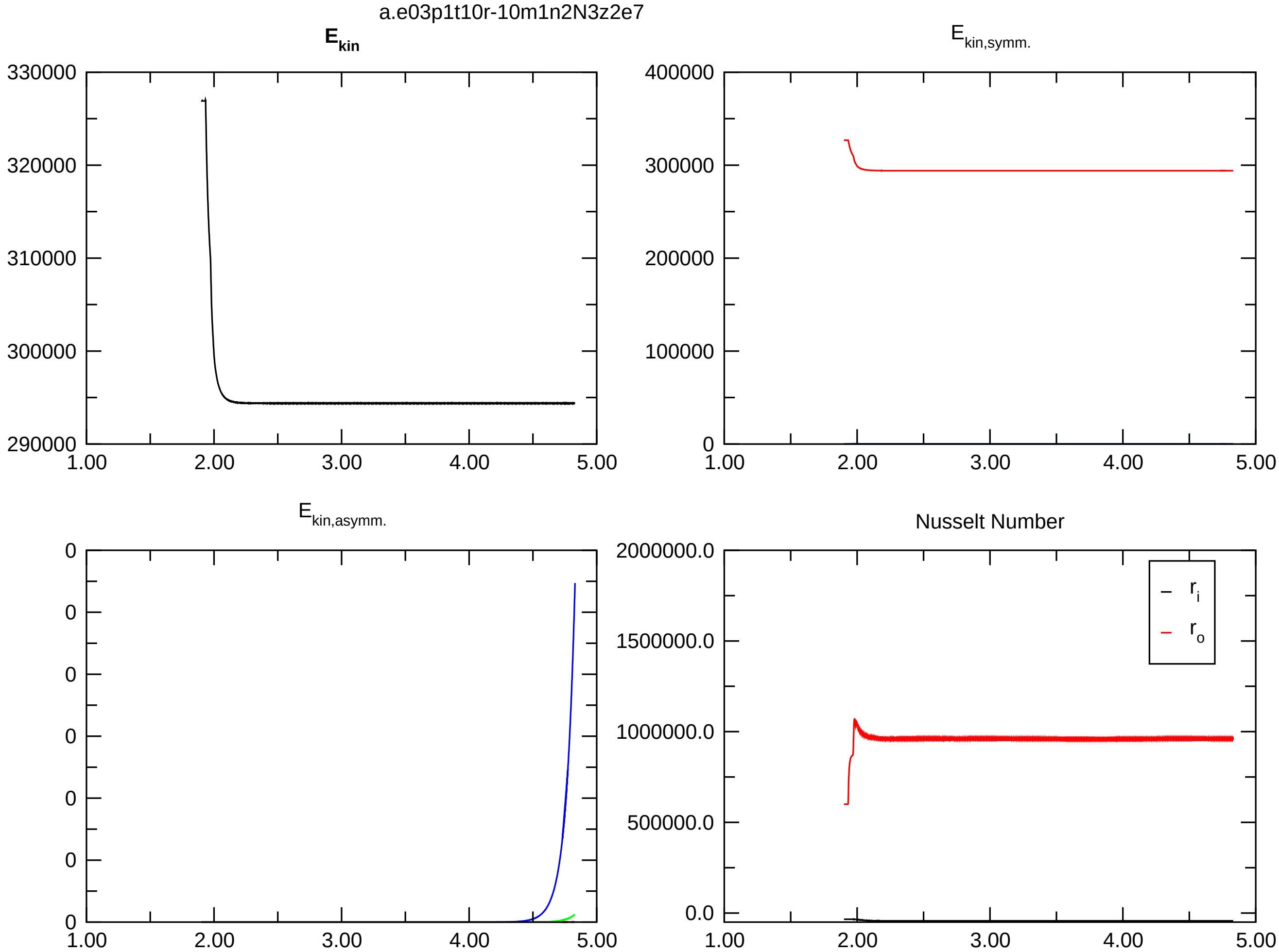

a.e03p1t10r-10m1n2N3z2.05e7

times: 2.250197 2.300198 2.350199 2.4002 2.450201 2.500202

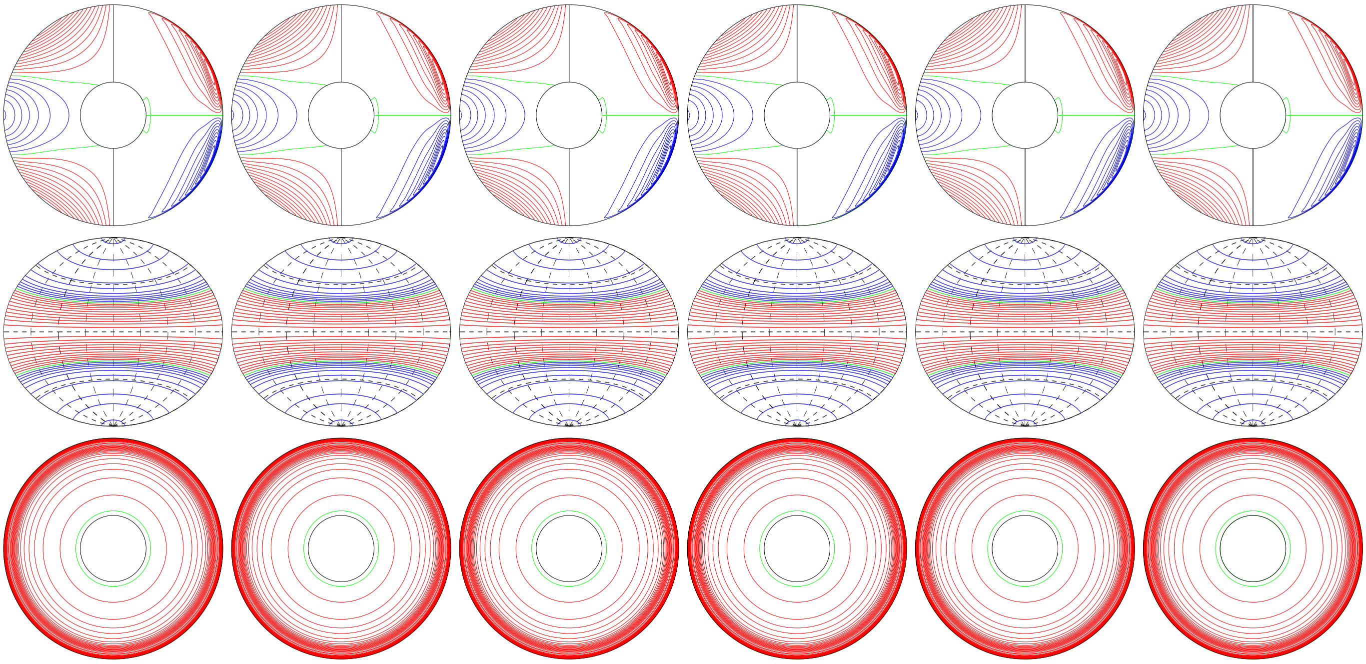

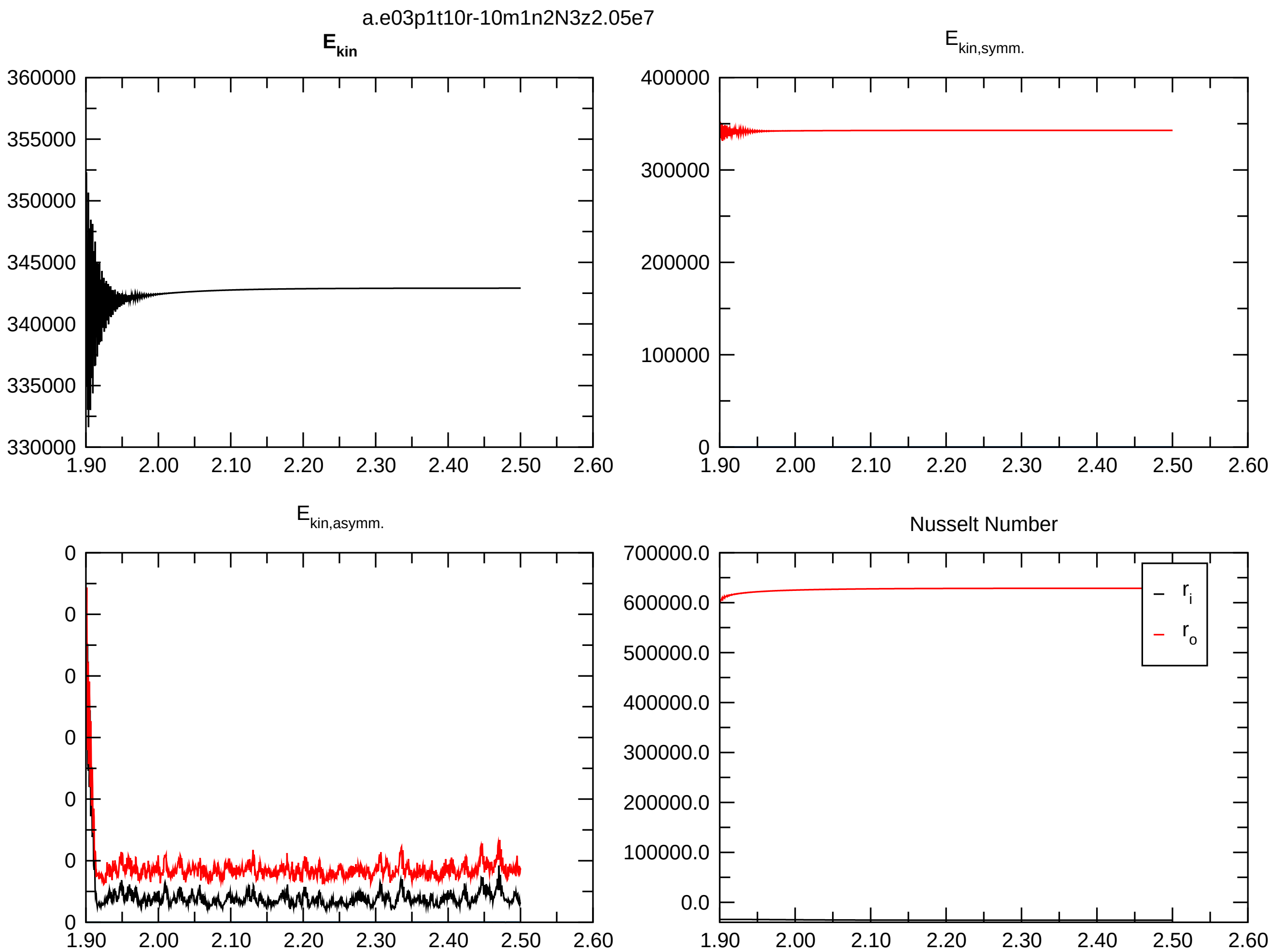

a.e03p1t10r-10m1n2N3z2.5e07

times: 2.250197 2.300198 2.350199 2.4002 2.450201 2.500202

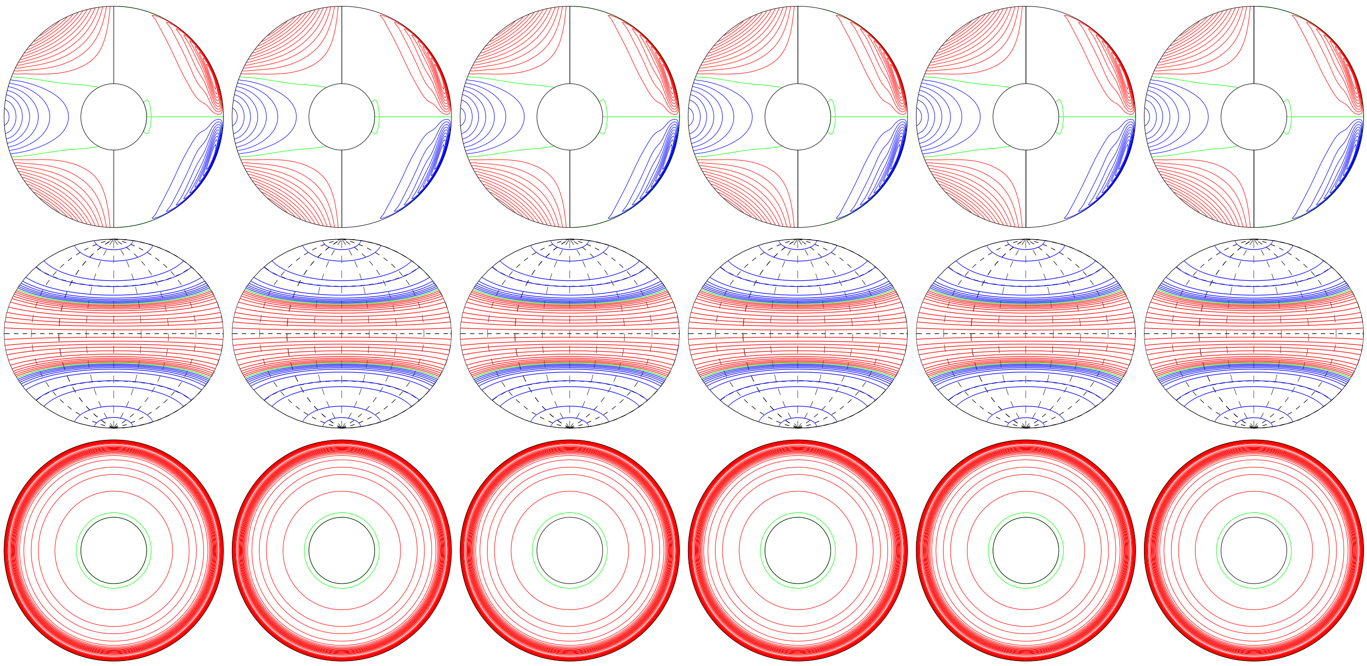

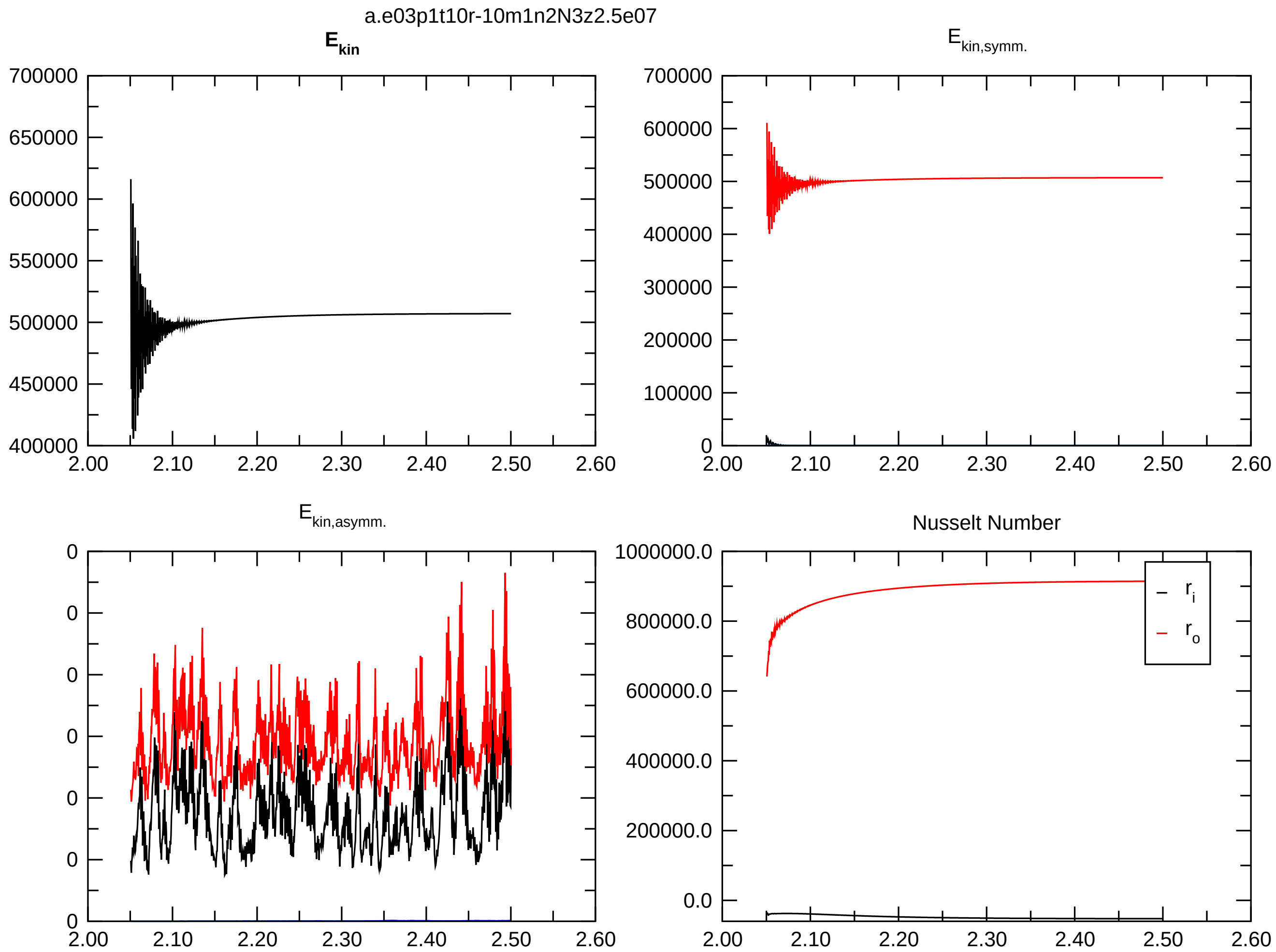

a.e03p1t10r-10m1n2N2z1.8e7

times: 0.1320066 0.1380069 0.1440072 0.1500075 0.1560078 0.1620081

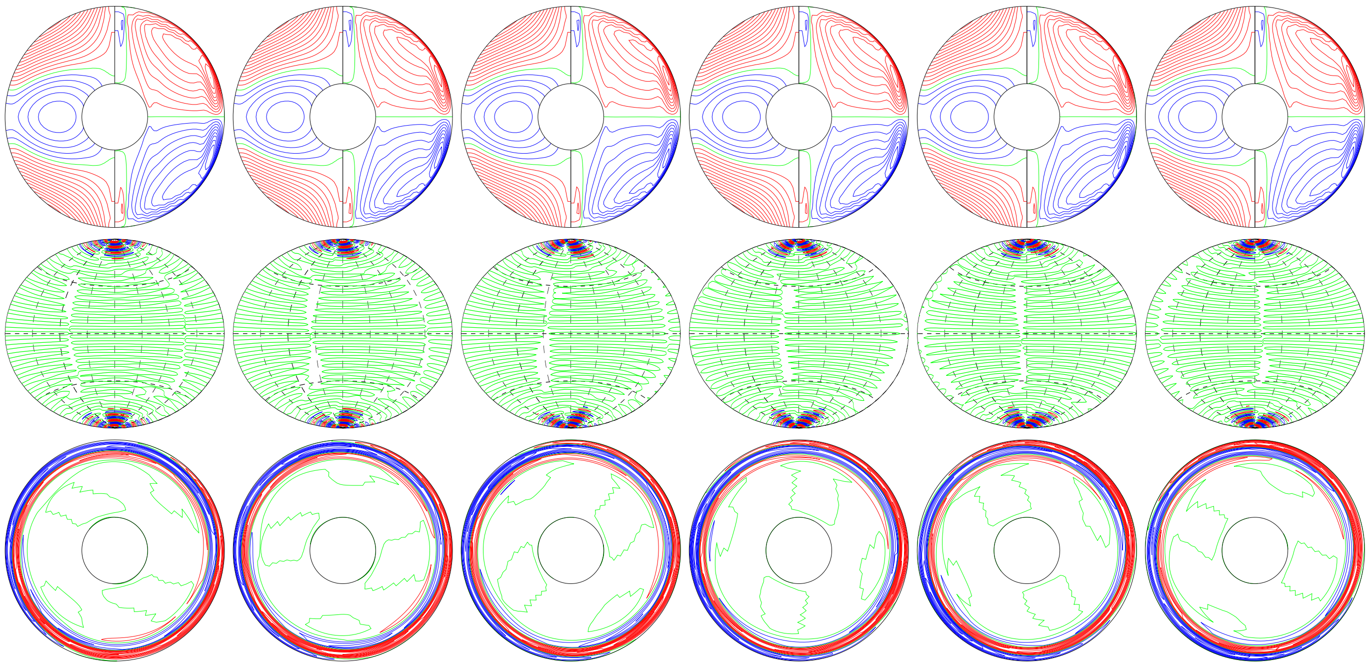

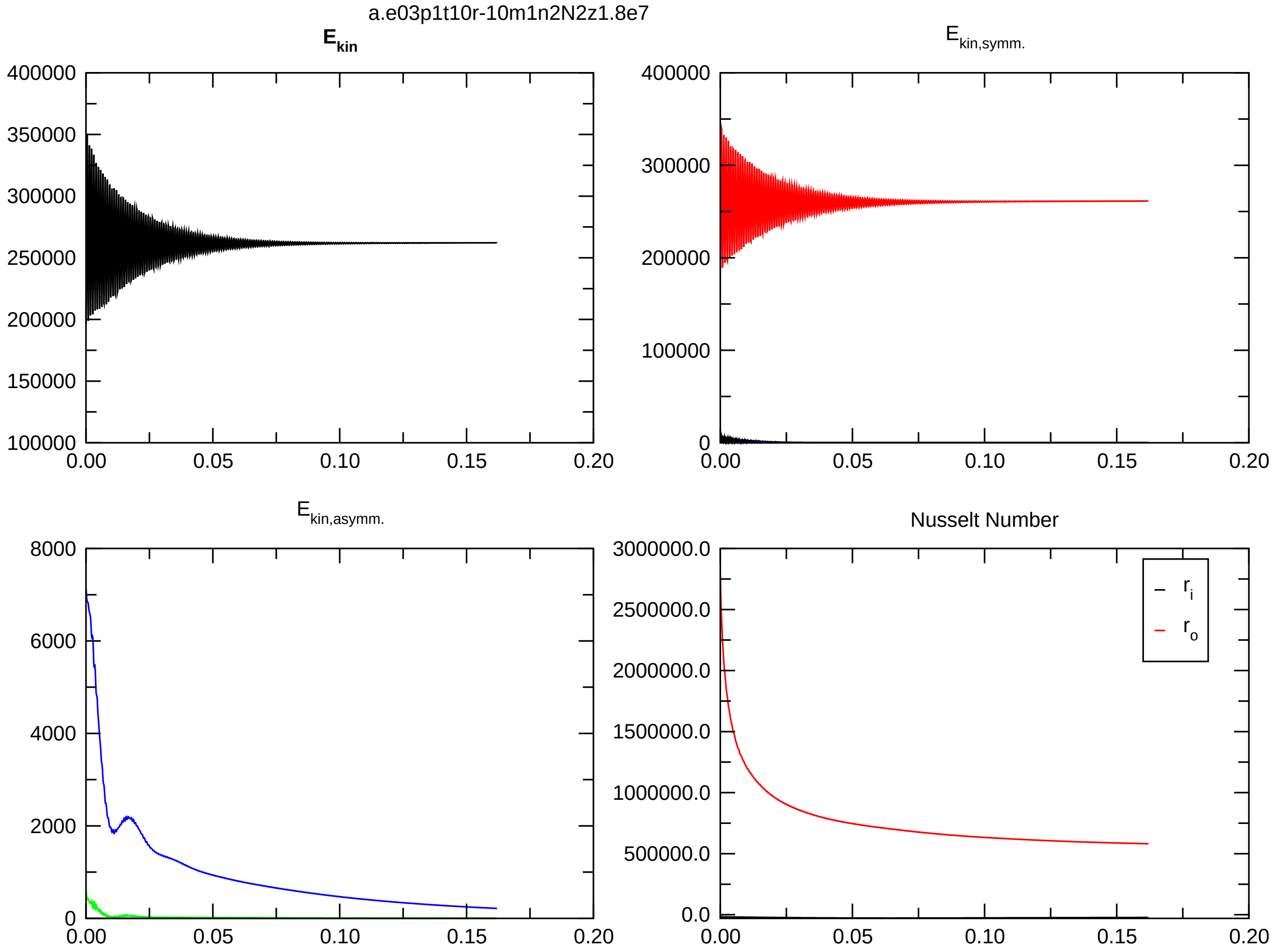

a.e03p1t10r-10m1n2N2z2e7
times: 0.1260063 0.1320066 0.1380069 0.1440072 0.1500075 0.1560078

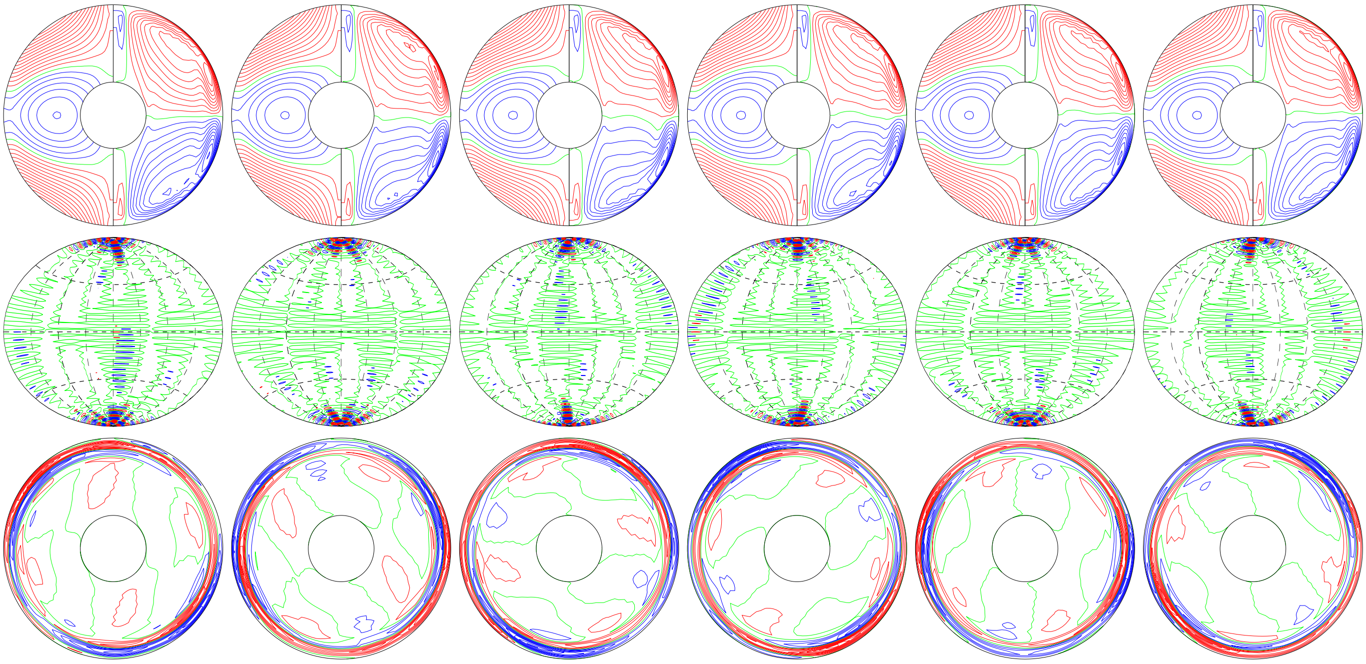

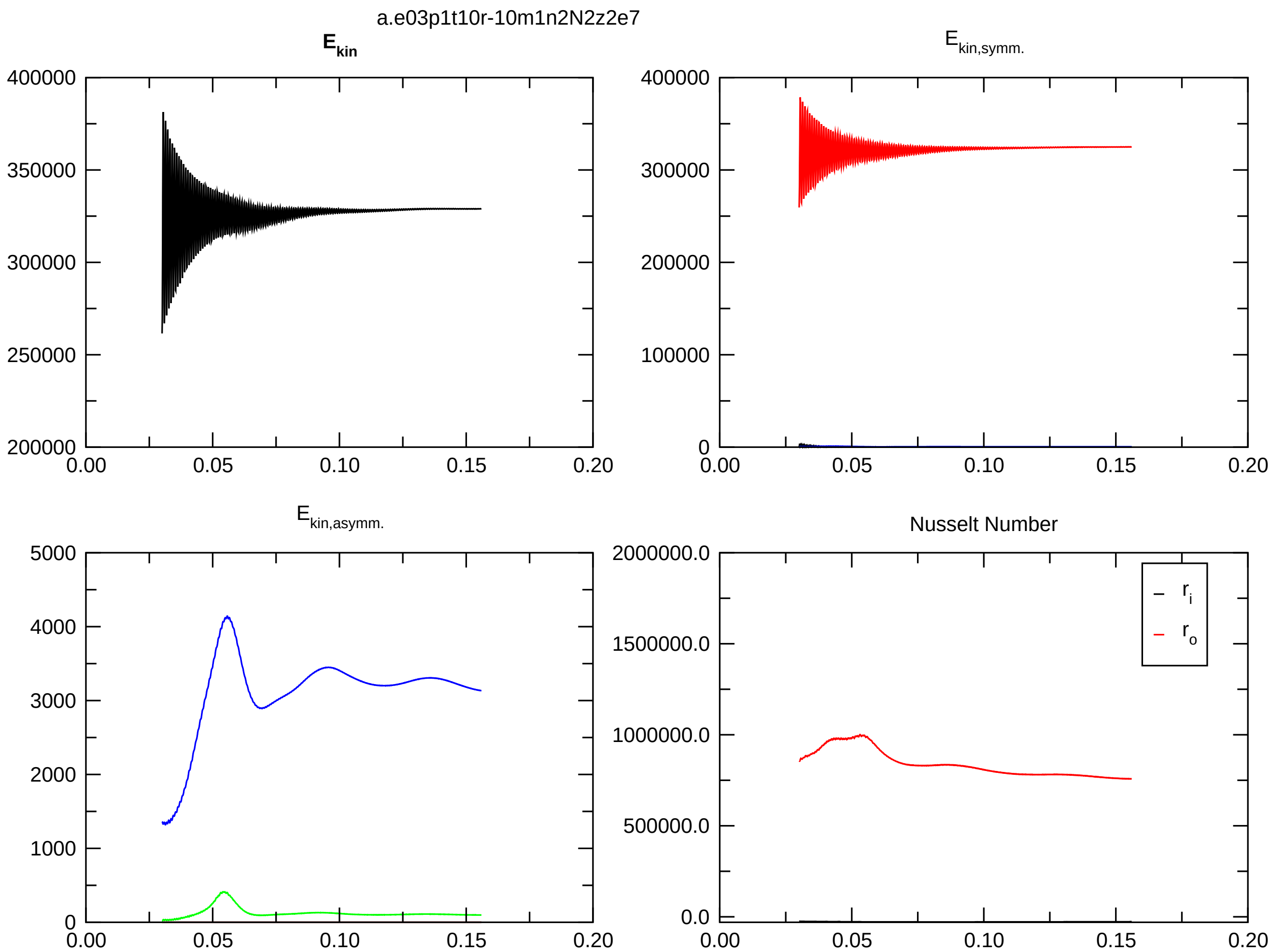

a.e03p1t10r-10m1n2N3z1e6
times: 2.80028 2.90029 3.0003 3.10031 3.20032 3.30033

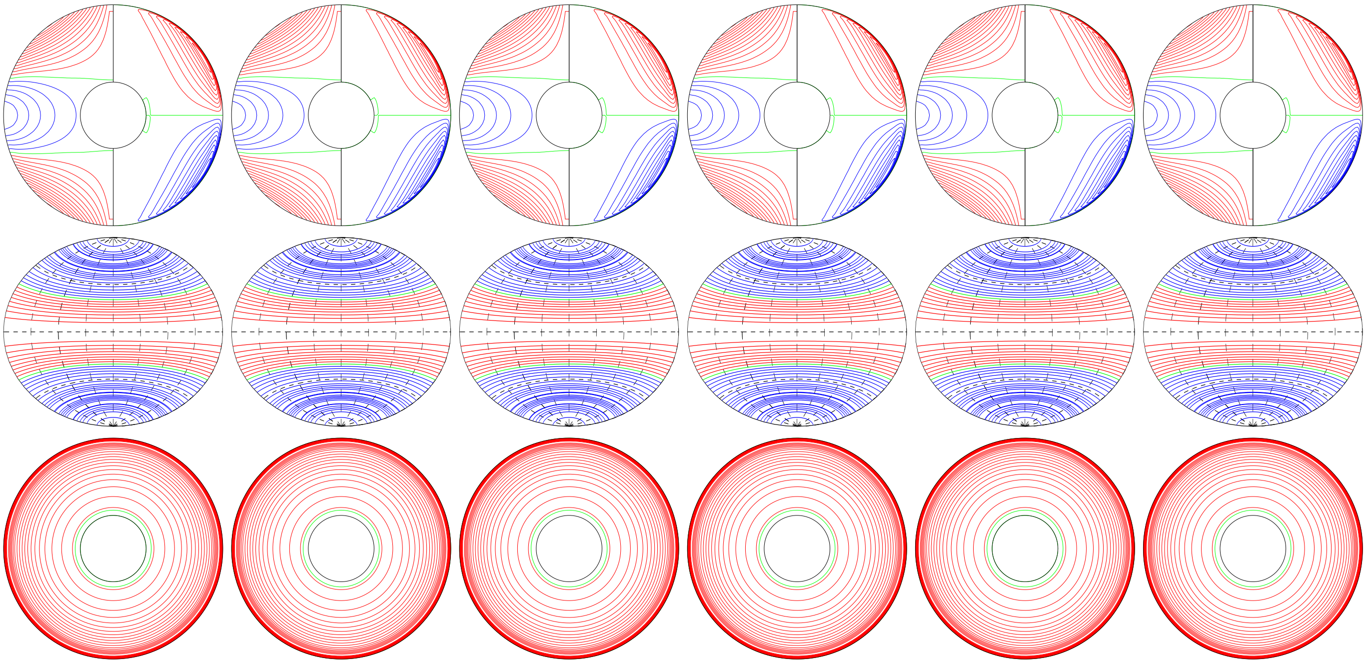

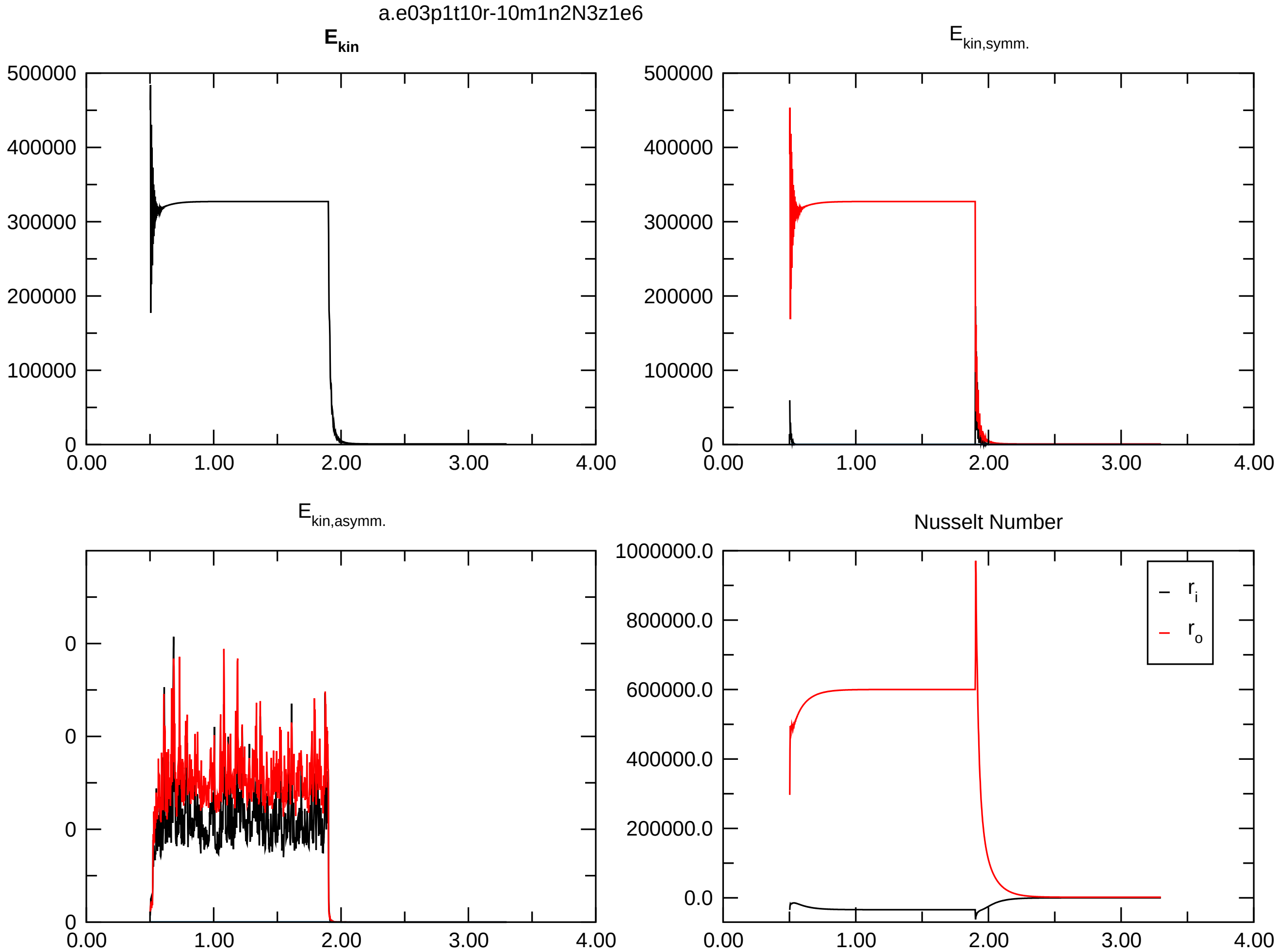

a.e03p1t10r-10m1n2N3z05e7

times: 2.80028 2.90029 3.0003 3.10031 3.20032 3.30033

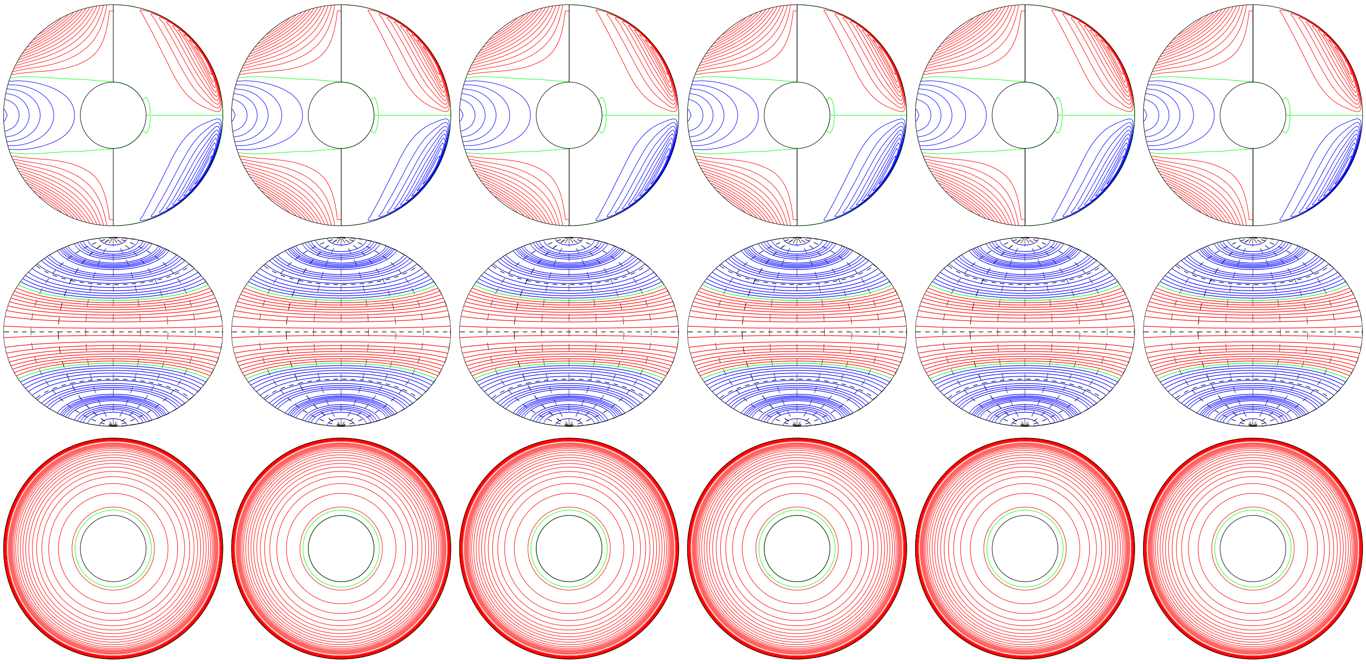

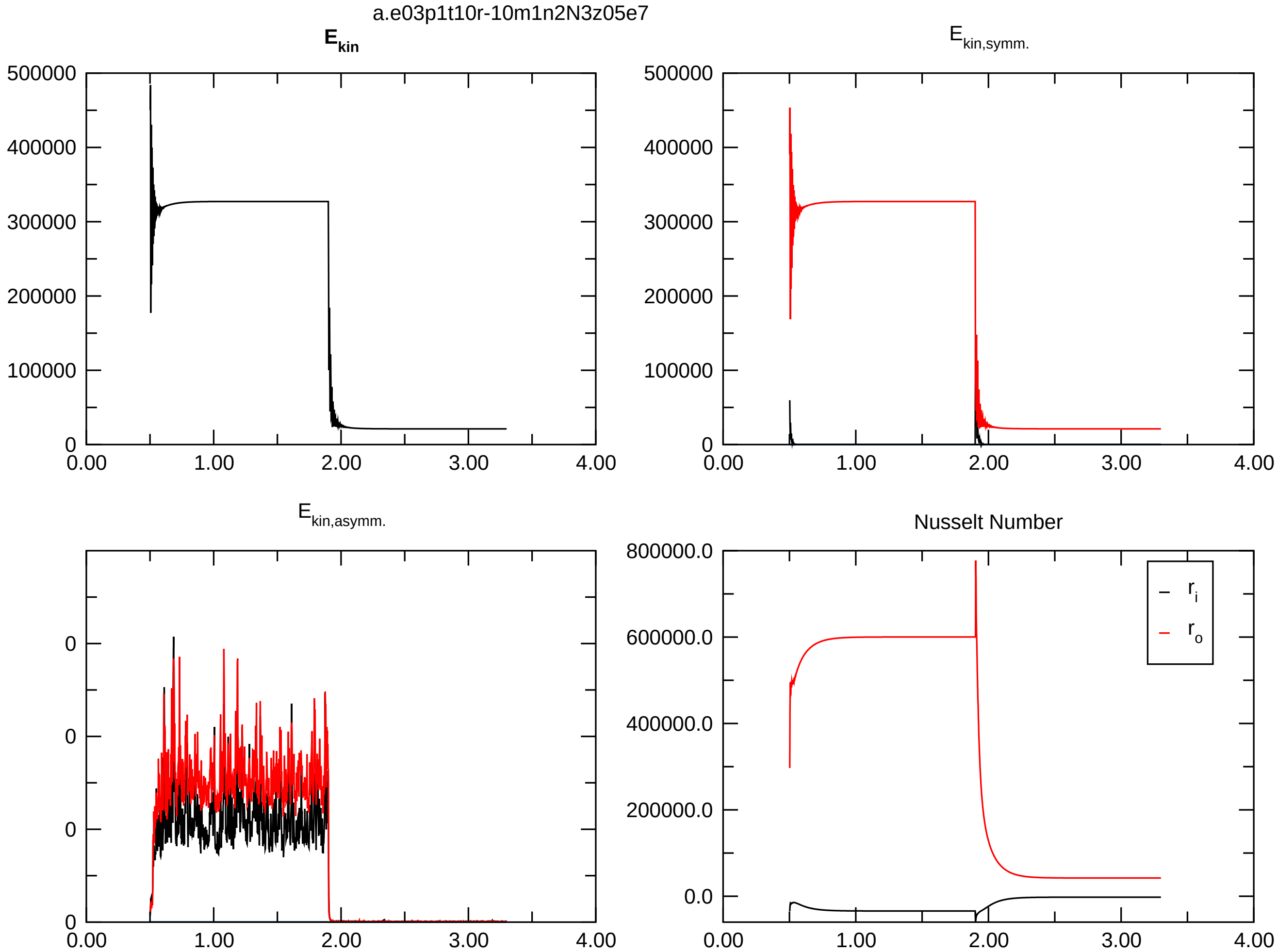

a.e03p1t10r-10m1n2N3z06e7
times: 2.80028 2.90029 3.0003 3.10031 3.20032 3.30033

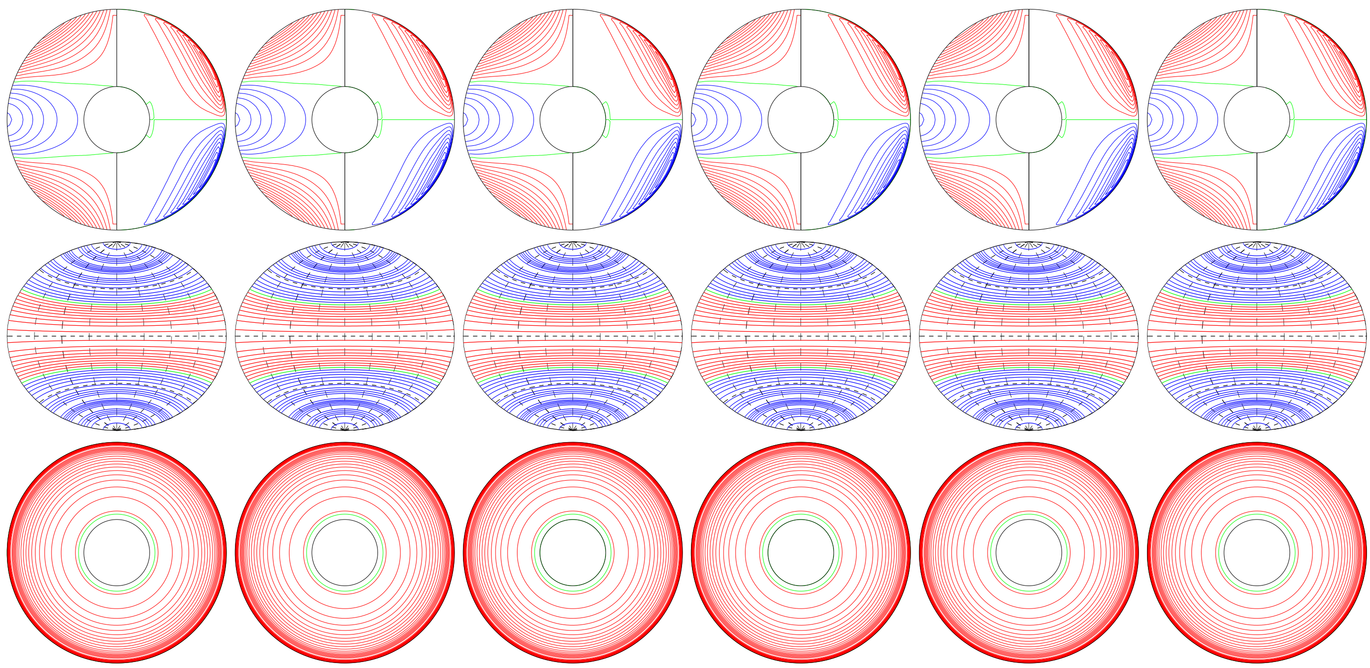

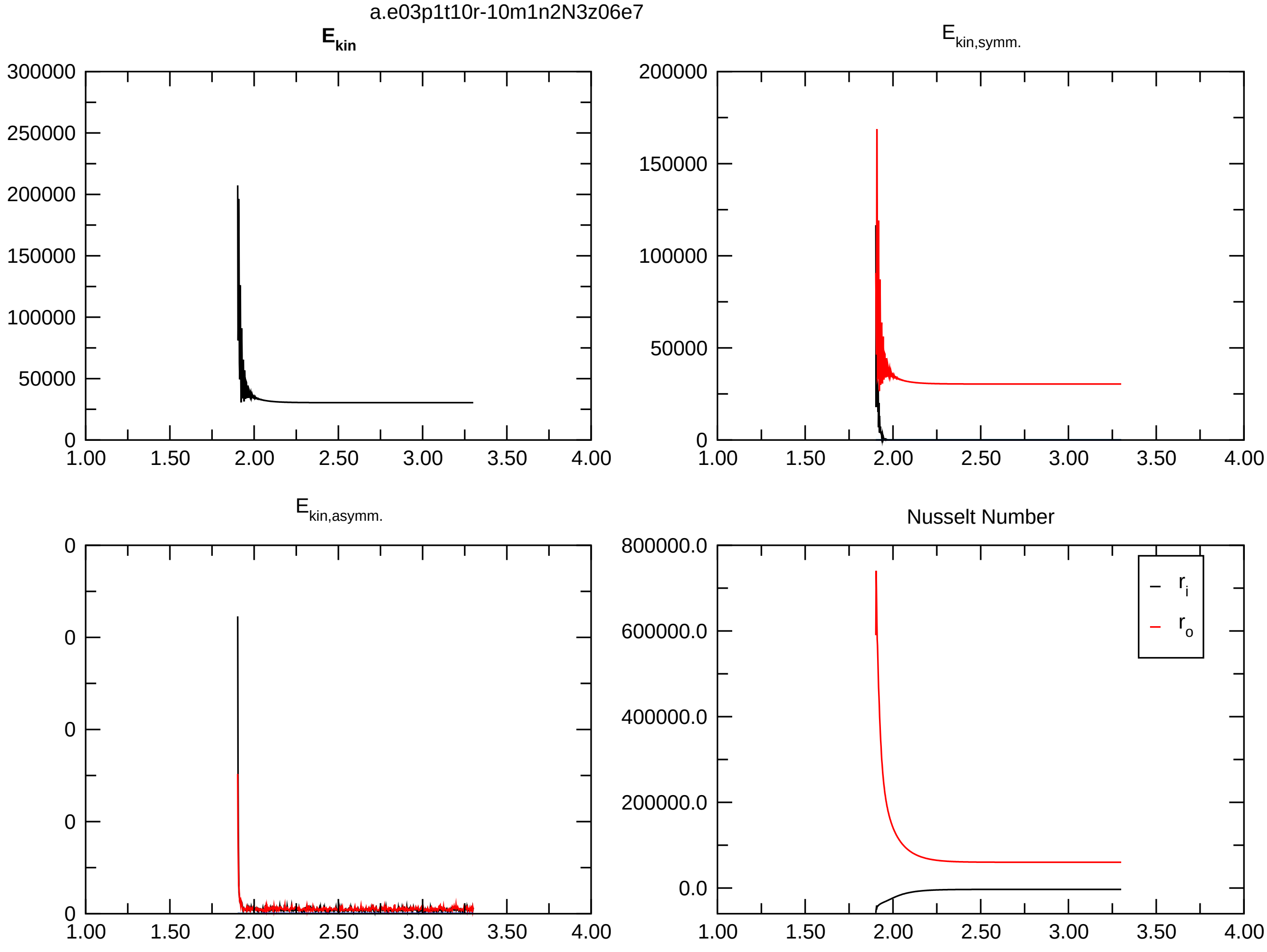

a.e03p1t10r-10m1n2N3z07e7
times: 2.80028 2.90029 3.0003 3.10031 3.20032 3.30033

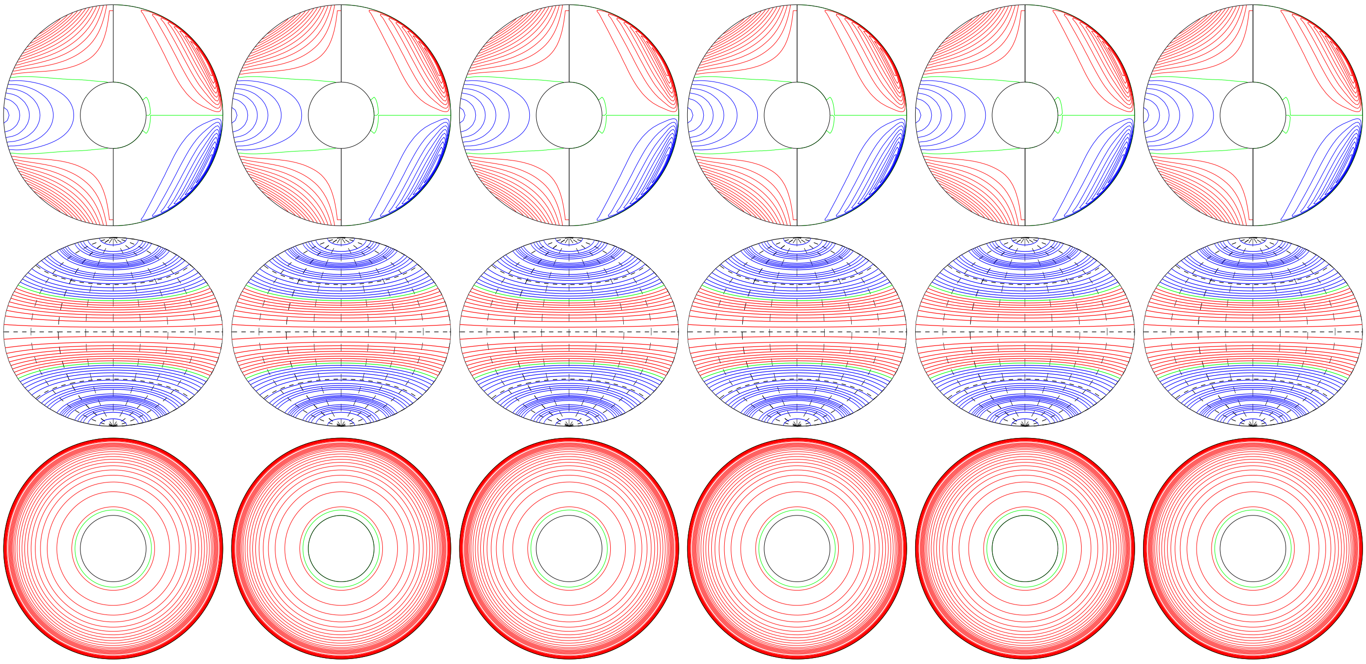

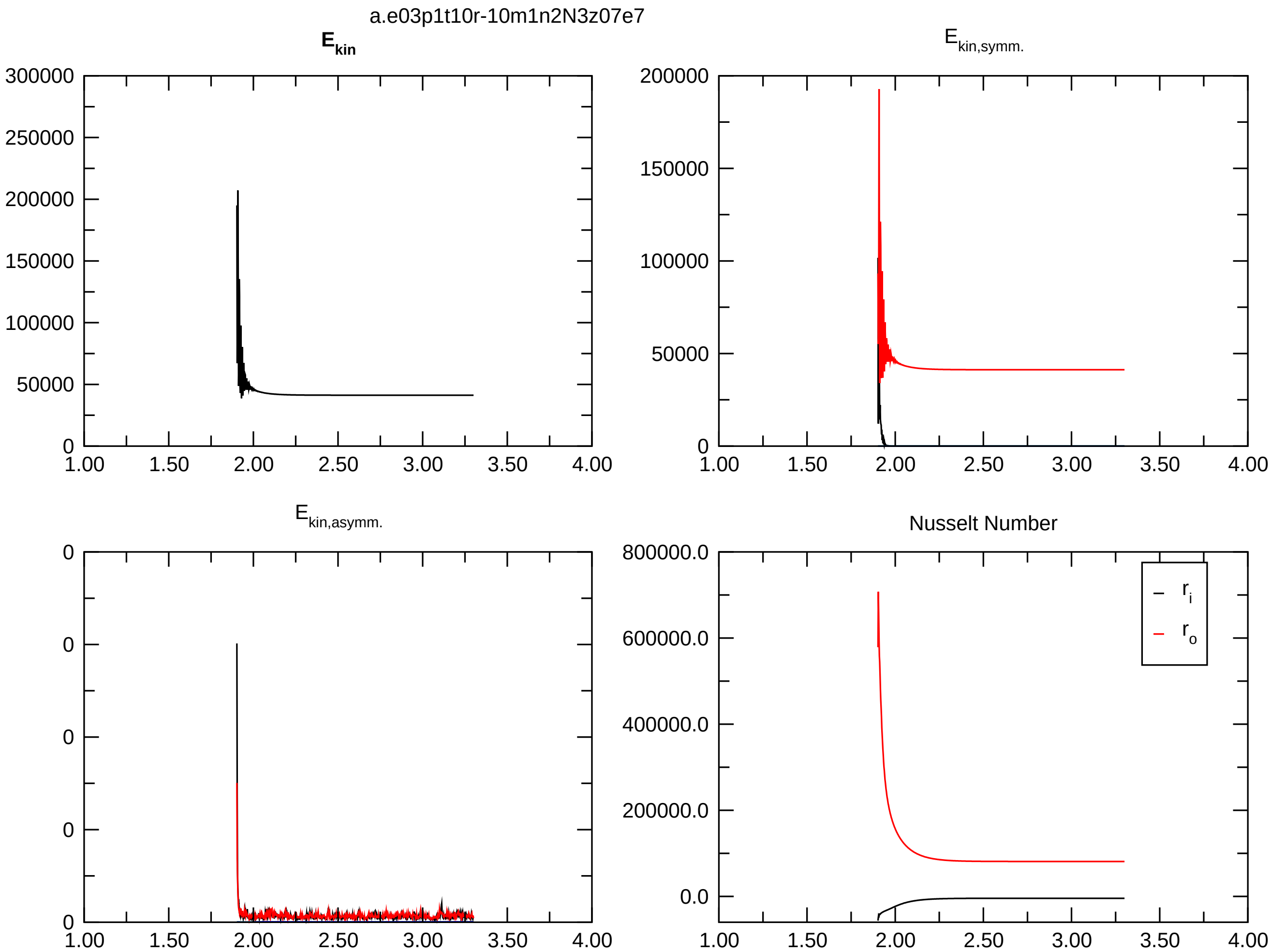

a.e03p1t10r-10m1n2N3z08e7
times: 2.80028 2.90029 3.0003 3.10031 3.20032 3.30033

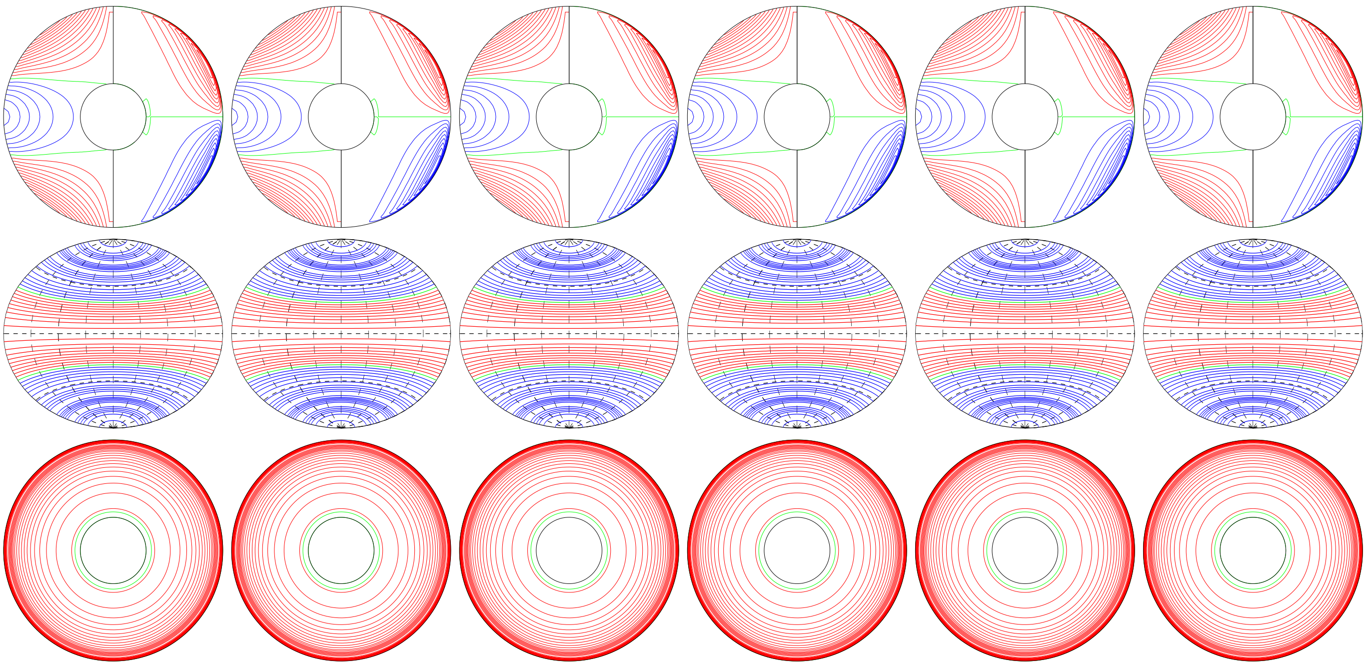

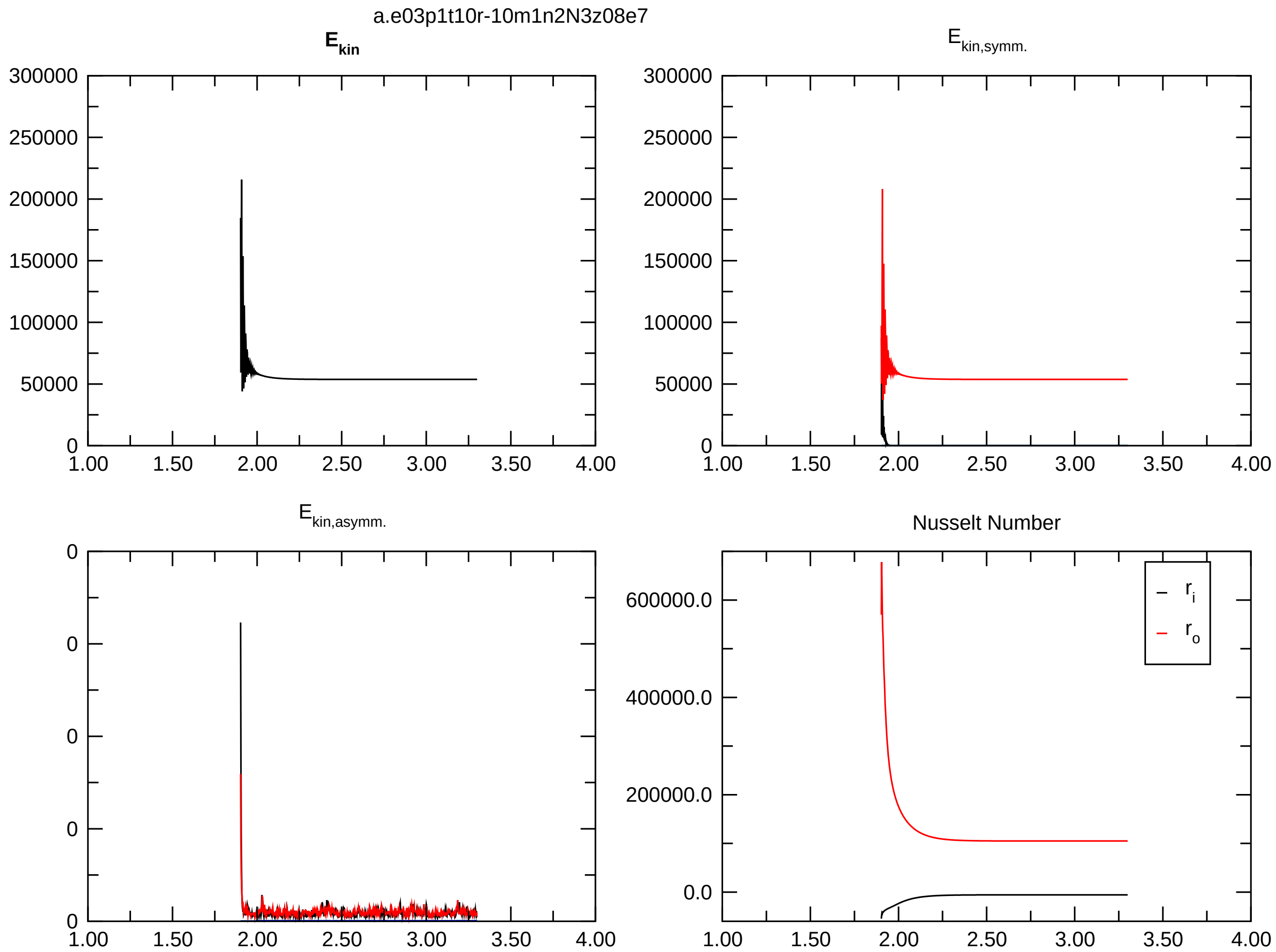

a.e03p1t10r-10m1n2N3z09e7
times: 2.80028 2.90029 3.0003 3.10031 3.20032 3.30033

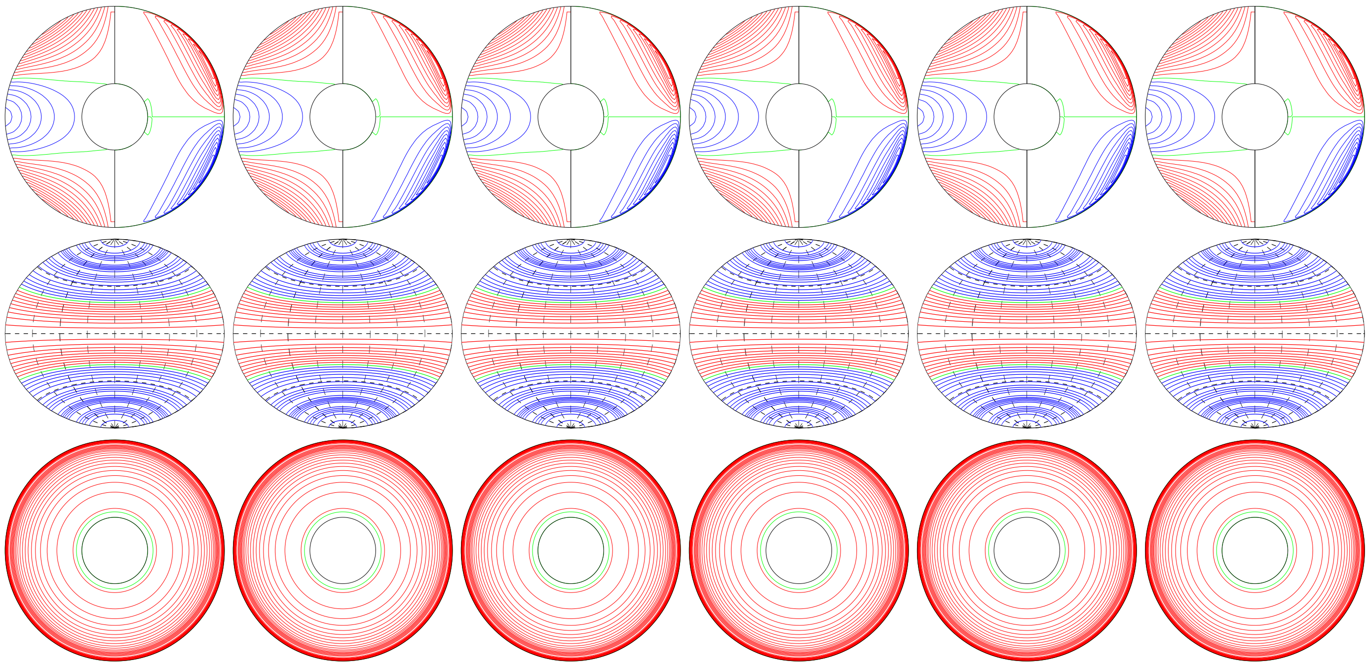

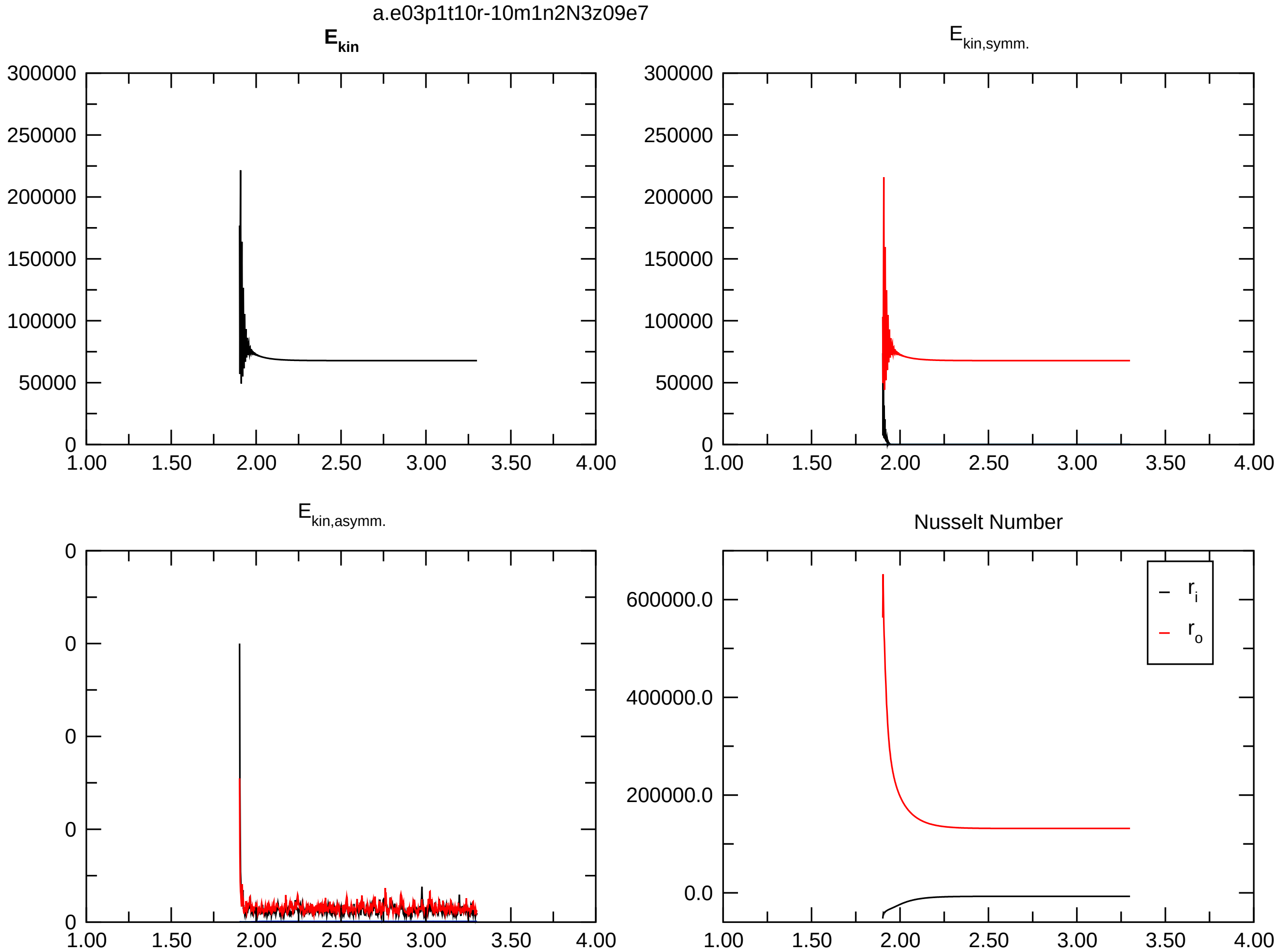

a.e03p1t10r-10m1n2N3z095e7
times: 3.650365 3.70037 3.750375 3.80038 3.850385 3.90039

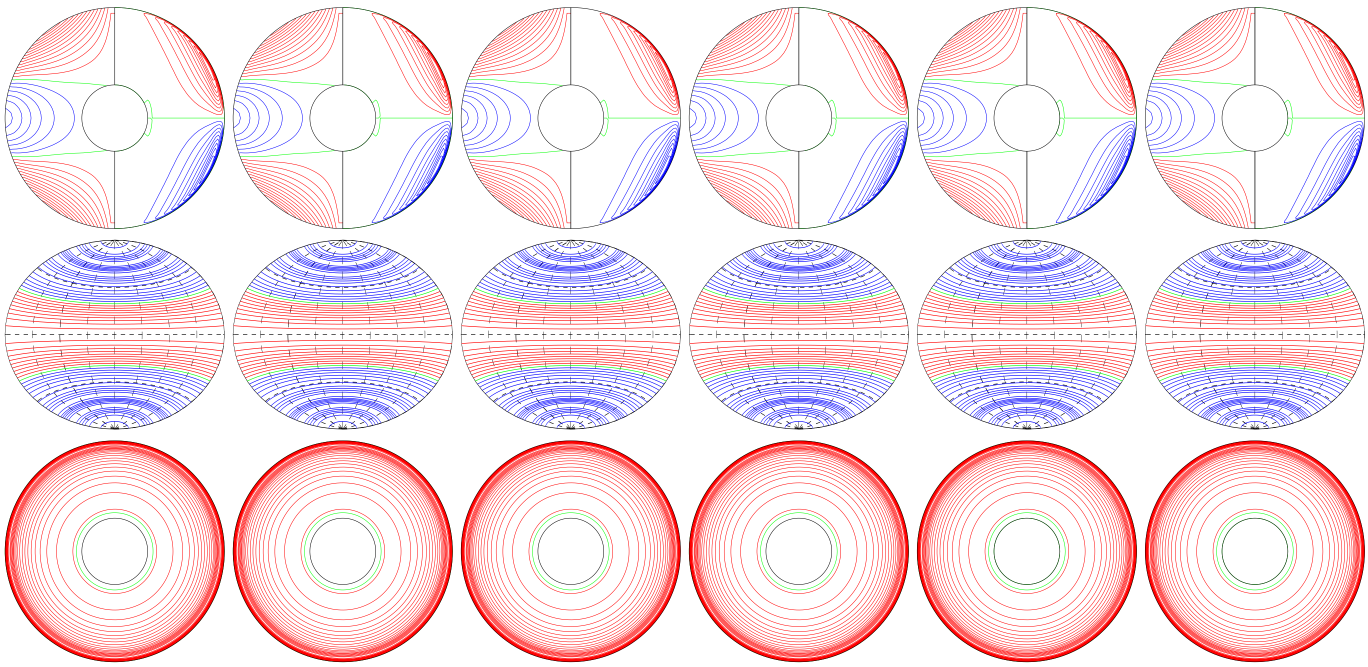

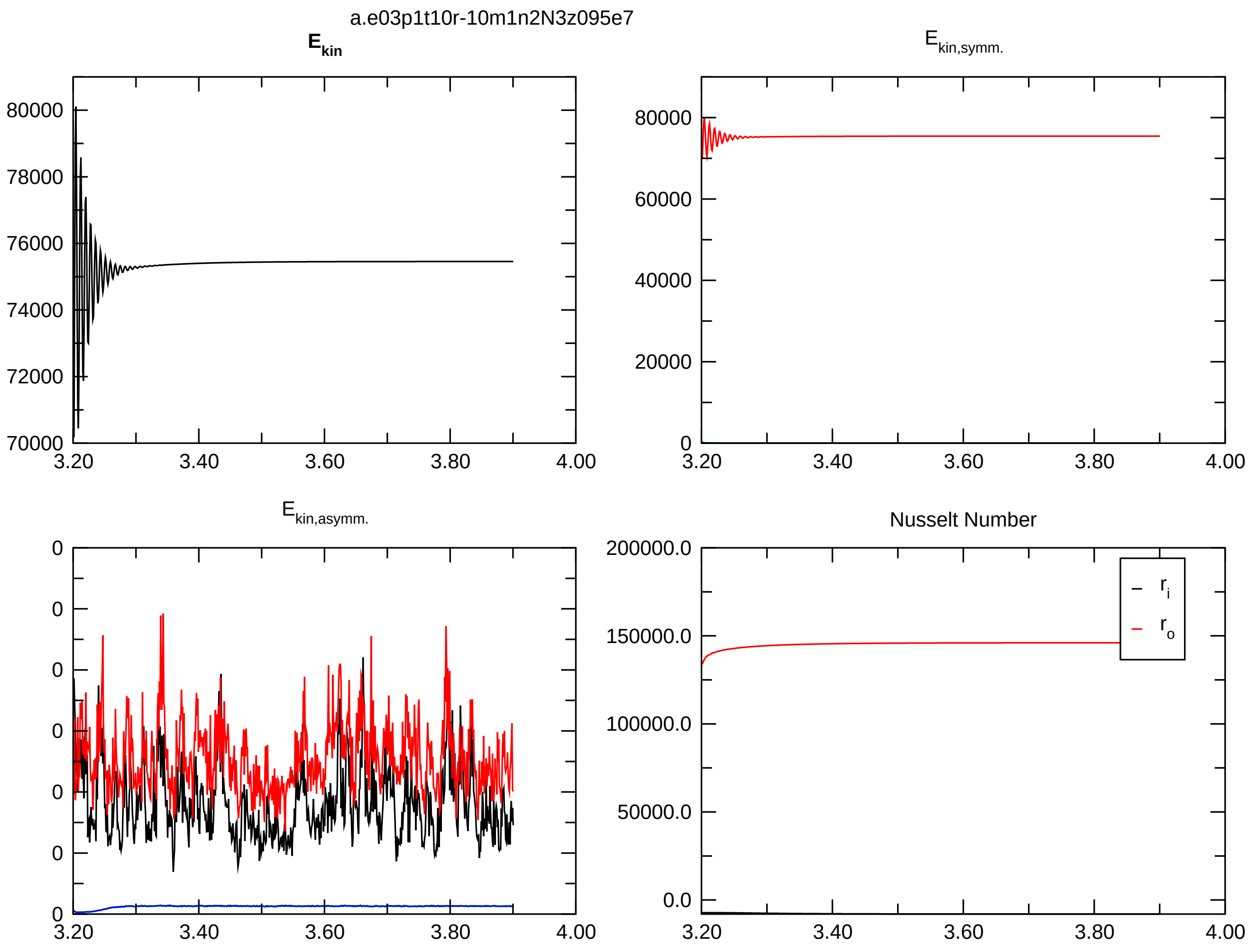

a.e03p1t10r-10m1n2N3z098e7

times: 3.560356 3.60036 3.640364 3.680368 3.720372 3.760376

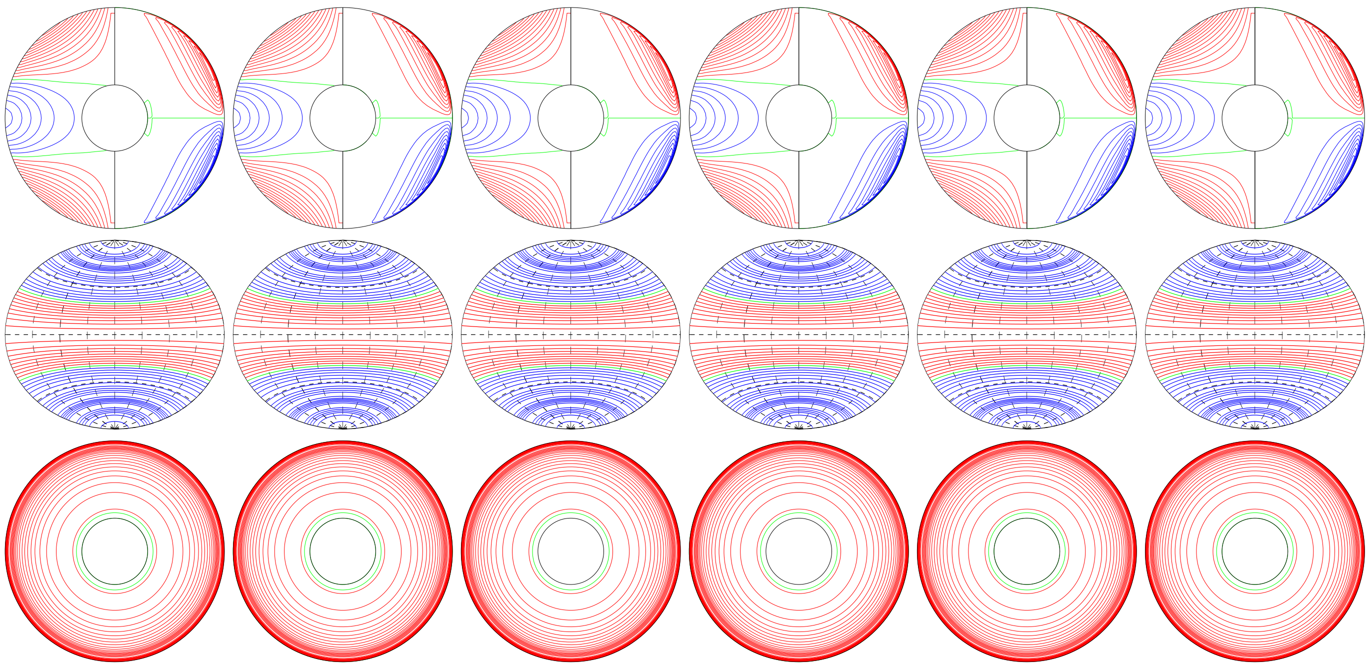

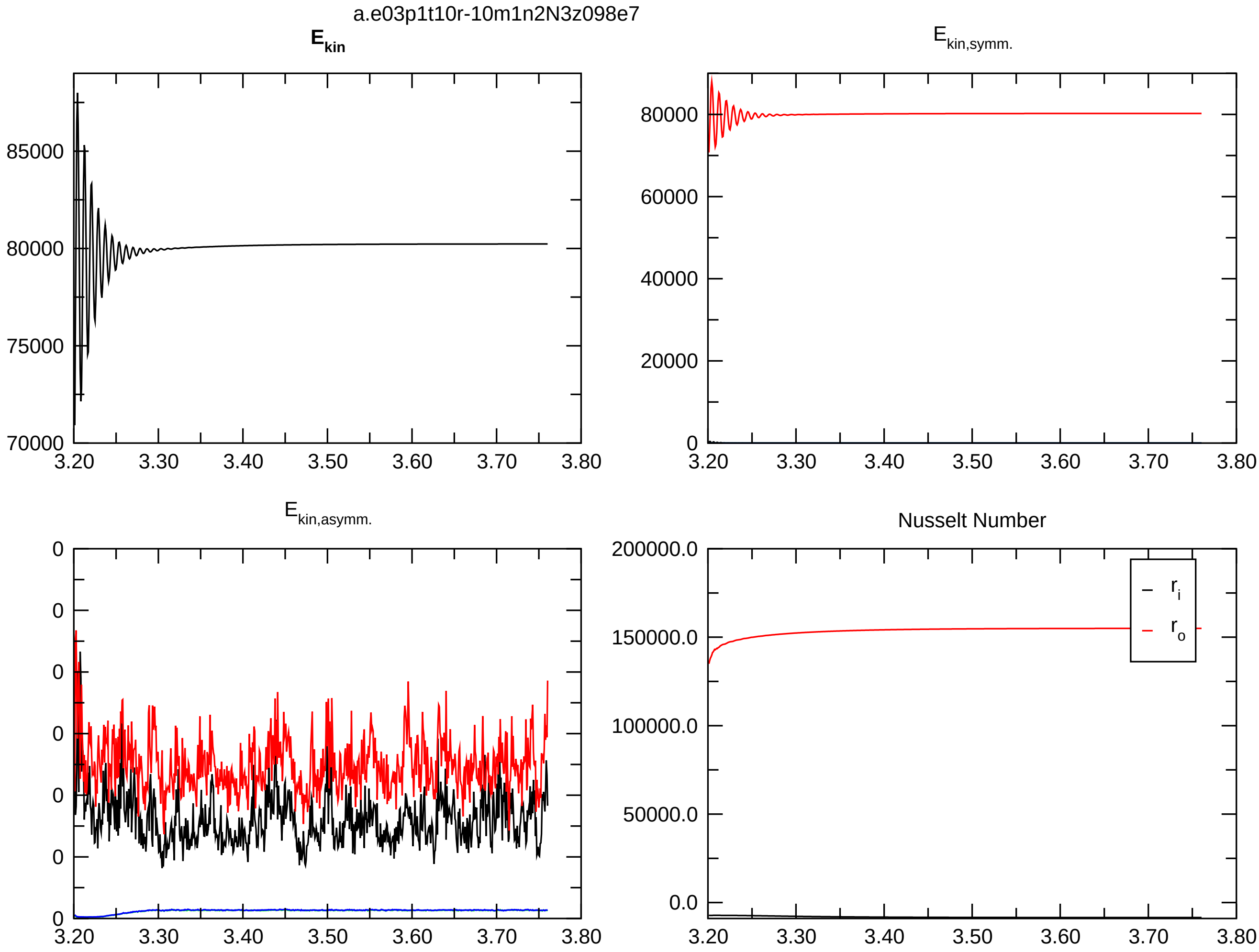

a.e03p1t10r-10m1n2N3z099e7
times: 3.940394 3.960396 3.980398 4.0004 4.020402 4.040404

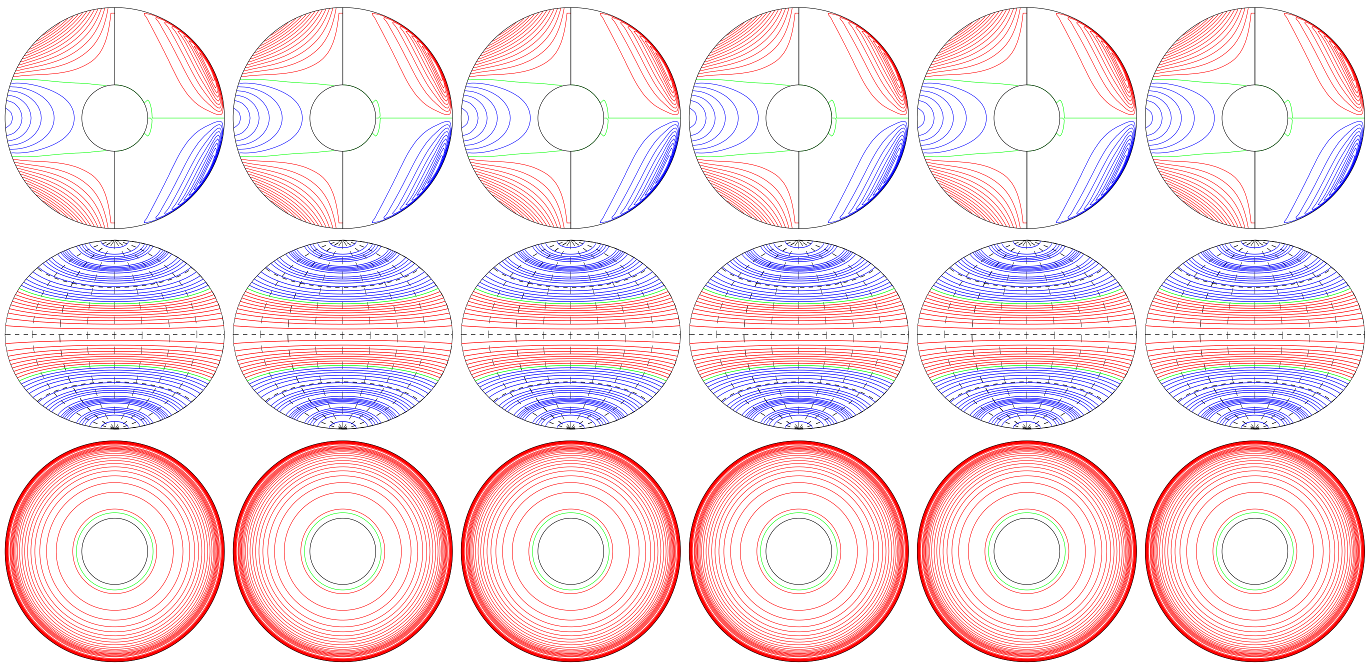

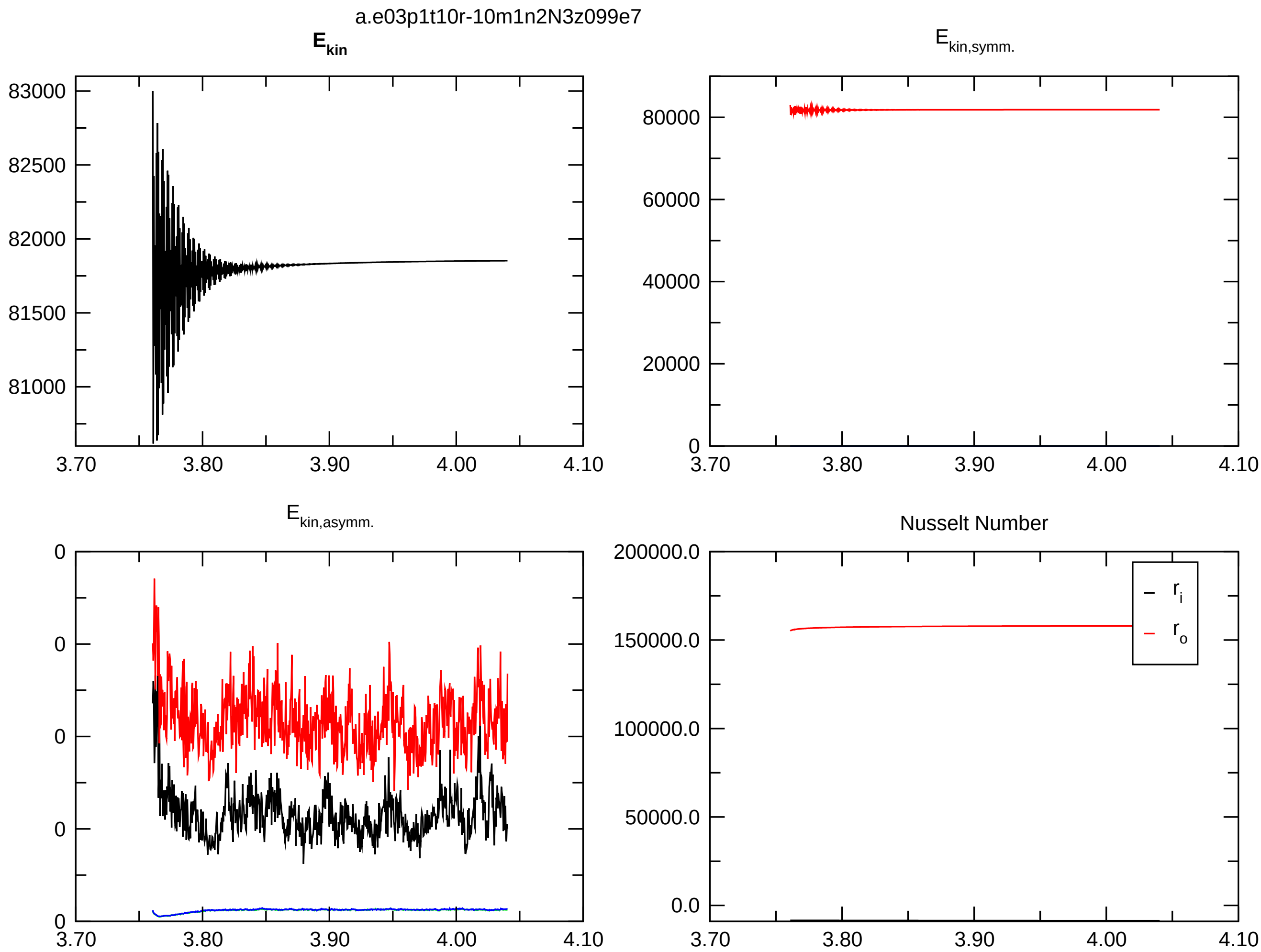

a.e03p1t10r-10m1n2N3z0995e7

times: 5.840464 5.900466 5.960468 6.02047 6.080472 6.140474

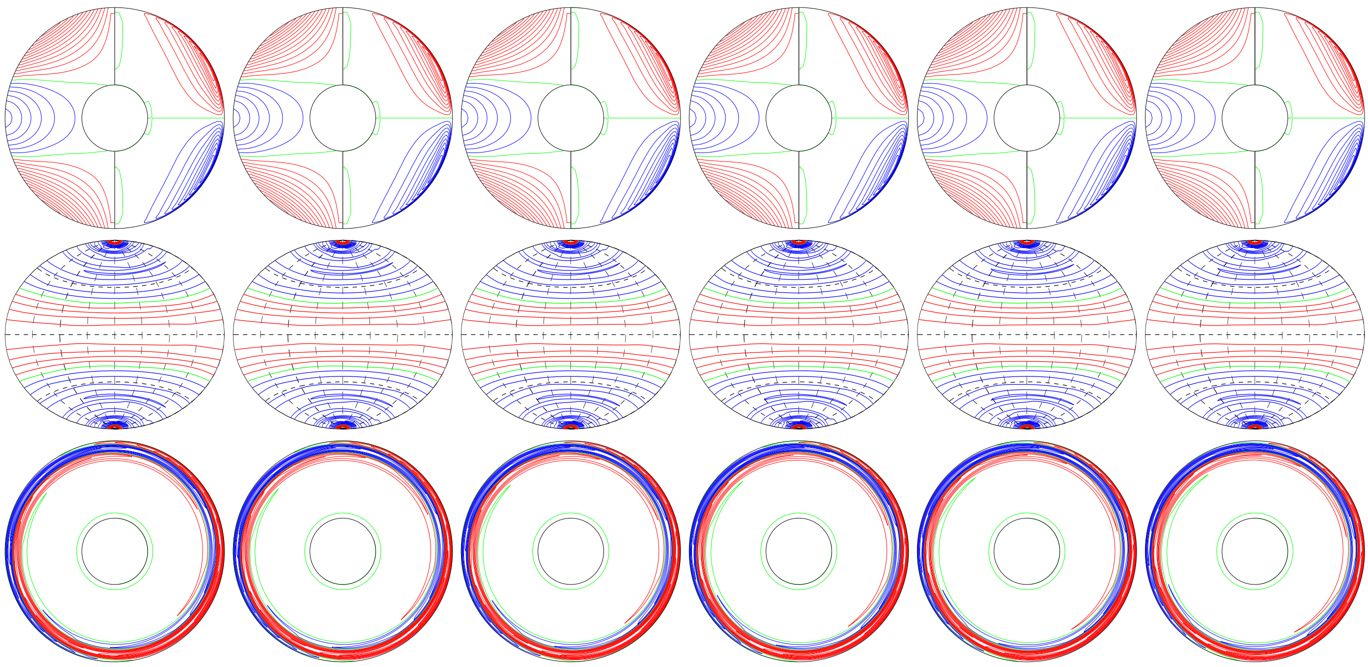

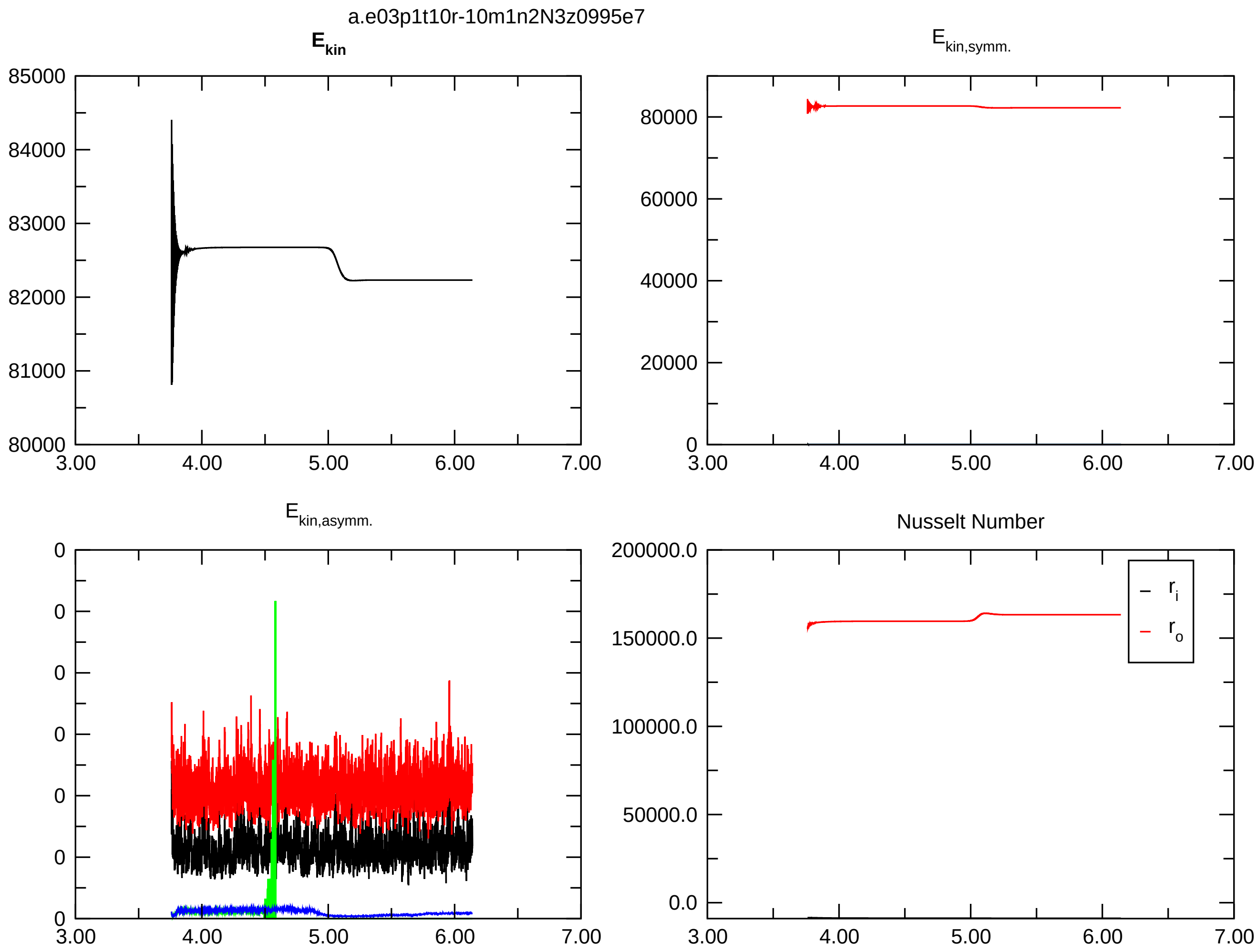

a.e03p1t10r-10m1n2N3z1e7
times: 2.910281 2.940282 2.970283 3.000284 3.030285 3.060286

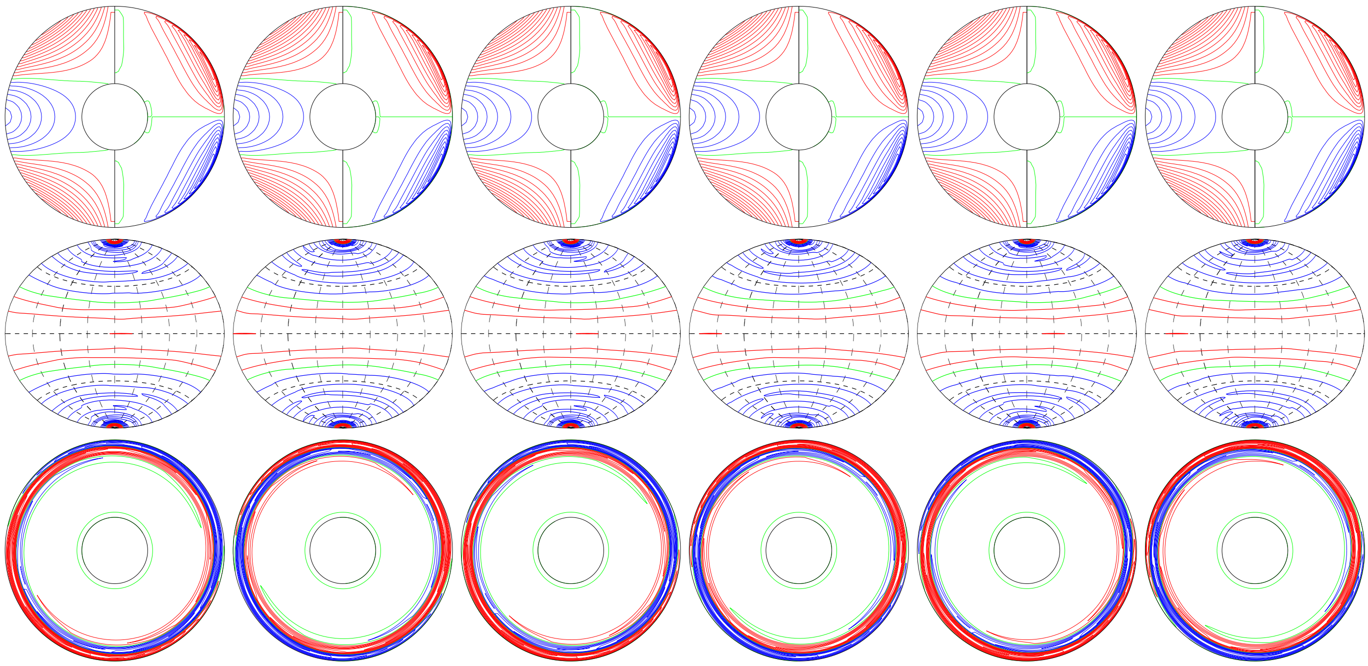

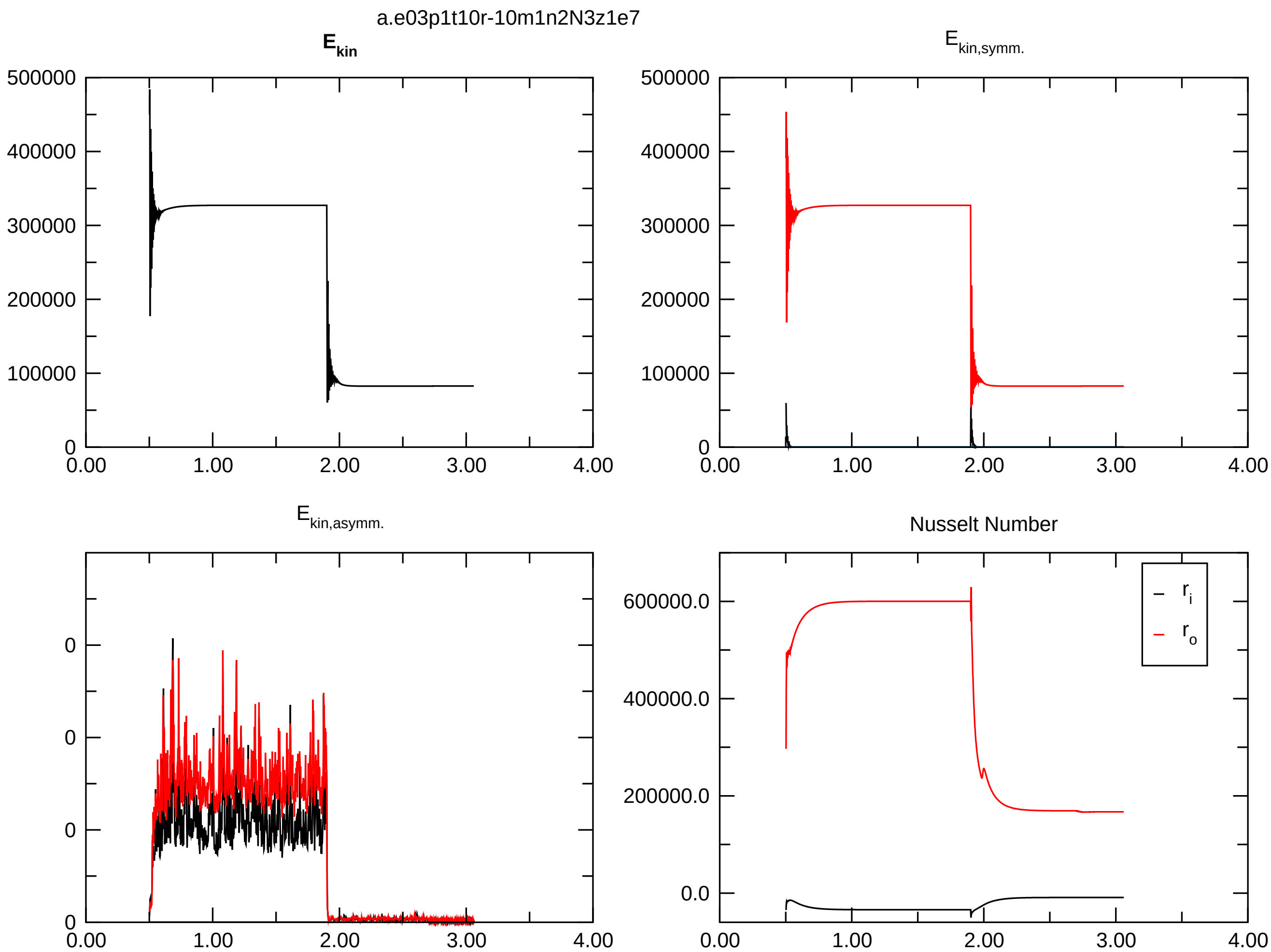

a.e03p1t10r-10m1n2N3z1e7a
times: 5.180488 5.22049 5.260492 5.300494 5.340496 5.380498

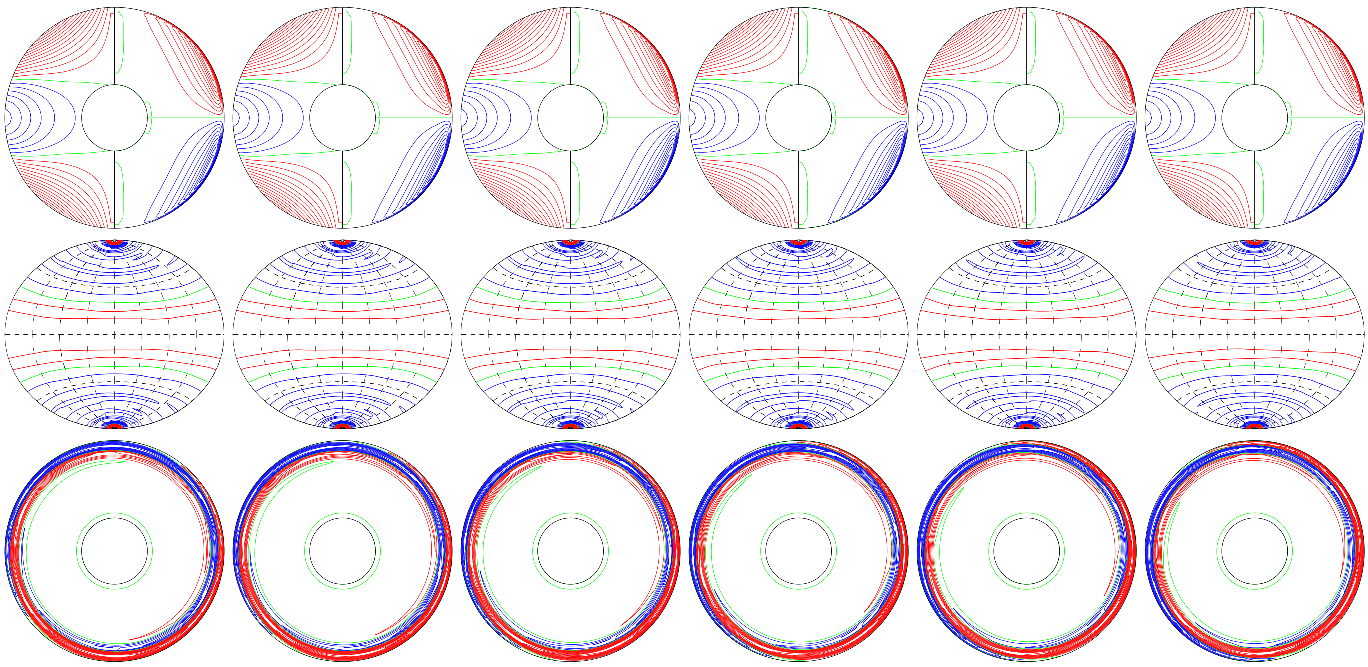

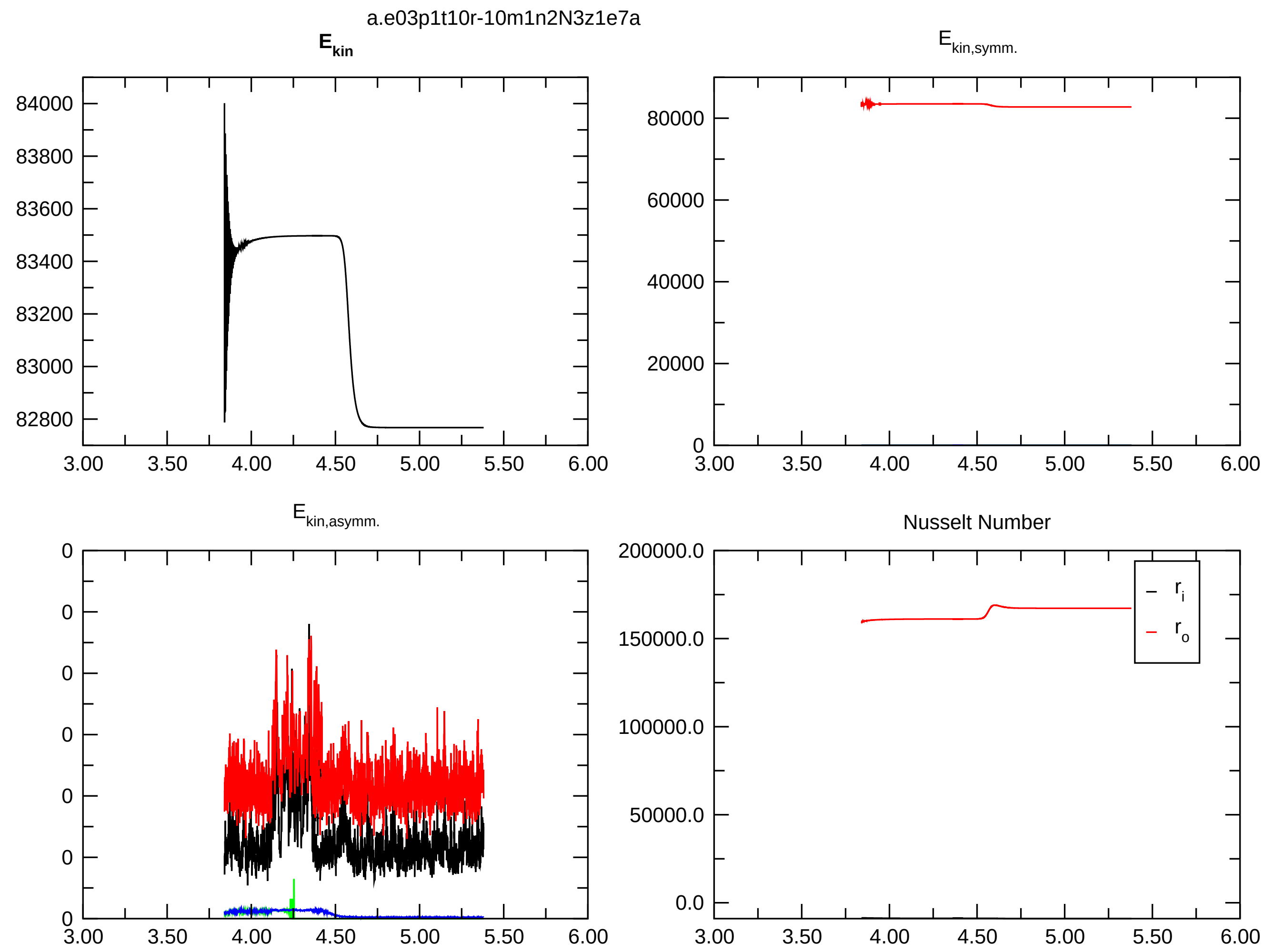

a.e03p1t10r-10m1n2N3z1.1e7
times: 5.820564 5.840566 5.860568 5.88057 5.900572 5.920574

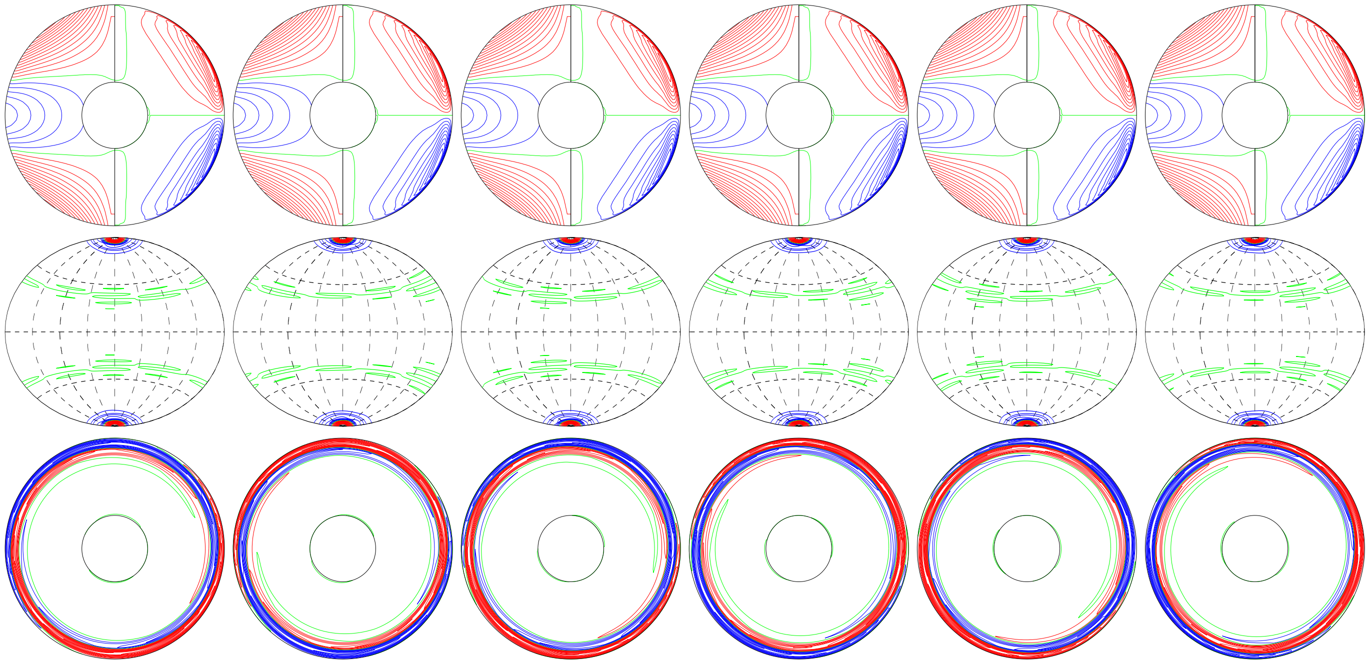

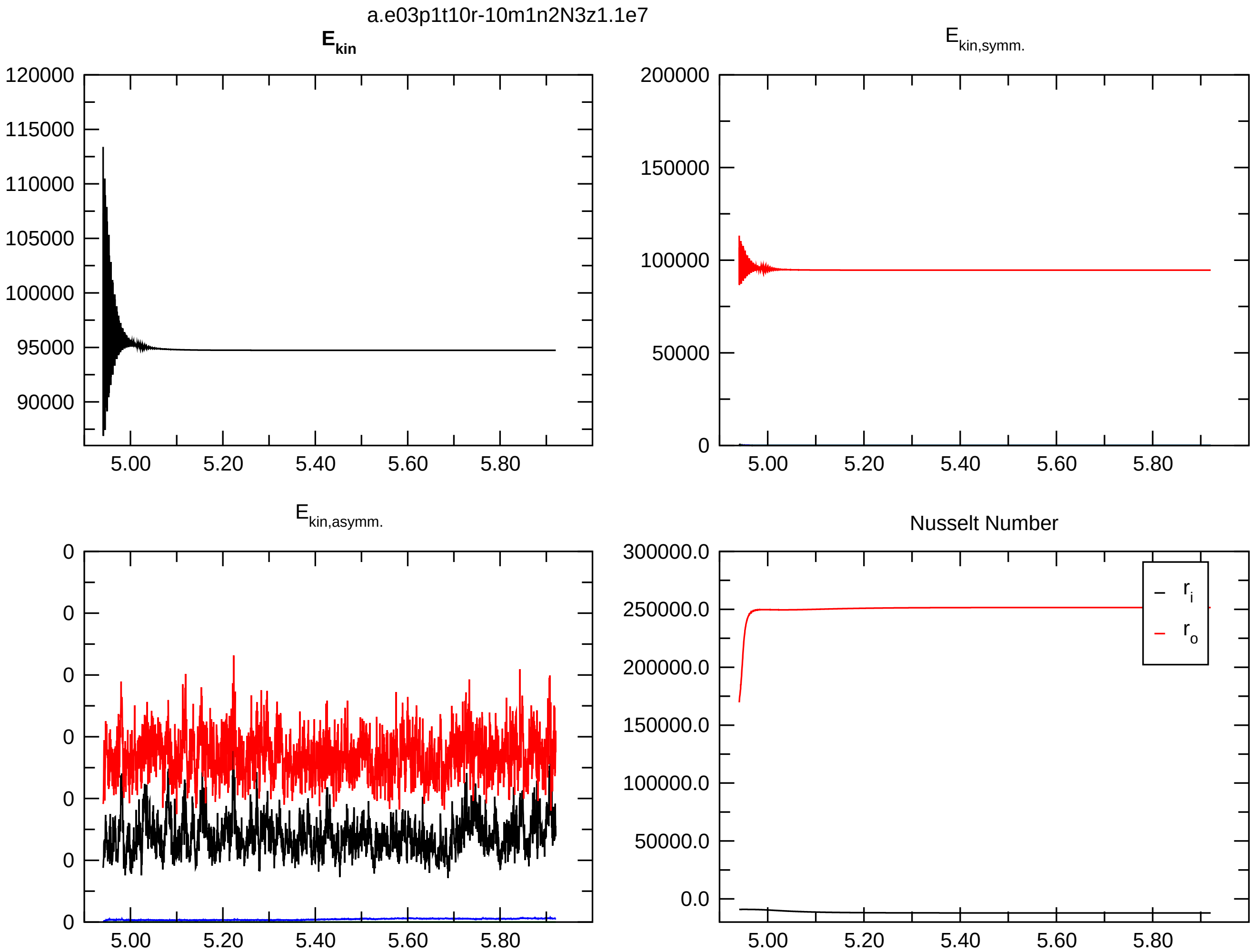

a.e03p1t10r-10m1n2N3z1.5e7
times: 7.67056 7.710561 7.750562 7.790563 7.830564 7.870565

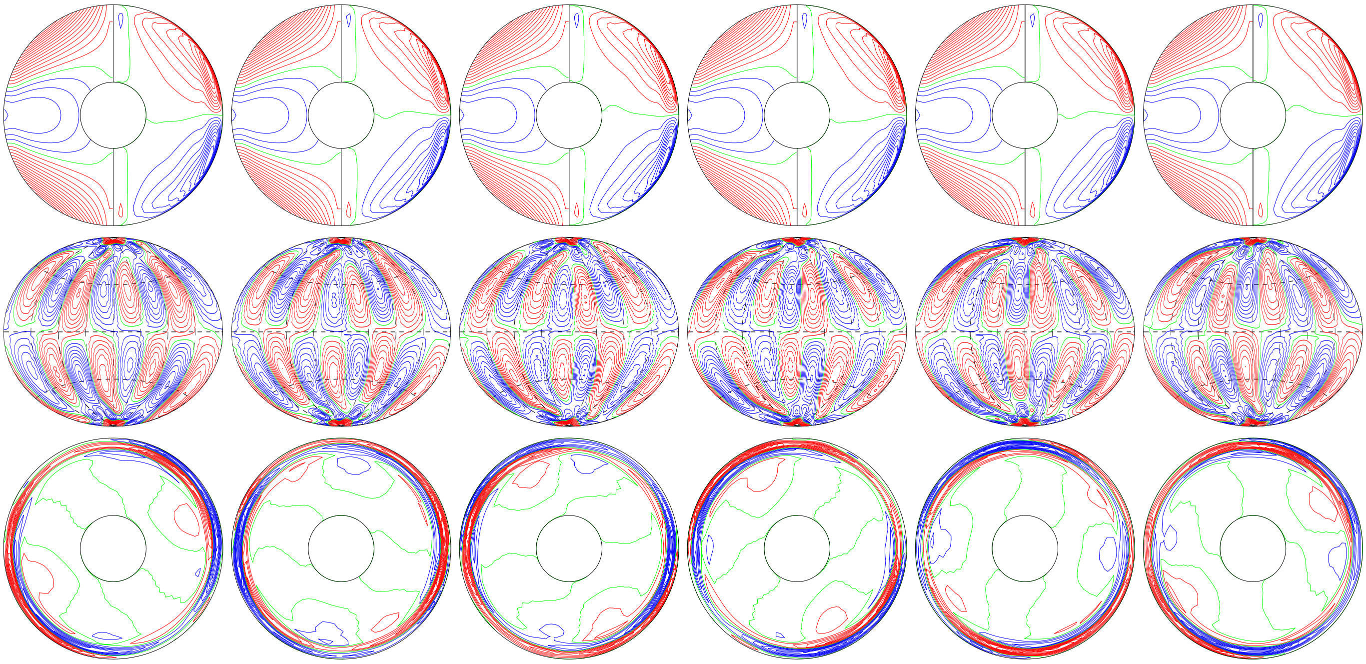

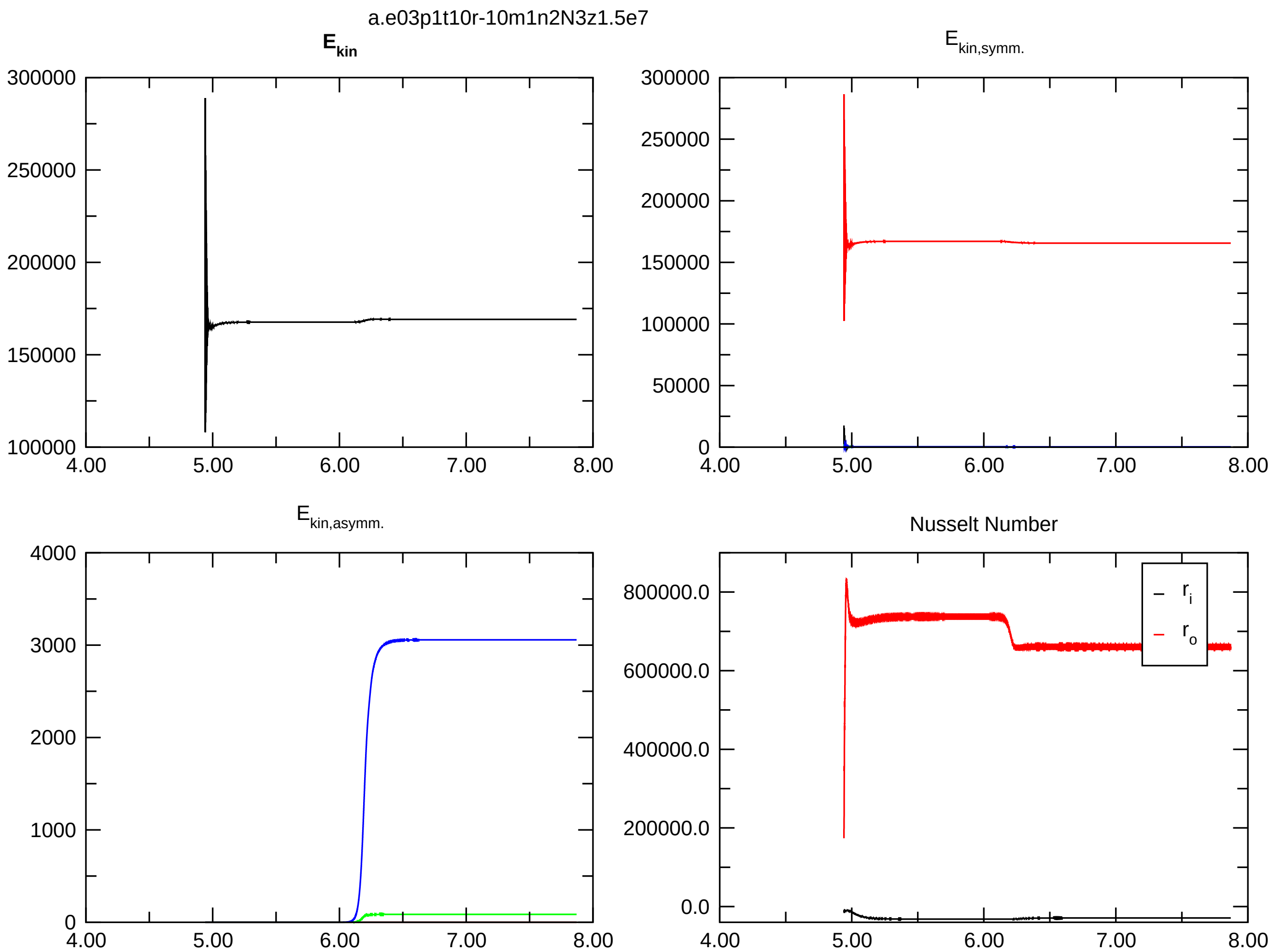

a.e03p1t10r-10m1n2N3z1.6e7

times: 8.040569 8.05057 8.060571 8.070572 8.080573 8.090574

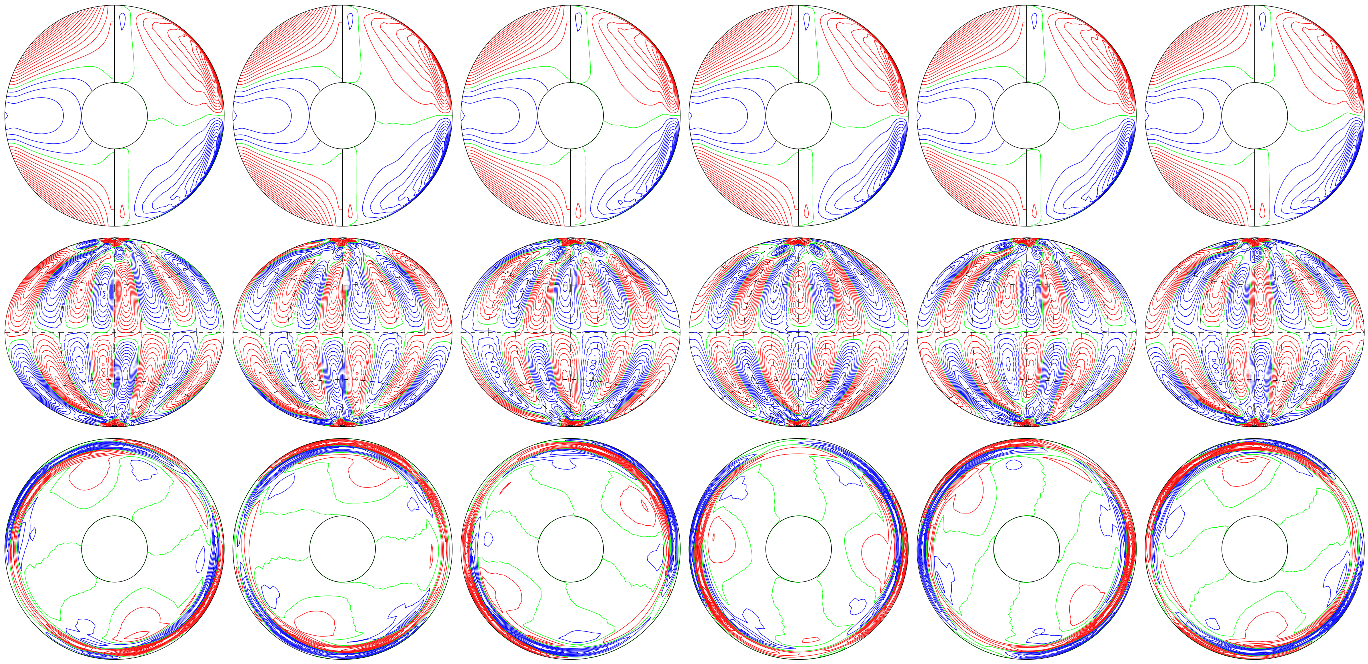

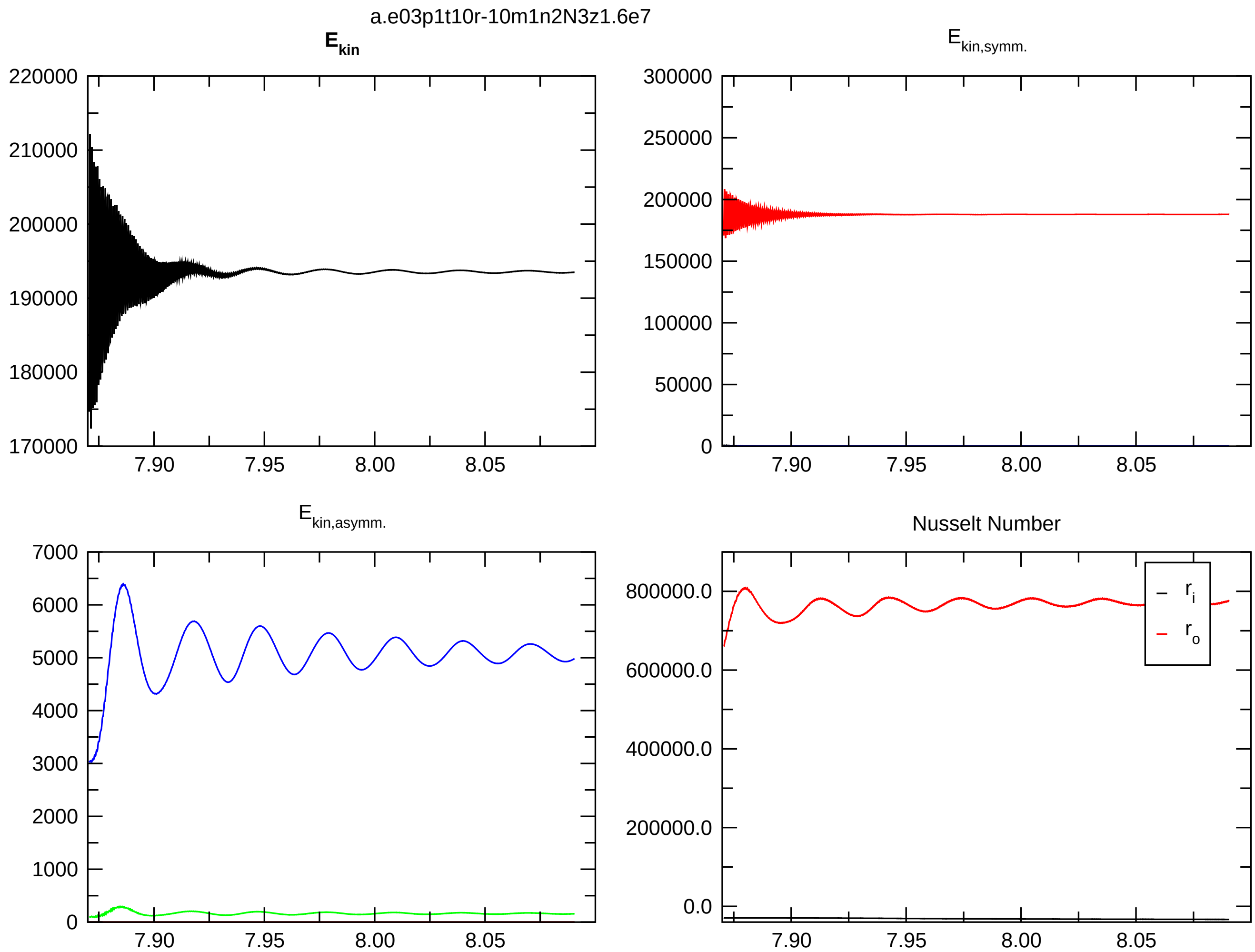

a.e03p1t10r-10m1n2N3z1.7e7
times: 8.040569 8.05057 8.060571 8.070572 8.080573 8.090574

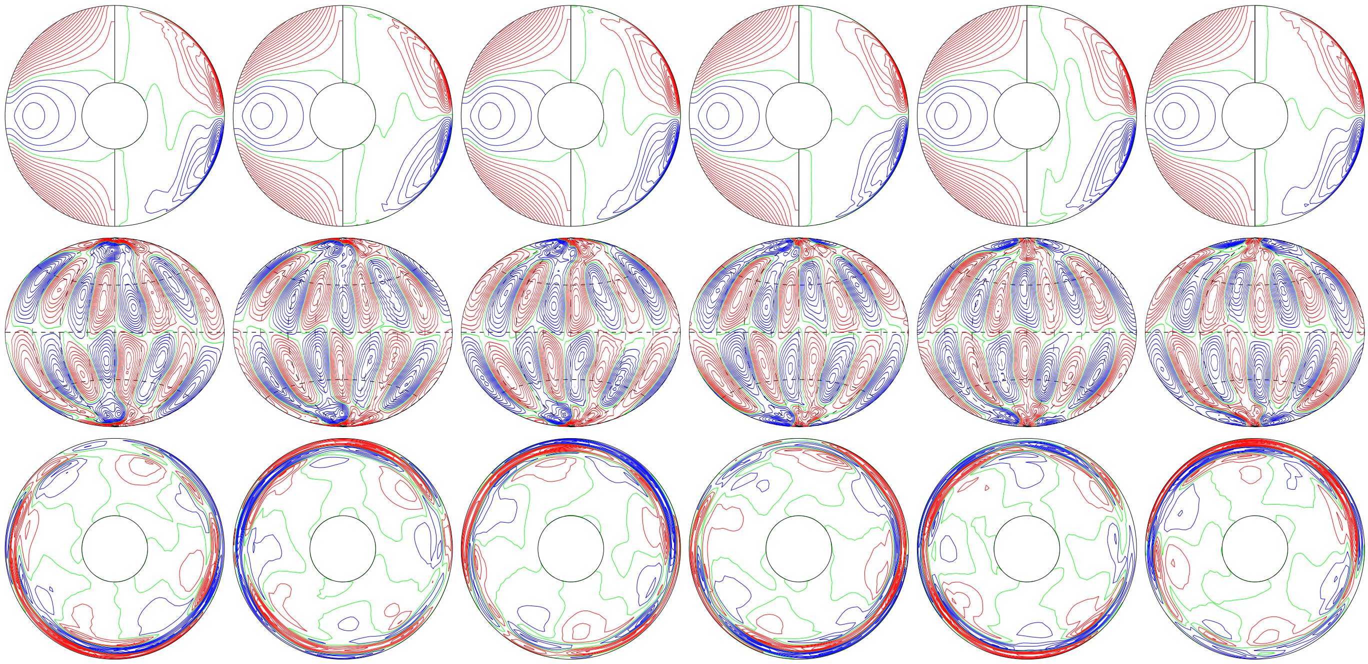

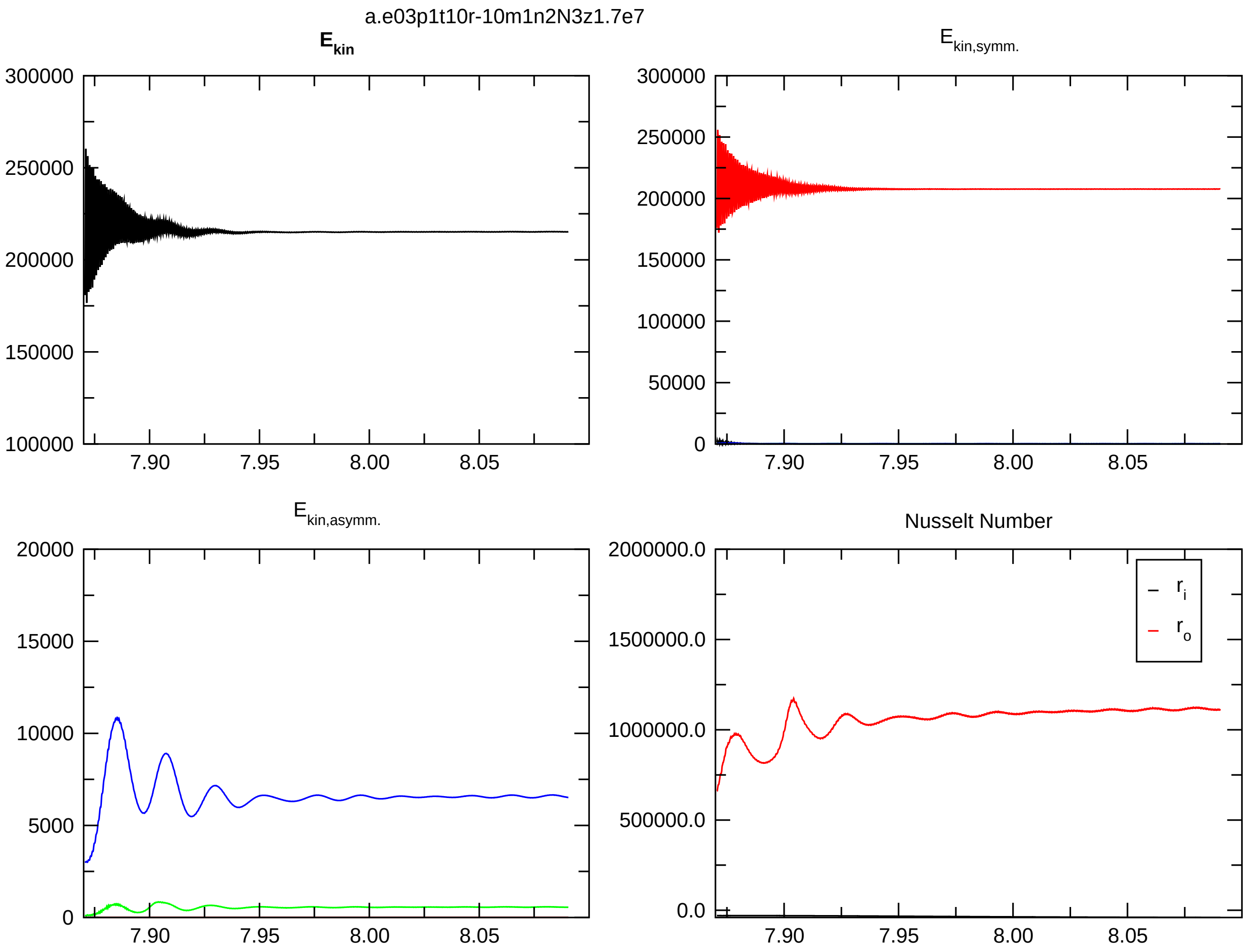

a.e03p1t10r-10m1n2N3z1.8e7

times: 7.998565 8.004565 8.010565 8.016565 8.022565 8.028565

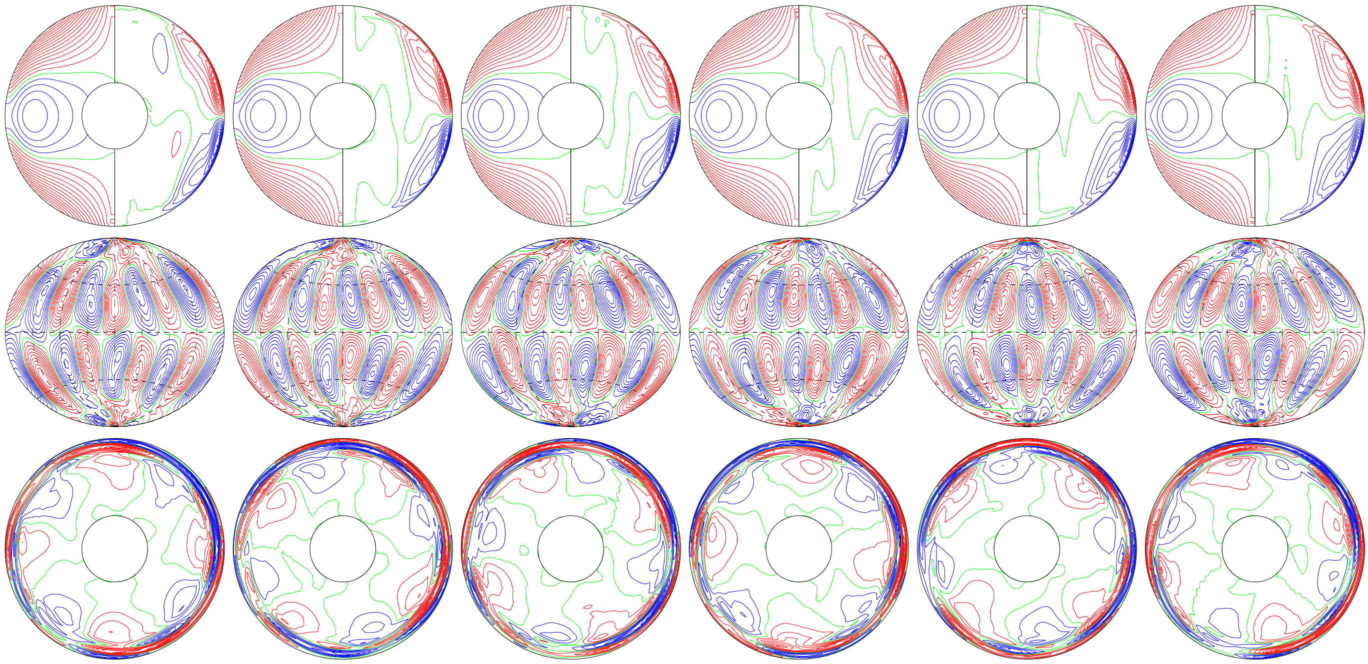

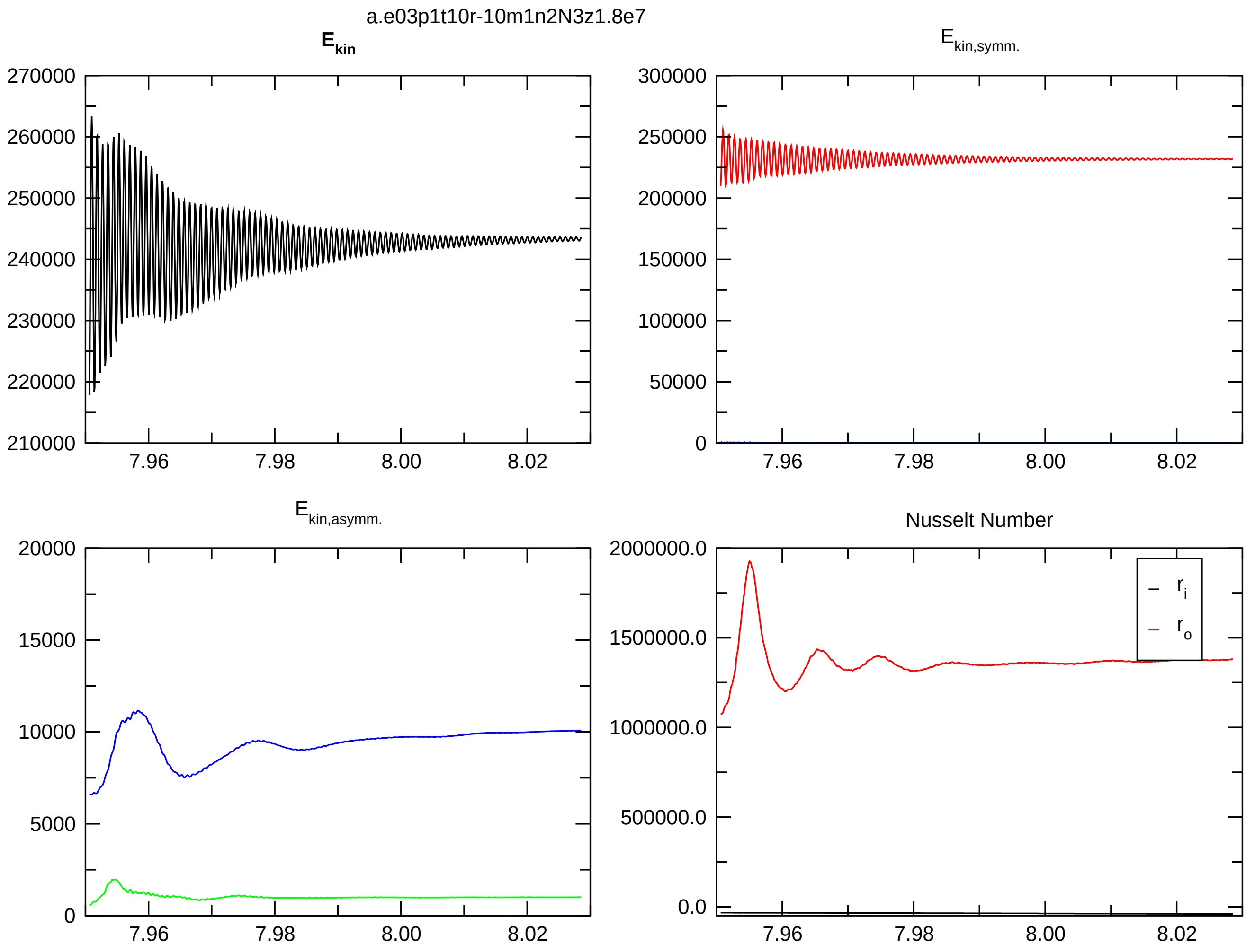

a.e03p1t10r-10m1n2N3z2e7

times: 4.330217 4.430218 4.530219 4.63022 4.730221 4.830222

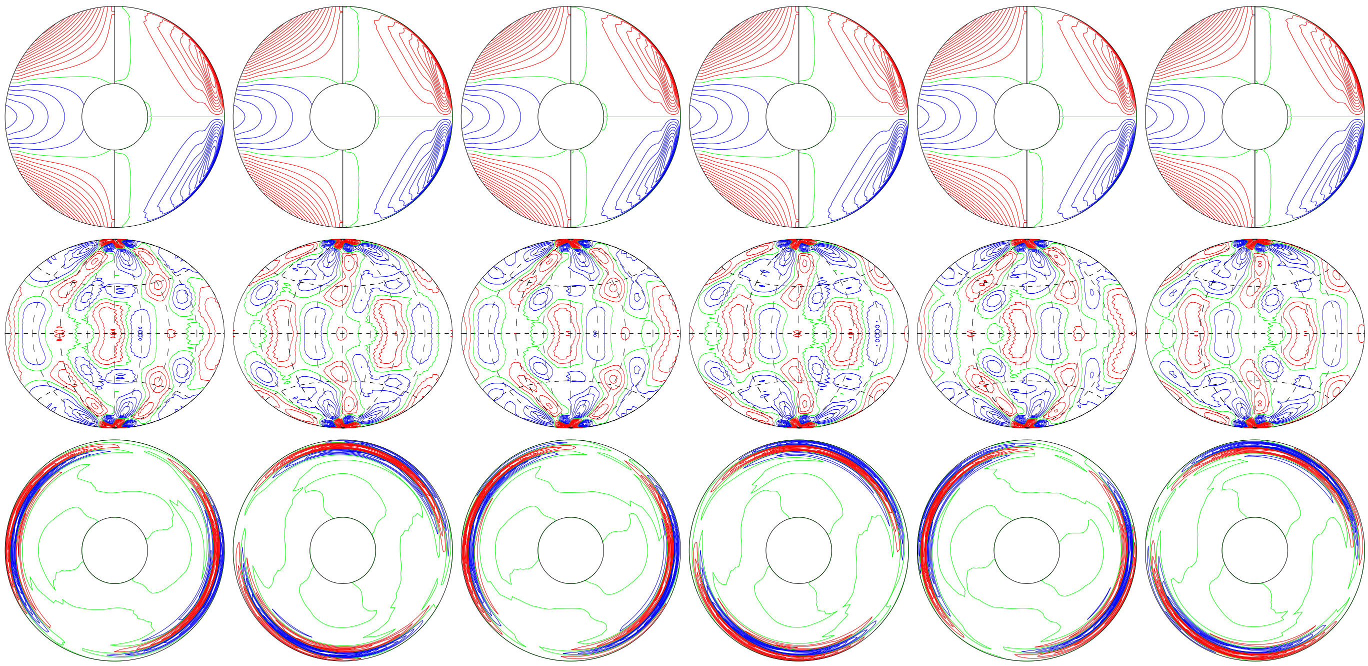

a.e03p1t10r-10m1n2N3z2e7

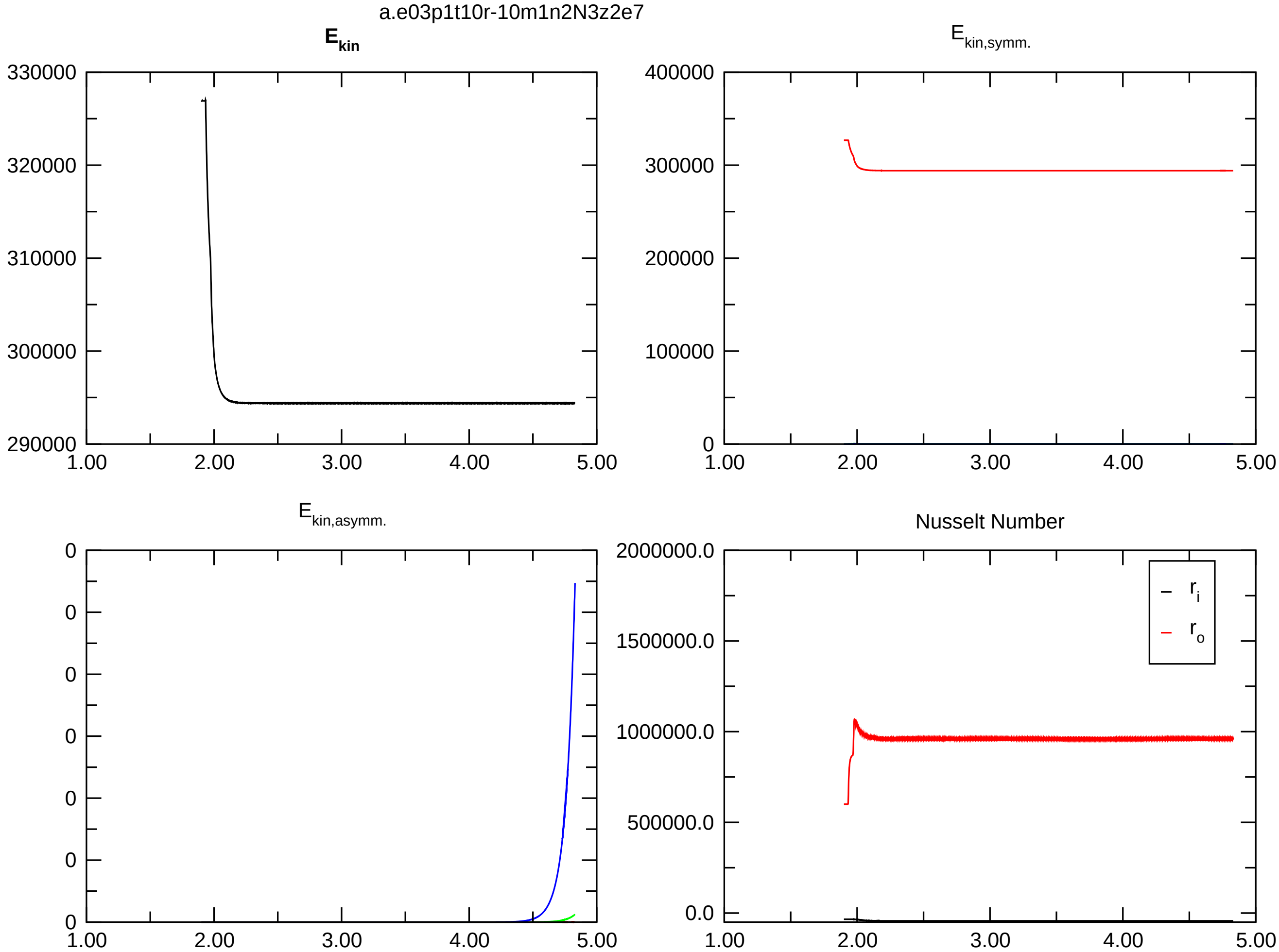

a.e03p1t10r-10m1n2N3z2.05e7
times: 2.250197 2.300198 2.350199 2.4002 2.450201 2.500202

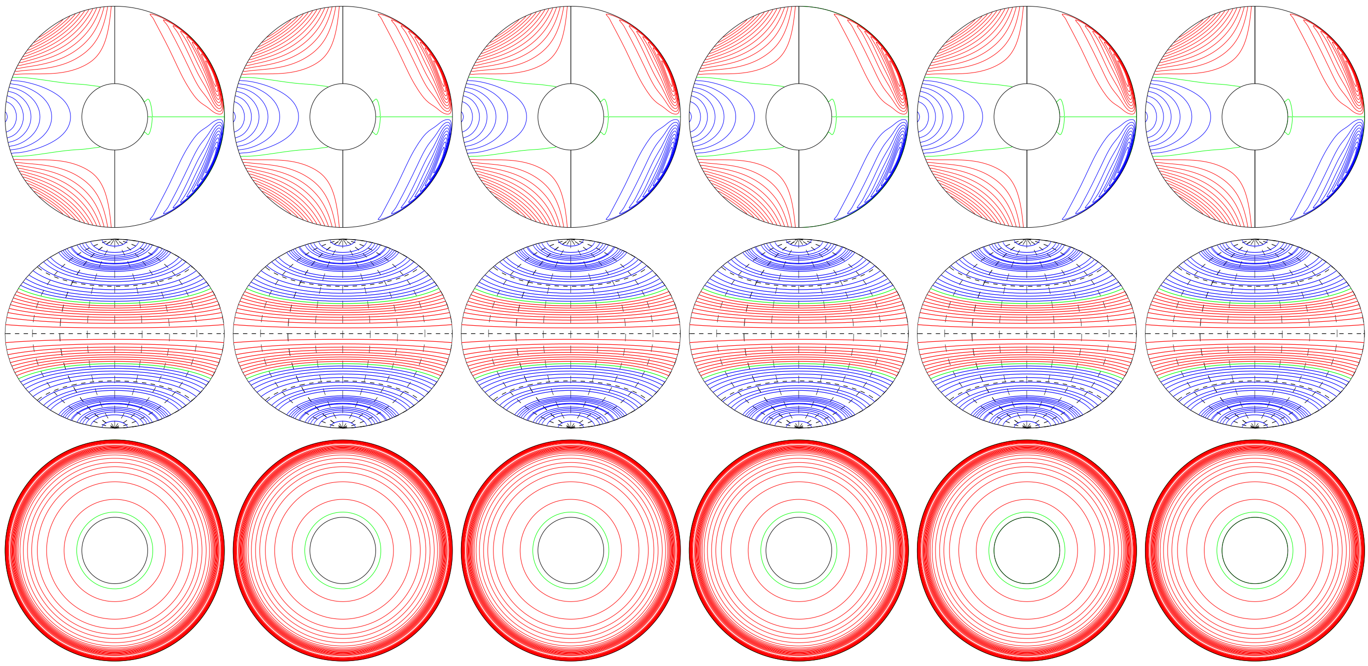

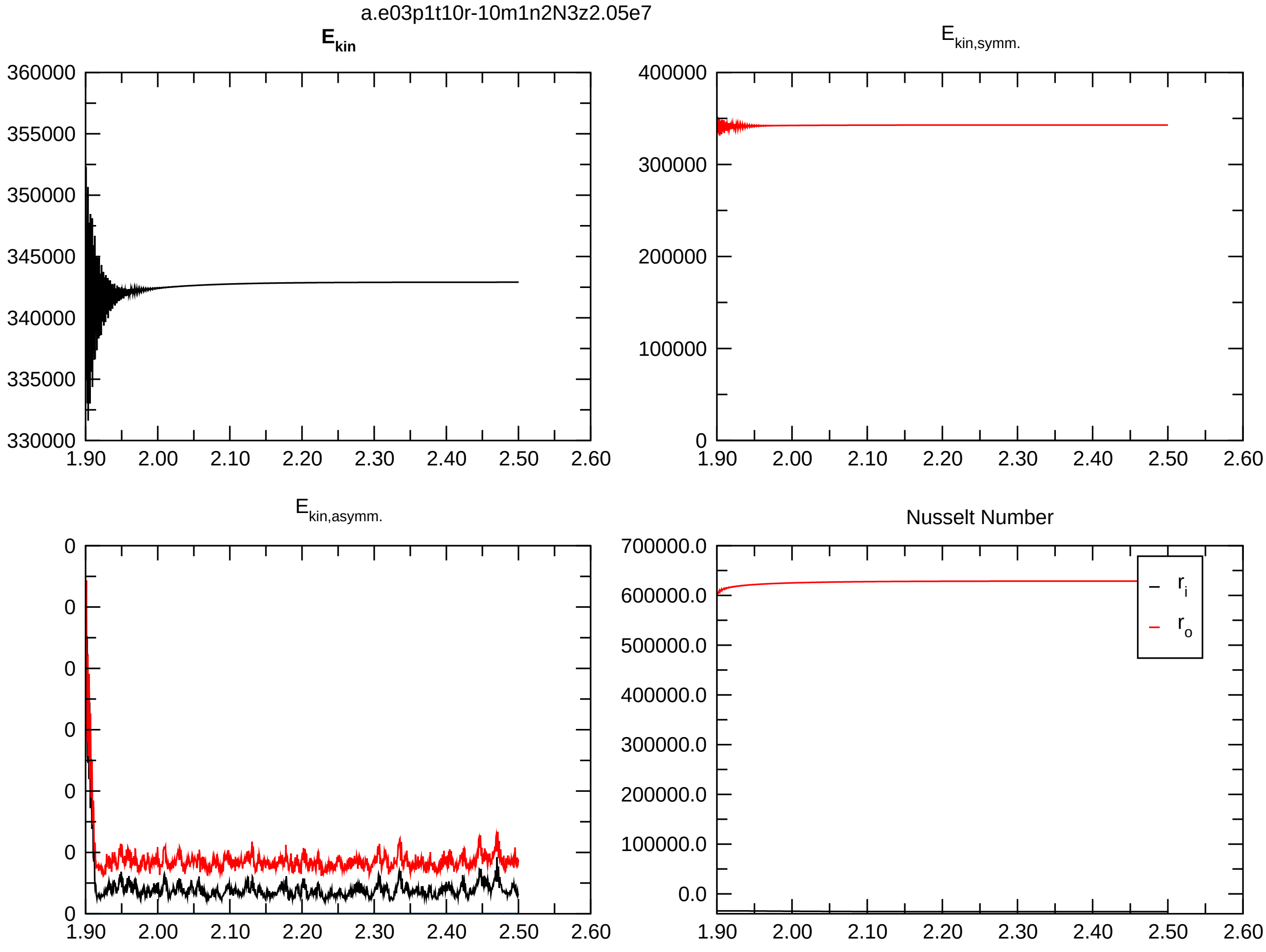

a.e03p1t10r-10m1n2N3z2.5e07
times: 2.250197 2.300198 2.350199 2.4002 2.450201 2.500202

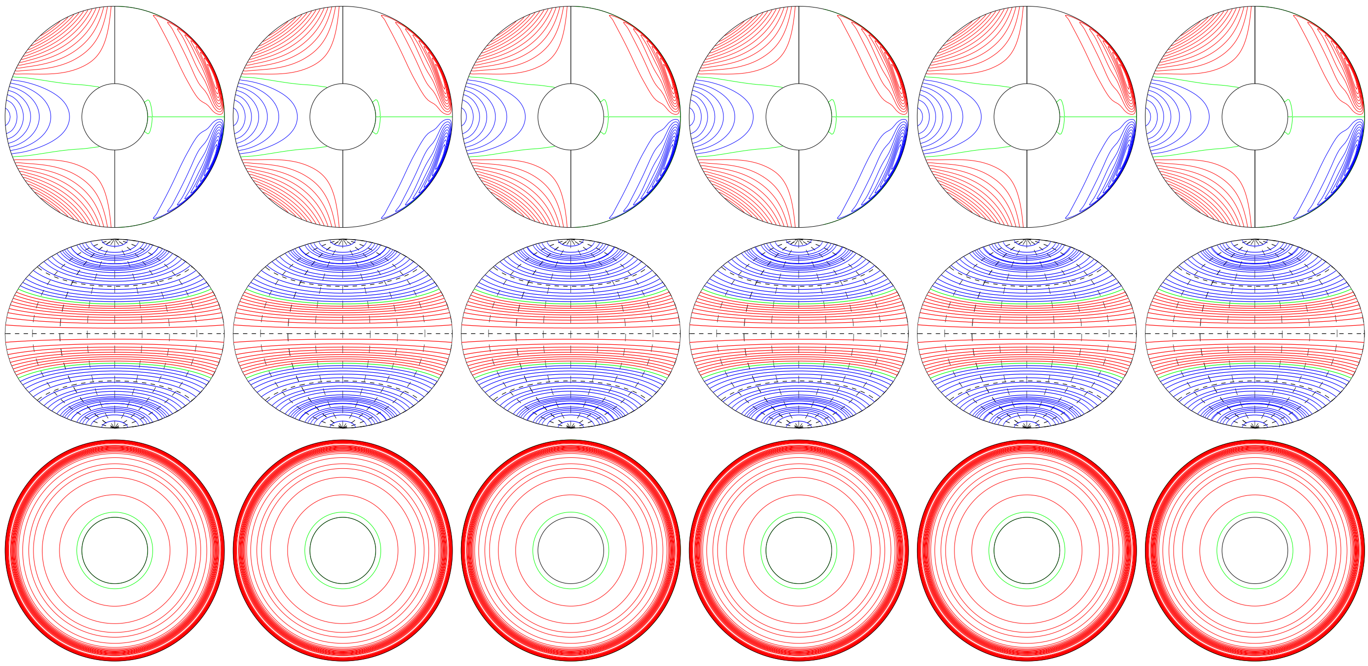

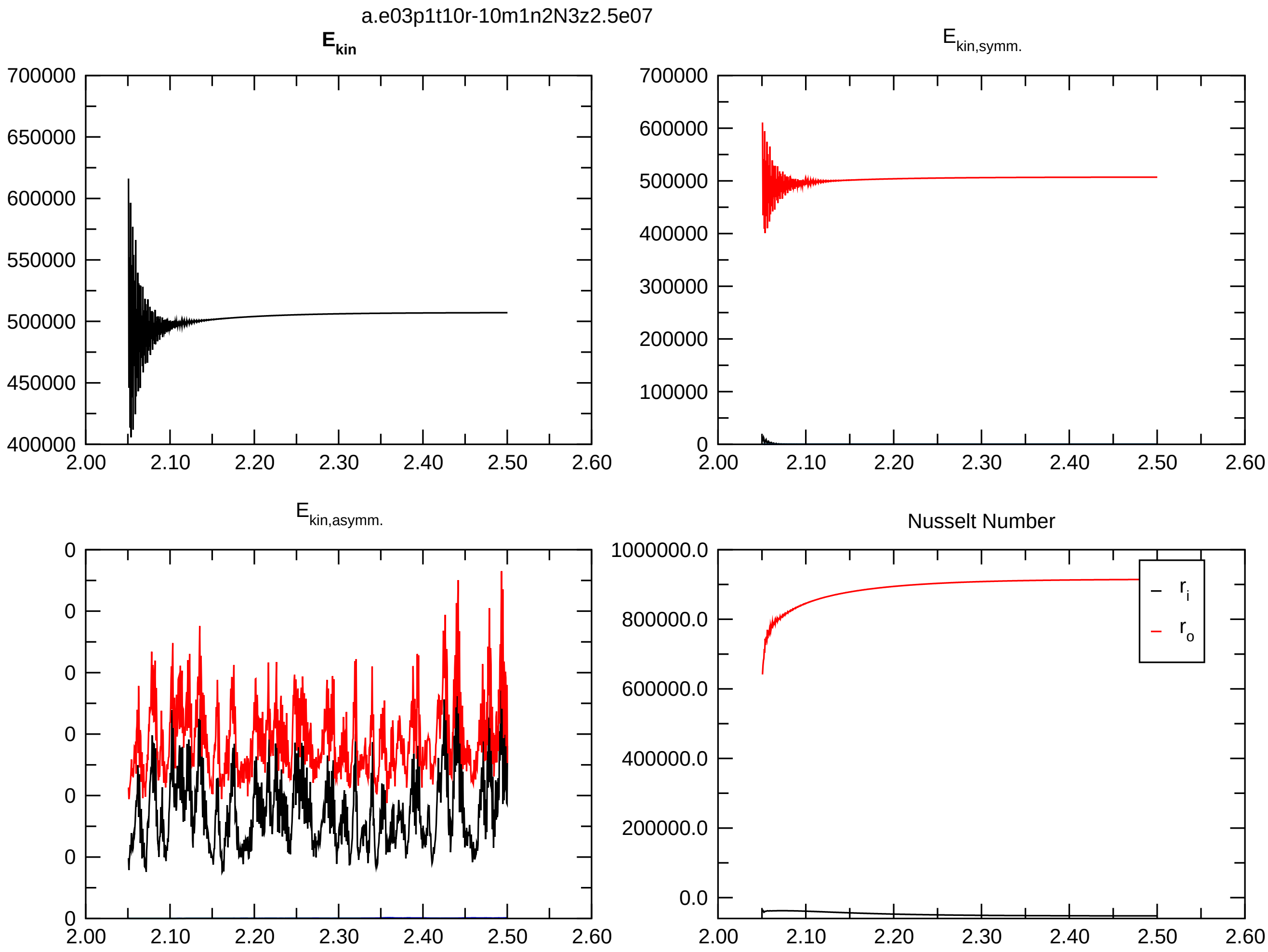

a.e03p1t10r-10m1n2N3z3e07

times: 2.050193 2.100194 2.150195 2.200196 2.250197 2.300198

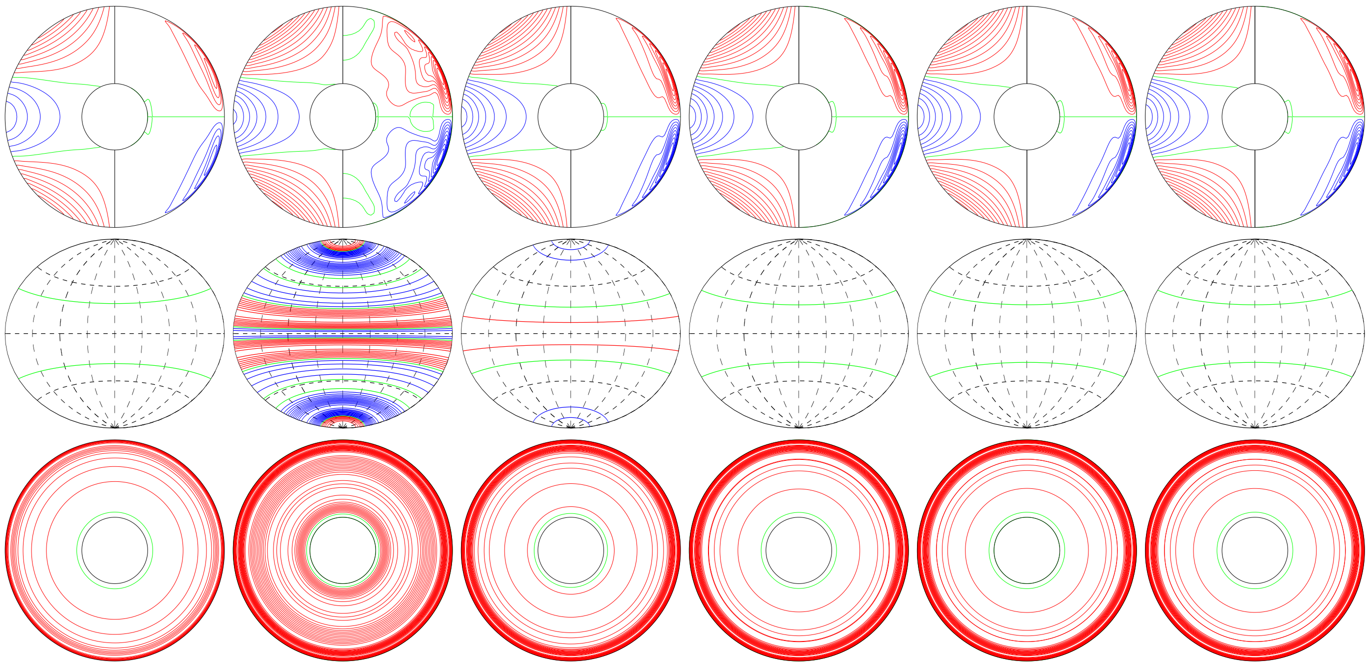

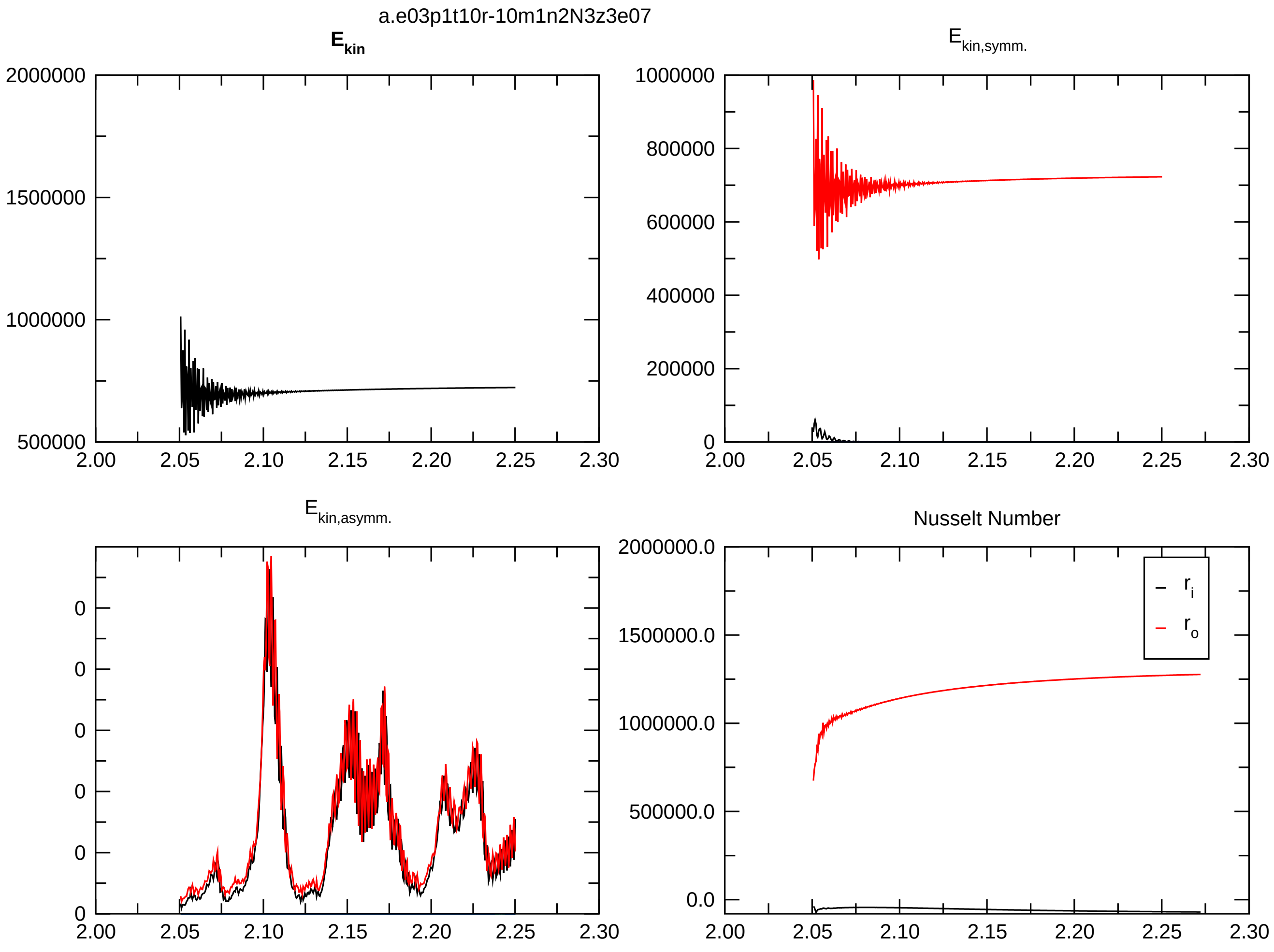

a.e03p1t10r-10m1n2N2z1.8e7
times: 0.1320066 0.1380069 0.1440072 0.1500075 0.1560078 0.1620081

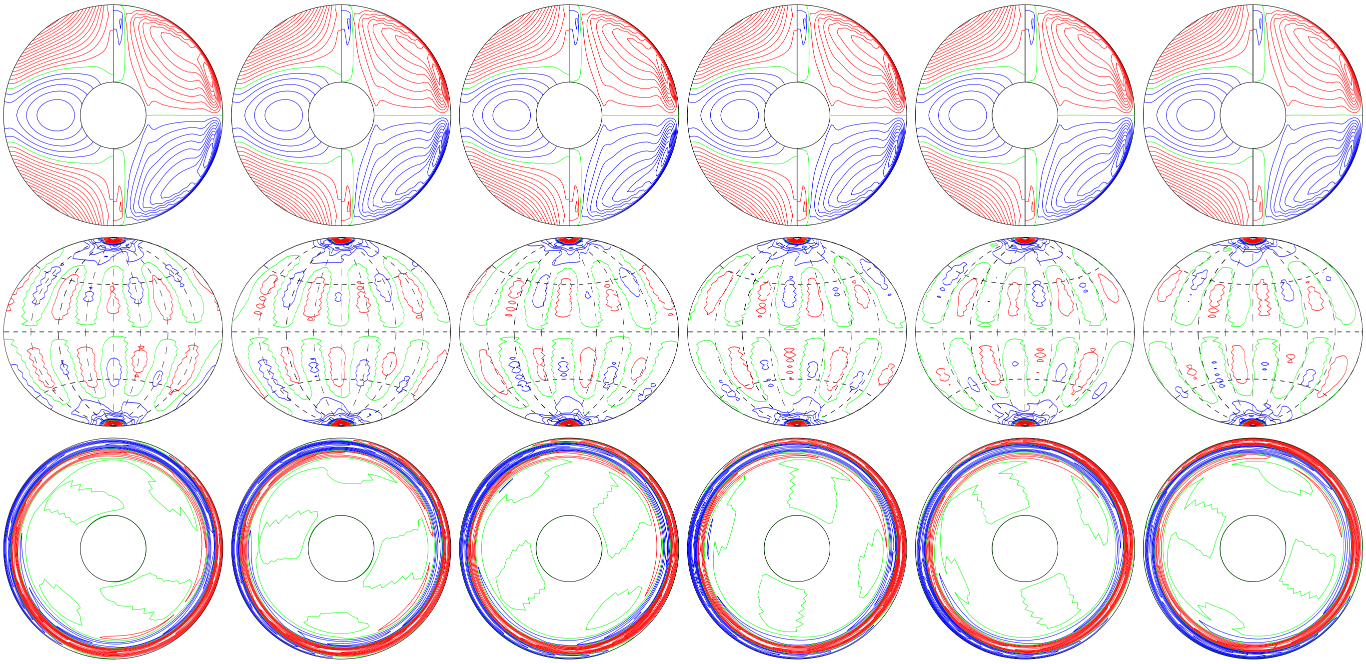

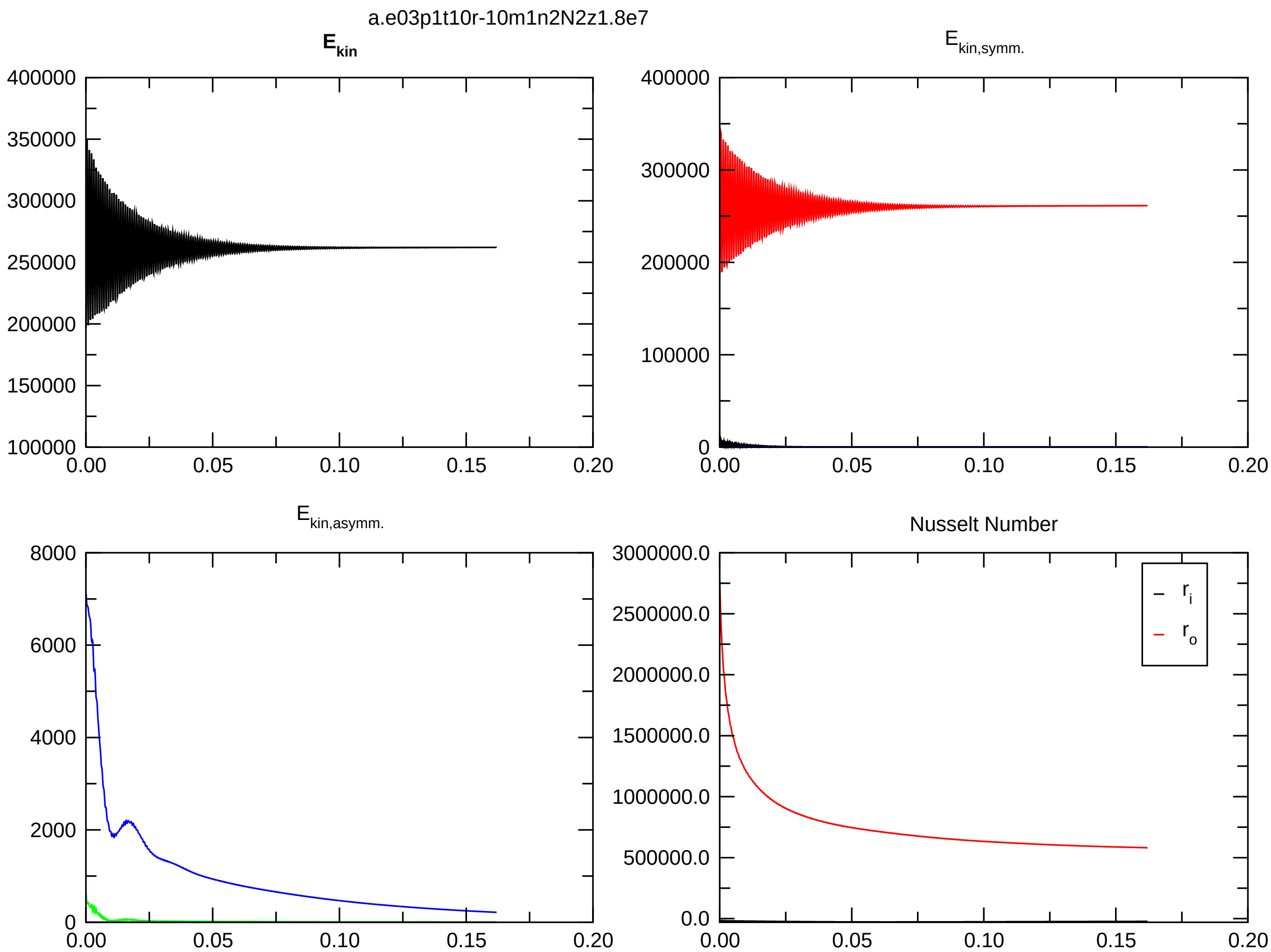

a.e03p1t10r-10m1n2N2z2e7
times: 0.1260063 0.1320066 0.1380069 0.1440072 0.1500075 0.1560078